Ultrasound Technology in Human Internal Organ Motion Tracking: An Application in Non-invasive Respiratory Monitoring

Amirhossein Shahshahani

Department of Electrical and Computer Engineering
Faculty of Engineering, McGill University
Montreal, Canada

April 2019

A thesis submitted to McGill University in partial fulfillment of the requirements for the degree of Doctor of Philosophy.

Acknowledgments

First and foremost, I would like to express my deep sense of gratitude to Prof. Zeljko Zilic and Sharmistha Bhadra for their commitment and worth advising. They shared the support and enthusiasm in my work and provided unlimited assistance throughout my research toward my Ph.D. degree.

I take this moment to extend my thankfulness to my committee members, Prof. Gordon Roberts and Prof. James J Clark for their insightful comments and suggestions during my dissertation proposal and seminar. I wish to thank Carl Laverdiere for his insights into the medical area and his contribution during my research. I would also like to thank my friends, Majid Janidarmian, Atena Roshan fekr, Junchao Wang, Anastasios Alexandridis, Soheyl Ziabakhsh, Farimah Poursafaei, Steve Ding and Andrey Tolstikhin who have been a source of friendships as well as good advice and collaboration in Integrated Microsystems Laboratory (IML). I would like to acknowledge Emile Traore for his contribution in speeding up the hardware design and French translation of the abstract.

Lastly, I would like to thank my family for all their love and encouragement. For my parents who raised me with a love of science and supported me in all my pursuits. And most of all I would like express appreciation to my beloved wife who has been my best friend and a great companion and helped me to keep things in perspective.

Thank you.

Abstract

Prolonged monitoring of breathing under different physical conditions is important in many applications, either for personal health tracking or in hospitals. Ultrasound technology has been used widely for imaging and diagnosis of the human body. In this dissertation, we introduce the use of the ultrasound for human respiratory monitoring. The proposed system measures the heart and respiration rates by capturing ultrasound reflections from the heart and surrounding organs. This system is based on ultrasound M-mode to measure the Time of Flight (TOF), amplitude and phase of reflected ultrasound waves generated by piezo transducers. Respiratory and heart rate signals are obtained by tracking the motion of the heart during tidal breathing. Practical tests applied on six subjects exhibited 94.5% sensitivity and 94.0% specificity in respiration detection compared to an SPR-BTA spirometer signal as a reference, and an average accuracy of 96.7% in heartbeats per minute (BPM) measurement.

The respiratory waveform obtained from the diaphragmatic motion of the heart contains errors when a subject is moving. Hence, instead of monitoring the diaphragm motions indirectly from the heart, we have tried to find the best place to monitor the diaphragm motions directly. The best place is the zone of apposition (ZOA) which is the area of the diaphragm encompassing the cylindrical portion. The sensor has been placed between ribs 8 and 9 at the mid-axillary line to see both contraction and relaxation of the diaphragm. Six different tests performed on six healthy adults demonstrated an average respiration detection sensitivity and specificity of 84% and 93%, respectively. All tests consisted of body motions, different breathing rate and patterns, apnea and breath-holds simulations.

Respiratory waveforms were affected by skin movement artifacts when the sensor is placed in front of rib cage. A sensor with an array of three transducers was designed to compensate the error in a way that at least one out of three transducers is able to track the diaphragm muscle movements. The effectiveness of this procedure has been verified in a comprehensive test including body motions and different sleep positions.

The designed low-power and low-complexity prototype delivers accurate respiratory signal tracking. The system can be integrated into a small size wearable device. The sensor is made of flexible hybrid printed circuit, enabling the conformal sensor interface to the human skin. The proposed sensor is examined against the spirometer output, which is the gold standard in all tests.

Abrégé

La surveillance prolongée de la respiration dans différents états physiques est importante dans plusieurs applications pour le suivi de la santé ou dans les hôpitaux. La technologie des ultrasons a été largement utilisée pour l'imagerie et le diagnostic du corps humain. Dans cette dissertation, nous introduisons l'usage des ultrasons pour la surveillance de la respiration humaine. Le système proposé mesure les rythmes respiratoire et cardiaque en capturant les réflexions des ultrasons par le cœur et les organes environnants. Ce système est basé sur les ultrasons en mode M et mesure le temps de vol (TDV), l'amplitude et la phase des ondes ultrasoniques réfléchies générées par des transducteurs piézoélectriques. Les signaux des rythmes respiratoire et cardiaque sont obtenus en suivant le mouvement du cœur durant la respiration courante. Les essais pratiques effectués sur six sujets ont démontré une sensibilité de 94.5 % et une spécificité de 94.0 % par rapport à un spiromètre SPR-BTA utilisé comme référence et une exactitude moyenne de 96.7 % dans la mesure de battements de cœur par minute (BPM).

La forme d'onde obtenue à partir du mouvement diaphragmatique du cœur contient des erreurs lorsque le sujet est en mouvement. Donc, au lieu de surveiller le mouvement du diaphragme indirectement à partir du cœur, nous avons tenté de trouver la meilleure position pour surveiller le mouvement du diaphragme directement. Cette position est la zone d'apposition (ZA) qui est la région du diaphragme comprenant la portion cylindrique. Le capteur était placé entre les côtes 8 et 9 sur la ligne médio-axillaire pour capter à la fois la contraction et la relaxation du diaphragme. Six essais différents effectués sur six adultes en bonne santé ont démontré respectivement une sensibilité et une spécificité de détection de la respiration de 89 % et de 93 %. Tous les essais comprenaient des mouvements du corps, des rythmes et profils de respiration différents et des simulations d'apnée et de rétention de la respiration. Les formes d'onde de la respiration étaient affectées par les artéfacts du mouvement de la peau lorsque le capteur est placé devant la cage thoracique. Un capteur avec un arrangement de trois transducteurs a été conçu pour compenser les erreurs de sorte qu'au moins un des trois transducteurs puisse suivre le mouvement musculaire du diaphragme. L'efficacité de ce procédé a été vérifiée par une étude complète.

Le prototype conçu, de faible puissance et complexité, transmet un signal respiratoire très exact. Le système peur être intégré dans un dispositif portable de petite taille. Le capteur est conçu de circuits imprimés hybrides flexibles, permettant au capteur de se conformer à la peau humaine. Le capteur proposé est examiné par rapport au spiromètre, l'étalon de référence pour tous les essais.

Contents

List of Figures

List of Tables

Nomenclature

Z Acoustic Impedance

ρ Density of medium

c Speed of sound in the medium

T Stress to transducer

P Polarization vector!!!

d Piezo electric strain constant

S Distortion , linear function of d

ϵ **or** ϵ_r Relative permittivity

S_{ij} Elastic Compliance

N_i Frequency coefficient

Q_m Mechanical quality factor

K Coupling factor

θ_z Axial resolution

t Piezo element thickness

λ Wave length

λ_t Wave length in piezo

Chapter 1

Introduction

1.1 Research Problem and Scope

Respiratory rate (RR), or the number of breath intakes per minute, is an important clinical sign representing ventilation. A change in RR is often the first sign of health deterioration as the body tries to balance oxygen delivery to the tissues. A real-time monitoring of respiratory parameters such as inhalation/exhalation duration, total time of the respiratory cycle, as well as respiration rate, are important diagnostic methods for planning medical care. Recently, demands for remote health monitoring systems have provided the driving force for development of wearable devices. There are plenty of methods and devices that are able to partially satisfy the demands in this domain. Innovations and advancements in this area are towards improvements in the following challenges:

- Accuracy: This is the most important parameter in monitoring a vital sign. Numerous health monitoring sensors are proposed, but the functionality of these sensors in different situations is a key point. The main role of a wearable sensor is providing trusted information for the patient's health condition without the presence of an expert such as a physician. Many existing methods suffer from motion artifacts that are unavoidable,

difficult to detect and to compensate.

- Convenience: Advances in the world of electronics have yielded integration of wearable systems into very small and portable packages. Although the size of sensor is not the only parameter for a sensor to be convenient, sensor position and the way it has to be mounted on the body are important as well. Some methods, such as Polysomnogaphy (PPG) and Electrocardiography (ECG), require the direct connection of adhesive electrodes which may cause injuries to sensitive skins [17].

- Signal complexity and computation power: Since most health monitoring devices are battery powered, the power consumption is another important criterion. Apart from the power consumption of the sensor and data transmission (or even storage), the signal processing efforts play a key role in this domain. There is much research done in processing the raw data towards obtaining the desired respiration signal from a sensor. However, most of the proposed techniques are not feasible to implement considering the limited hardware resources in portable or wearable devices.

- Safety and security: The safety of e-health products must be addressed in a similar way as for medical devices in hospitals. Since the device is supposed to be used for a long time, hazards such as electrical shocks and skin injuries should be taken into account with a higher importance. Also, the security of data transmission and storage are other key points to consider.

- Privacy: It could be categorized into the privacy of collected data and the utilization of the wearable device. Some patients may desire to use a wearable device that is not visible to other people. Therefore, ambient sensors such as cameras and microphones are less private than the on-body sensors. However, sensors that have to be placed on the face, hands, and fingers could be categorized as less private than other methods that are hidden under the clothes.

Considering the importance and the challenges of designing a real-time portable respiratory monitoring system, this thesis will focus on proposing an ultrasound-based organ motion tracking to continuously monitor internal organs involved in the respiratory system to provide the respiratory signal. A wearable sensor output should be robust to human motion artifacts. In this research, I evaluate the proposed system in the rest condition, as well as under body motions of normal daily activities. Also, the proposed technique is in direct contact with the chest skin and could be hidden for the patient's convenience.

1.2 Motivation Behind the Research

Increasing health care and nursing costs in hospitals apply enormous stress on society and the government. Therefore, smart assistive technology that promotes the independence of patients for visiting hospitals is a major motivating factor for wearable sensor-based systems. The U.S. health care system reports a $200 billion cost reduction over the next 25 years if remote monitoring tools were utilized in congestive heart failure, diabetes, chronic obstructive pulmonary disease (COPD), and chronic wounds or skin ulcers [26]. Almost 3.7 million people in UK live with COPD (predicted to increase by one-third by 2030), costing about 1.2 billion pound per year [36]. In addition to the elderly, it is also necessary to monitor the babies breathing to prevent disease such as sudden infant dead syndrome (SIDS) [19]. Also, it is highly desirable to monitor infant respiratory signals without using adhesive pads or wire bonded methods.

The majority cases for shortness of breath are due to chronic cardiopulmonary conditions such as asthma, heart disease, chronic obstructive pulmonary disease, and psychological conditions that cause anxiety and panic attacks [35][31]. While anxiety can cause shortness of breath and other physical symptoms, it is important to acknowledge that experiencing shortness of breath for other reasons may also create anxiety. There are different types of breath disorders that are characterized by their patterns such as Bradypnea [43], Tachypnea, Cheyn-

stokes and Kussmaul [10][7]. Monitoring ventilation during sleep, in terms of hypopneas and apneas (i.e. finding the occurrence of periods with low or no ventilation), is a necessity in the screening of sleep disorder.

In a research by Cretikos *et al*[11], over half of the examined patients suffering a serious adverse event on the general wards (such as a cardiac arrest or ICU admission) had a respiratory rate of 24 breaths/minute and more. These patients could have been identified as high risk up to 24 hours earlier by RR information. A respiratory rate higher than 27 breaths/minute could be the most important predictor of cardiac arrest in hospital wards [15]. Another research by Jonsson *et al*[22] found that respiratory failure was the primary cause of emergency admission to the ICUs, while the RR was the least documented vital sign. By having early detection and monitoring of changes in vital signs, particularly RR, serious health conditions might be avoided.

Recent technological advancements in wearable sensors make monitoring systems low-cost, intelligent, and lightweight [2]. As technology grows, a large potential exists for more advanced techniques with higher capabilities in health care systems in order to enhance diagnosis and monitoring. The measurement of human vital signals is crucial in cyber-biological systems, since any disorder pattern can be the first symptom of different physiological, mechanical, or psychological dysfunctions. The main objective of this chapter is to describe the motivations and purposes behind this research. The proposed solution showed a noticeable error reduction in breath detection based on comprehensive tests done in this research.

1.2.1 Literature review of respiratory monitoring systems

Nowadays, a variety of respiratory monitoring systems and sensors are proposed with different advantages and disadvantages, considering their applications in hospital, at home or in athletic fields. Table 1.1 lists the most known techniques of breath monitoring systems utilized in markets and researches, including their pros and cons. These systems are cat-

egorized as direct and indirect methods of measurements. For example, some respiratory rate measurement systems based on direct method are flow meters (pressure transducer, thermal and ultrasound flow meters) [3], [5], such as a spirometer shown in Figure 1.1-A. These methods have a direct relationship with the source of operation, which is the airflow of respiratory system. It could be the flow detection of air from nasal or mouth. However, these methods are not eligible as a comfortable gadget for long-term respiratory monitoring, due to the position of the sensor. Also, oral breathing makes people tired if it lasts long. In this dissertation, we found that breathing longer than 2 minutes is exhausting for subjects.

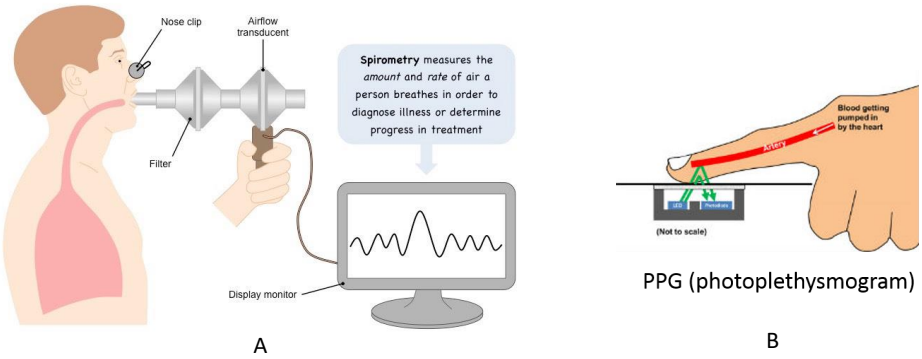

Figure 1.1 (A) Spirometer for oral breathing flow metering, (B) Pulse oximetry (PPG) sensor [1].

In another example, respiratory waveform was obtained by using a piezoelectric transducer using flexible piezoelectric film made of aluminum nitride [8]. This sensor measured pressure fluctuations on the skin surface due to the breathing and heart operations when a subject was lying on it. In a similar work, a strain gauge transducer was utilized for classifying normal respiration or respiration with motion categories (such as apnea)[34]. They used second-order auto-regressive modeling and zero-cross algorithm in which the square root of energy index is considered as the baseline for respiration rate calculation. Although techniques based on chest and abdomen motions tracking are cheap and easy to mount on the patient's body, they suffer from human motion artifacts.

An image-based system for real-time respiratory monitoring system was proposed using a

camera-based technique [33][47]. Their image- and signal-processing methods used information from chest and abdominal movements from a sequence of video recordings by a single camera. They reached an estimation error of 3% in respiration rate detection for a 3–10 min test on a single subject in sitting position. Such systems, not only demand high cost, but also may be considered to be an invasion of patients' privacy. Furthermore, the accuracy directly depends on the patients' clothing patterns as well as their distance from the camera.

Recently, motion sensors were introduced to detect small motions of the body due to the expansion and contraction of the lungs in each respiration cycle. In a study [37], a combined oximeter with an accelerometer sensor is used to diagnose sleep apnea, COPD, and asthma. In other works [14][20], they also examined the body posture impacts in analyzing the respiration. They proposed a method to detect the apnea and hypoapnea events in real time and apnea/hypoanpea index (AHI) calculation. The beauty of this technique is in the low cost and comfortable implementation of this system. The system is supposed to detect mild motions on the surface of the body due to the respiration. Therefore, human body motions will hide smaller motions due to breathing. In addition, if the user sleeps on the sensor, no breathing motions will be sensed by this sensor.

A method for respiration rate estimation based on the ECG signal was proposed by Lazaro *et al* [25]. A different combination of 12-leads ECG was examined and the data were digitized with a sampling rate of 1000 Hz. Their results were referenced with an airflow thermistor-based device. The lowest error in respiration rate estimation with normal breathing pattern was $1.07 \pm 8.86\%$, based on using a three vector cardiographic (VCG) leads. The main issue with ECG-based instruments is that the electrodes are attached directly on the skin (by at least three adhesive pads) and making the use of such technique uncomfortable. Removing the adhesive bonding will cause skin injuries (especially for children and people with sensitive skins) and skin dermatitis [49]. So, minimizing the number of adhesive pads will be preferable.

Another well-known method for respiratory monitoring, called electrical impedance tomography (EIT), obtains the respiratory signal through impedance changes in thorax [9][6]. Typically, the EIT device uses 16 or 32 electrodes distributed around the thorax to inject high-frequency and low-amplitude alternating electrical currents. Then, the measured electrical potentials on the skin surface are used to obtain the electrical impedance. Again, this method requires an almost 16 electrodes (standard) [24], or 4 electrodes in [53], connected to the skin surface. However, this method provides more information such as cardiac volume.

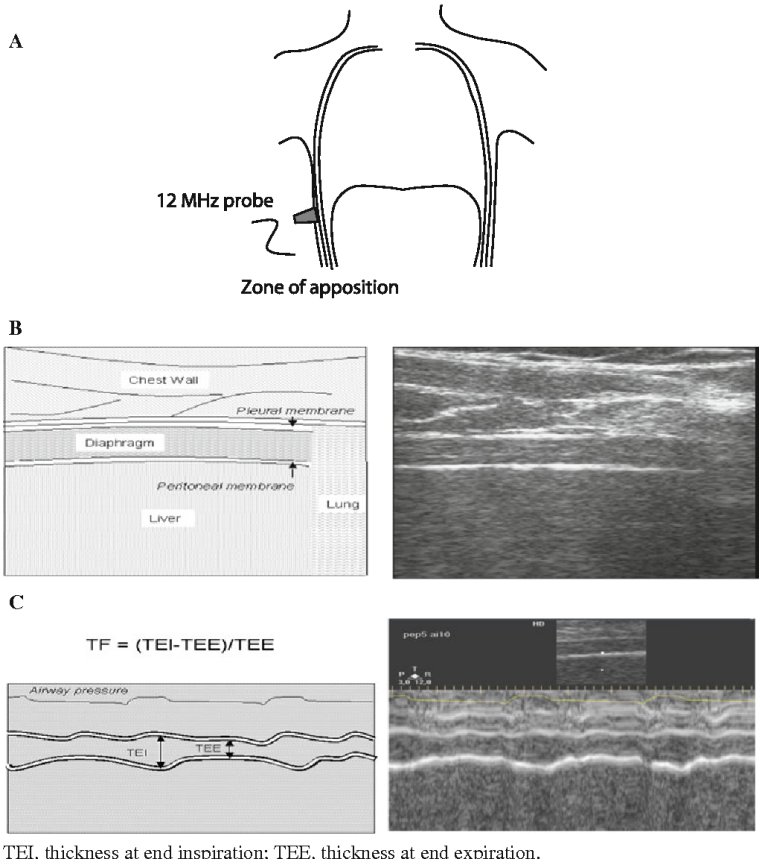

Figure 1.2 Probe placement to explore the diaphragm in the zone of apposition (a), with the ultrasonographic view of the normal diaphragm in the zone of apposition (b) and illustration of the measurement of diaphragm thickness at end inspiration and end-expiration in TM mode (c). TEI thickness at end-inspiration, TEE thickness at end-expiration [48] (reprint with copyright permission from Springer Nature).

Ultrasound technology (US) is inexpensive, safe, real-time and can be used as a direct

method for pulmonary monitoring. This technology has been utilized for imaging the human body for over half a century. Ultrasound imaging systems with an array of piezo transducers are widely used in diagnosis and imaging [45]. Imaging of the diaphragm using ultrasound imaging machine was assessed by Zambon *et al.*[52] and E. Vivier *et al.*[48], but it required a technician to hold the probe. Moreover, this is not a wearable or hand-held solution for RR monitoring and it requires extensive processing efforts to analyze signals from many transducers integrated in the probe. As shown in the Fig. 1.2, the ultrasound system monitors the diaphragm wall position and thickness at end inspiration (TEI) and expiration (TEE). Since the liver is a big tissue and positioned behind the diaphragm wall, there is no reflection sensed right after the reflections from the diaphragm. This makes the processing effort simpler and more clear to obtain the desired data.

Indirect methods are based on a consequence of an organ activity like oxygen level variation measurements during the breathing or small blood pressure variation due to the diaphragm pressures on the cardiac system [30][16]. Such indirect methods are not accurate and reliable because of many parameters. For instance, for the above mentioned oxygen level measurement sensor, the oxygen level depends on the oxygen level of area the person is breathing, bad functioning of lungs or airflow, latency between the breathing and oxygen level variation [16]. A study on oxygen level measurements examined parameters that impact the estimations, such as S_aO_2 level, sensor type, skin color, and gender are predictive of errors [13]. They have found that skin color has impacts on accuracy of oxygen level measurements. Pulse oximetry (PPG) sensor measures the arterial hemoglobin saturation and blood pressure through changes in ambient and infrared light absorption, as shown in Fig. 1.1-B. This sensor is usually placed on the index finger, great toe and ear lobes. Cretikos *et al* [11] found that pulse oximetry (PPG) is not a replacement for measuring respiratory rate. This sensor alone does not provide adequate ventilation monitoring information due to reasons such as reduced perfusion at the site of measurement and motion artifact [23].

Another indirect method for respiratory monitoring is based on the sound processing heard from tracheal [51],[50]. Although it can be an efficient way of detecting deep and low breathing sound amplitude, the noise background (like speech) is dominant to the breathing sounds. Therefore, finding a relationship between the sound amplitude and air flow is complicated and requires extensive processing.

Table 1.1 A summary of respiratory monitoring systems

Sensor type	Placement	Portability	Technique	Other points	Reference
Flow meter	Mouth or nose	only nose type	Measuring the airflow from mouth or nose	Uncomfortable, under certain conditions	[3], [5]
Piezo film	Around the thorax	Yes	Measuring pressure fluctuation	Sensitive to body motions	[8]
Strain gauge	Abdomen	Yes	Measuring strain due to the breathing	Sensitive to body motions	[34]
Microphone	On tracheal	Yes	Measuring tracheal sound signal	Work only in silence area	[50]
Camera	In front of subject	No	Video processing	Higher power consumption	[33],[47]
Accelerometer	Chest/Sternum region	Yes	Correlation with a reference	Sensitive to body motions	[14],[37]
ECG	Different places on chest	No	QRS slop and RR processing	Not comfortable	[25]
Ultrasound (Low Freq)	In front of subject, like a camera	No	Measuring distance or Doppler	Sensitive to body motions and patients clothes	[4]
Pulse Oximeter	Finger or ear	Yes	Measuring blood flow/Oxygen level	Sensitive to movements, indirect	[16]
Ultrasound (High Freq)	Chest	Yes	Organ physical motion detection and Doppler	Less sensitive to motions, more features in one sensor	[38]

1.2.2 Signal processing evaluation

Another important criterion in selecting the right sensor for the purpose of respiratory monitoring is the complexity of the signal obtained from the sensor. A complex signal requires extensive processing such as fine filtering and classification. A correct selection of filter is significant. For example, an Infinite Impulse Response (IIR) filter is not linear in the phase, while a Finite Impulse Response (FIR) filter is. Hence, the FIR filter will not alter the signal in the time domain. However, an FIR filter with the same frequency response than the IIR

filter has a higher order, which makes the processing slower. Accordingly, using fewer filters in the design and utilizing filters with lower order are preferable. As for the classification of the signal, one of the most common techniques to extract the respiratory signal is filtering the raw signal by rejecting signals beyond the expected frequency of breathing. However, the respiratory signal is a non-stationary signal, and the frequency of that is unknown. For example, it is evident that the maximum RR rate is lower than 40 breaths per minute for healthy people in rest [27]. But, the lower bound of this frequency is unknown. Dysfunctioning of the pulmonary system may result in breathing shortage or even blockage of the airway. So, the respiratory signal is similar to a DC signal.

Apart from the respiration operation, the human motion rates are comparable to the breathing rate. For example, regular activity of a subject in a sitting position or when the subject is walking can have a similar frequency than the breathing rate. So, if the respiratory monitoring system's signal is susceptible to motion artifact, it is hard to separate the desired signal from the undesired component of the signal.

Among the previously mentioned systems for respiratory monitoring, some methods are based on physical motions of the human body. For instance, resistive strain gauge [18] and piezo film sensors generate the respiratory signal based on skin surface deformation and abdomen (and/or chest) elongation. Therefore, the respiratory waveform of these methods is subject to motion artifact.

There are many efforts to derive the respiratory signal from ECG and PPG signals. Researchers are using different processing methods either in time or frequency domains [12]. One uses an ensemble empirical mode decomposition (EEMD) to remove the motion artifact from the respiratory waveform obtained from the ECG signal [46]. Since the PPG sensor is very cheap, low-power and wearable, it is the most interesting sensor for heart and respiratory monitoring. However, as mentioned before, this sensor is an indirect method for respiratory monitoring. There are many techniques adopted by researchers to obtain the respiratory

signal as discussed before. Most of these methods involve complex processing efforts [32][28]. In some studies, the researcher considers a windowing technique in which an extensive signal processing is performed over a recorded window of 32 seconds for instance [21].

Figure 1.3 presents a raw PPG signal for a subject when he is breathing and motioning his hand. In this figure, it is evident that the baseline of the PPG signal varies by motions. Since by breathing operation the overall arterial blood pressure changes, its impact is in direct contact with the PPG baseline amplitude. So, the respiratory signal separation from the motion artifact is complicated.

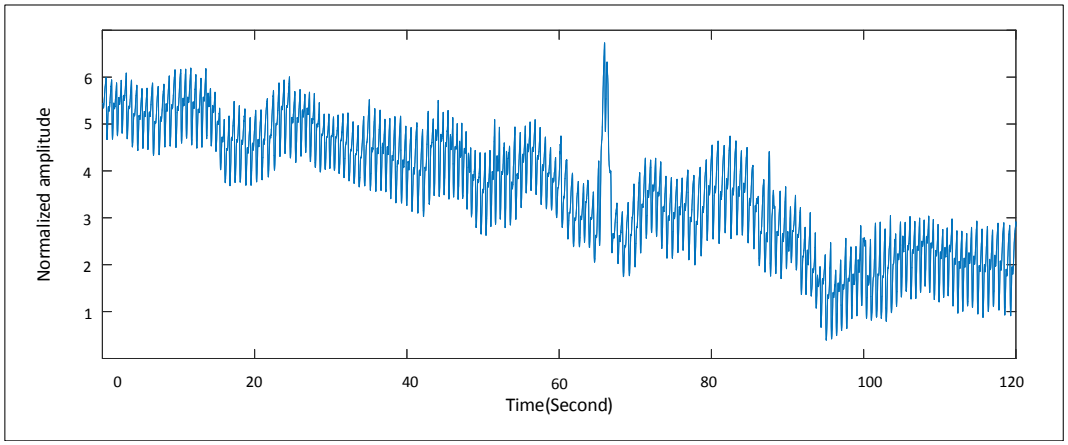

Figure 1.3 An example of a raw PPG signal contaminated with motion artifact while the subject is breathing.

As a summary of concerns regarding the processing efforts needed to obtain a respiratory signal using the systems mentioned above, most of these methods are sensitive to motion artifacts. The cost of time and energy used to process the signal should be taken into account when selecting a method for a wearable vital sign monitoring. It is worth noting that most of the wearable devices are powered by batteries, and have modest memory space to store and process signals. Therefore, an ideal sensor with a well-suited processing method would have the best performance.

In this dissertation, I tried to propose and develop a method which is less sensitive to motion artifacts and requires an effortless processing effort. Therefore, it can provide an

instantaneous respiratory signal with the least delay to the breathing function.

1.3 Thesis Contribution

1.3.1 Objective

This dissertation aims to design and implement a respiratory monitoring system that is comfortable, portable, inexpensive and less sensitive to human body movements. Additionally, it is preferred to have fewer sensors mounted on the body with adhesive pads. These pads may cause sweating, irritation for sensitive skins such as for newborn infants, kids or injured bodies. Piezo ultrasound transducers are a good candidate to make a diagnostic system. These transducers require only a soft medium such as an ultrasound gel in contact with the skin. An array of these transducers with a complex hardware unit are used for imaging. In this work, I developed a system based on ultrasound piezo transducers to observe internal organs physical motions, such as the heart or diaphragm. By classifying signals of heart motions, respiratory rate (RR), heart beats per minute (BPM), heart rate variation (HRV) and heart cycles (systole and diastole) could be extracted. Diaphragm motion tracking provides a robust respiratory signal than heart motion tracking. But, it lacks information about the heart. This method is noninvasive and requires a semi-complex hardware setup for pulse generation and reflection detection. In addition, they only require a conductive material like an ultrasound gel being rubbed on the skin surface to remove air gaps. There are many solutions for the entire ultrasound gel such as water, baby oil, some hand cream, etc. So, the patient is not limited to have the ultrasound gel.

1.3.2 Contributions

The main contributions in this thesis includes:

- Developing a new method for heart and respiratory monitoring using only one sensor:

The circumference of the normal adult human rib cage expands by 3 to 5 cm during inhalation [44]. Moreover, in a study for respiratory motion of the heart on some patients [42][29], researchers showed that during inspiration the heart moves inferiorly and underwent a cranio-dorsal rotation, and in eight patients, they observed anterior movements as well. Considering all these motions due to the respiration, we demonstrated the possibility of extracting a respiratory waveform as well as heart rate out of ultrasound reflections from the heart. Chapter 3 is a reprint of a paper under review in the IEEE Transaction on Biomedical Engineering (TBME) [41]. This chapter describes the proposed ultrasound sensor for heart and respiratory monitoring when the US sensor is placed in front of heart. Results were compared with references on six subjects.

- A new method for robust respiratory monitoring: Instead of heart motion tracking, we can obtain the respiratory signal by tracking the motion of diaphragm muscle inside the body. In this way, the sensor has to be placed on the zone of apposition (ZOA) which is in the right side of the chest, between ribs 8^{th} and 9^{th}, at the mid-axillary line. We found that the derived respiratory waveform in this position was extremely robust to human motion artifacts. However, it provides only the respiratory signal. As explained before about the necessity of having a trustable sensor to detect breathing operation, the proposed system barely generates false breath detection which is a distinct feature of this method compared to the other methods. The sensor's performance is compared with pulse oximetry (PPG) sensor and spirometer (as the gold standard). We concluded that the performance of our sensor is considerably higher than the inertial sensor and PPG sensor as the most competitive method in RR monitoring. However, we found the respiratory signal of this sensor susceptible to errors due to big skin motions and stretches. Chapter 4 is a published journal paper reprinted with the permission from the publisher [39].

- An enhanced motion-independent respiratory monitoring method: In this part, I designed a 3-channel sensor with an array of three piezo transducers, in a triangular shape. In this format, the system accuracy was found higher than the single channel sensor design. This sensor was tested on six subjects in six different body motions and positions with more emphasis on body motions and stretches. This work has been submitted to another journal [40] and presented in Chapter 5.

As part of the work of this thesis, ethical approval was received from McGill University Ethics Committee. All the participants were informed about the experimental procedures before starting the trial sessions.

1.4 Thesis Organization

This thesis is written based on three journals published or submitted. A general introduction for all chapters is brought to the Chapter 1. In Chapter 2, I will discuss the basics of ultrasound technology and the way this method is used in this thesis. Chapter 3 presents a sensor that is able to monitor heart and respiratory signals. In this method, I put the ultrasound sensor in front of the heart to observe heart motions, including every heart beat motions and respiratory motion of the heart. In Chapter 4, I introduce a novel method for respiratory monitoring which tracks the diaphragm motions, in which the sensor should be placed in the zone of apposition (ZOA) on the mid-auxiliary region. The ZOA is a window to observe the diaphragm wall motions. This method had a really interesting performance for breath monitoring, compared to inertial and PPG sensors. In the Chapter 5, I show performance and reliability improvements of this method against the motion artifact.

1.5 List of Publications

- **A. Shahshahani**, Z. Zilic, S. Bhadra, "*Diaphragmatic Motion Tracking Using Ultrasound Sensors for a Motion Independent Non-invasive Respiratory Monitoring,*" IEEE Sensors Journal, submitted in 2019.

- **A. Shahshahani**, Z. Zilic, S. Bhadra, "*An Ultrasound Based Biomedical System for Continuous Cardiopulmonary Monitoring: A Single Sensor for Multiple Information,*" IEEE Transaction on Biomedical Engineering (TBME), 2019.

- **A. Shahshahani**, C. Laverdiere, S. Bhadra, Z. Zilic, "*Ultrasound Sensors for Diaphragm Motion Tracking: An Application in Non-invasive Respiratory Monitoring,*" Sensors 2018, 8, 2617.

- **A. Shahshahani**, Z. Zilic, S. Bhadra, "*Motion Artifact Reduction in an Ultrasound Based Respiratory Monitoring System Using a 4-Channel Piezo Transducer,*" 17th IEEE International NEWCAS Conference, submitted in 2019.

- **A. Shahshahani**, S. Bhadra, Z. Zilic, "*Ultrasound Based Respiratory Monitoring Evaluation Under Human Body Motions,*" IEEE Sensors Conference, 1-4, 2018.

- **A. Shahshahani**, S. Bhadra, Z. Zilic, "*A Piezo Transducer Based Flexible Hybrid Sensor for Health Monitoring,*" International Flexible Electronics Technology Conference (IFETC), 1-2, 2018.

- **A. Shahshahani**, S. Bhadra, Z. Zilic, "*A Continuous Respiratory Monitoring System Using Ultrasound Piezo Transducer,*" IEEE International Symposium on Circuits and Systems (ISCAS), 1-4, 2018.

- **A. Shahshahani**, Z. Zilic, "*Ultrasound Sensors and its Application in Human Heart Rate Monitoring,*" IEEE International Symposium on Circuits and Systems (ISCAS),

1-4, 2017.

- **A. Shahshahani**, Z. Zilic, "*Enabling Debug in IoT Wireless Development and Deployment with Security Considerations,*" IEEE 25^{th} North Atlantic Test Workshop (NATW), 1-4, 2016.

Bibliography

[1] Measuring ventilation with a spirometer.

[2] Andrea Aliverti. Wearable technology: role in respiratory health and disease. *Breathe*, 13(2):e27–e36, 2017.

[3] GAL Araujo, RCS Freire, JF Silva, A Oliveira, and EF Jaguaribe. Breathing flow measurement with constant temperature hot-wire anemometer for forced oscillations technique. In *Instrumentation and Measurement Technology Conference, 2004. IMTC 04. Proceedings of the 21st IEEE*, volume 1, pages 730–733. IEEE, 2004.

[4] Philippe Arlotto, Michel Grimaldi, Roomila Naeck, and Jean-Marc Ginoux. An ultrasonic contactless sensor for breathing monitoring. *Sensors*, 14(8):15371, 2014.

[5] Ying-Wen Bai, Wen-Tai Li, and You-Wei Chen. Design and implementation of an embedded monitor system for detection of a patient's breath by double webcams. In *Medical Measurements and Applications Proceedings (MeMeA), 2010 IEEE International Workshop on*, pages 171–176. IEEE, 2010.

[6] Marc Bodenstein, Matthias David, and Klaus Markstaller. Principles of electrical impedance tomography and its clinical application. *Critical care medicine*, 37(2):713–724, 2009.

[7] Thomas Brack, Irene Thüer, Christian F Clarenbach, Oliver Senn, Georg Noll, Erich W Russi, and Konrad E Bloch. Daytime cheyne-stokes respiration in ambulatory patients with severe congestive heart failure is associated with increased mortality. *Chest*, 132(5):1463–1471, 2007.

[8] N. Bu, N. Ueno, and O. Fukuda. Monitoring of respiration and heartbeat during sleep using a flexible piezoelectric film sensor and empirical mode decomposition. In *2007*

29th Annual International Conference of the IEEE Engineering in Medicine and Biology Society, pages 1362–1366, Aug 2007.

[9] Margaret Cheney, David Isaacson, and Jonathan C Newell. Electrical impedance tomography. *SIAM review*, 41(1):85–101, 1999.

[10] Jeanne Craft. Current diagnosis and treatment in pediatrics. *Pediatric Critical Care Medicine*, 9(6):670–671, 2008.

[11] Michelle A Cretikos, Rinaldo Bellomo, Ken Hillman, Jack Chen, Simon Finfer, and Arthas Flabouris. Respiratory rate: the neglected vital sign. *Medical Journal of Australia*, 188(11):657, 2008.

[12] Shishir Dash, Kirk H Shelley, David G Silverman, and Ki H Chon. Estimation of respiratory rate from ecg, photoplethysmogram, and piezoelectric pulse transducer signals: a comparative study of time–frequency methods. *IEEE Transactions on Biomedical Engineering*, 57(5):1099–1107, 2010.

[13] John R Feiner, John W Severinghaus, and Philip E Bickler. Dark skin decreases the accuracy of pulse oximeters at low oxygen saturation: the effects of oximeter probe type and gender. *Anesthesia & Analgesia*, 105(6):S18–S23, 2007.

[14] Atena Roshan Fekr, Katarzyna Radecka, and Zeljko Zilic. Design of an e-health respiration and body posture monitoring system and its application for rib cage and abdomen synchrony analysis. In *Bioinformatics and Bioengineering (BIBE), 2014 IEEE International Conference on*, pages 141–148. IEEE, 2014.

[15] John F Fieselmann, Michael S Hendryx, Charles M Helms, and Douglas S Wakefield. Respiratory rate predicts cardiopulmonary arrest for internal medicine inpatients. *Journal of general internal medicine*, 8(7):354–360, 1993.

[16] Sotirios Fouzas, Kostas N Priftis, and Michael B Anthracopoulos. Pulse oximetry in pediatric practice. *Pediatrics*, 128(4):740–752, 2011.

[17] S Furdon. Challenges in neonatal nursing: Providing evidence-based skincare. *Medscape Nurses*, 2003.

[18] Gaetano D Gargiulo, Aiden O'Loughlin, and Paul P Breen. Electro-resistive bands for non-invasive cardiac and respiration monitoring, a feasibility study. *Physiological measurement*, 36(2):N35, 2015.

[19] Ruth Gilbert, Georgia Salanti, Melissa Harden, and Sarah See. Infant sleeping position and the sudden infant death syndrome: systematic review of observational studies and historical review of recommendations from 1940 to 2002. *International journal of epidemiology*, 34(4):874–887, 2005.

[20] J. E. Hernandez and E. Cretu. Respiratory effort monitoring system for sleep apnea screening for both supine and lateral recumbent positions. In *2017 8th IEEE Annual Information Technology, Electronics and Mobile Communication Conference (IEMCON)*, pages 191–197, Oct 2017.

[21] Delaram Jarchi, Dario Salvi, Lionel Tarassenko, and David Clifton. Validation of instantaneous respiratory rate using reflectance ppg from different body positions. *Sensors*, 18(11):3705, 2018.

[22] Thorsteinn Jonsson, Helga Jonsdottir, Alma D Möller, and Lovísa Baldursdottir. Nursing documentation prior to emergency admissions to the intensive care unit. *Nursing in critical care*, 16(4):164–169, 2011.

[23] Amal Jubran. Pulse oximetry. *Critical care*, 3(2):R11, 1999.

[24] T Koivumäki, M Vauhkonen, JT Kuikka, and MA Hakulinen. Bioimpedance-based measurement method for simultaneous acquisition of respiratory and cardiac gating signals. *Physiological measurement*, 33(8):1323, 2012.

[25] Jesús Lázaro, Alejandro Alcaine, Eduardo Gil, Pablo Laguna, and Raquel Bailón. Electrocardiogram derived respiration from qrs slopes. In *Engineering in Medicine and Biology Society (EMBC), 2013 35th Annual International Conference of the IEEE*, pages 3913–3916. IEEE, 2013.

[26] D Lindeman. Technologies for remote patient monitoring in older adults. *Center for Technology and Aging Google Scholar*, 2009.

[27] Wilburta Q Lindh, Marilyn Pooler, Carol D Tamparo, Barbara M Dahl, and Julie Morris. *Delmar's comprehensive medical assisting: administrative and clinical competencies*. Cengage Learning, 2013.

[28] K Venu Madhav, E Hari Krishna, and K Ashoka Reddy. Extraction of respiratory activity from ppg signals using an adaptive fourier coefficient estimator. In *2016 International Conference on Control, Instrumentation, Communication and Computational Technologies (ICCICCT)*, pages 446–451. IEEE, 2016.

[29] Kate McLeish, Derek LG Hill, David Atkinson, Jane M Blackall, and Reza Razavi. A study of the motion and deformation of the heart due to respiration. *IEEE transactions on medical imaging*, 21(9):1142–1150, 2002.

[30] DJ Meredith, D Clifton, P Charlton, J Brooks, CW Pugh, and L Tarassenko. Photoplethysmographic derivation of respiratory rate: a review of relevant physiology. *Journal of medical engineering & technology*, 36(1):1–7, 2012.

[31] Kenneth M Moser, Birgitta Ellis, and Carol Archibald. Shortness of breath: A guide to better living and breathing, 1983.

[32] Mohammod Abdul Motin, Chandan Kumar Karmakar, and Marimuthu Palaniswami. An eemd-pca approach to extract heart rate, respiratory rate and respiratory activity from ppg signal. In *2016 38th Annual International Conference of the IEEE Engineering in Medicine and Biology Society (EMBC)*, pages 3817–3820. IEEE, 2016.

[33] Kazuki Nakajima, Atsushi Osa, Shunji Kasaoka, Ken Nakashima, Tsuyoshi Maekawa, Toshiyo Tamura, and Hidetoshi Miike. Detection of physiological parameters without any physical constraints in bed using sequential image processing. *Japanese Journal of Applied Physics*, 35(2B):L269, 1996.

[34] Kundan Nepal, Eric Biegeleisen, and Taikang Ning. Apnea detection and respiration rate estimation through parametric modelling. In *Bioengineering Conference, 2002. Proceedings of the IEEE 28th Annual Northeast*, pages 277–278. IEEE, 2002.

[35] Monique C Pfaltz, Paul Grossman, Tanja Michael, Jürgen Margraf, and Frank H Wilhelm. Physical activity and respiratory behavior in daily life of patients with panic disorder and healthy controls. *International Journal of Psychophysiology*, 78(1):42–49, 2010.

[36] Klaus F Rabe, Suzanne Hurd, Antonio Anzueto, Peter J Barnes, Sonia A Buist, Peter Calverley, Yoshinosuke Fukuchi, Christine Jenkins, Roberto Rodriguez-Roisin, Chris Van Weel, et al. Global strategy for the diagnosis, management, and prevention of chronic obstructive pulmonary disease: Gold executive summary. *American journal of respiratory and critical care medicine*, 176(6):532–555, 2007.

[37] Tuomas Reinvuo, Manne Hannula, Hannu Sorvoja, Esko Alasaarela, and R Myllyla. Measurement of respiratory rate with high-resolution accelerometer and emfit pressure sensor. In *Sensors Applications Symposium, 2006. Proceedings of the 2006 IEEE*, pages 192–195. IEEE, 2006.

[38] A. Shahshahani, D. R. Nafchi, and Z. Zilic. Ultrasound sensors and its application in human heart rate monitoring. In *2017 IEEE International Symposium on Circuits and Systems (ISCAS)*, pages 1–4, May 2017.

[39] Amirhossein Shahshahani, Carl Laverdiere, Sharmistha Bhadra, and Zeljko Zilic. Ultrasound sensors for diaphragm motion tracking: An application in non-invasive respiratory monitoring. *Sensors*, 18(8):2617, 2018.

[40] Amirhossein Shahshahani, Zeljko Zilic, and Sharmistha Bhadra. Diaphragmatic motion tracking using ultrasound sensors for a motion independent non-invasive respiratory monitoring. *(Under review). IEEE Sensors journal*, 2019.

[41] Amirhossein Shahshahani, Zeljko Zilic, and Sharmistha Bhadra. An ultrasound based biomedical system for continuous cardiopulmonary monitoring: A single sensor for multiple information. *IEEE Transaction on Biomedical Engineering (TBME)*, 2019.

[42] Guy Shechter, Cengizhan Ozturk, Jon R Resar, and Elliot R McVeigh. Respiratory motion of the heart from free breathing coronary angiograms. *IEEE transactions on medical imaging*, 23(8):1046–1056, 2004.

[43] Thomas Lathrop Stedman et al. *Stedman's medical dictionary*. Lippincott Williams & Wilkins Philadelphia, 2000.

[44] Thitiporn Suwatanapongched, David S Gierada, Richard M Slone, Thomas K Pilgram, and Peter G Tuteur. Variation in diaphragm position and shape in adults with normal pulmonary function. *CHEST Journal*, 123(6):2019–2027, 2003.

[45] Daniel A Sweeney. Point-of-care ultrasound. *Critical Care Medicine*, 43(8):e330, 2015.

[46] Kevin T Sweeney, Damien Kearney, Tomás E Ward, Shirley Coyle, and Dermot Diamond. Employing ensemble empirical mode decomposition for artifact removal: ex-

tracting accurate respiration rates from ecg data during ambulatory activity. In *2013 35th Annual International Conference of the IEEE Engineering in Medicine and Biology Society (EMBC)*, pages 977–980. IEEE, 2013.

[47] K Song Tan, Reza Saatchi, Heather Elphick, and Derek Burke. Real-time vision based respiration monitoring system. In *Communication Systems Networks and Digital Signal Processing (CSNDSP), 2010 7th International Symposium on*, pages 770–774. IEEE, 2010.

[48] Emmanuel Vivier, Armand Mekontso Dessap, Saoussen Dimassi, Frederic Vargas, Aissam Lyazidi, Arnaud W Thille, and Laurent Brochard. Diaphragm ultrasonography to estimate the work of breathing during non-invasive ventilation. *Intensive care medicine*, 38(5):796–803, 2012.

[49] John G Webster. Medical instrumentation-application and design. *Journal of Clinical Engineering*, 3(3):306, 1978.

[50] A. Yadollahi and Z. M. K. Moussavi. A robust method for estimating respiratory flow using tracheal sounds entropy. *IEEE Transactions on Biomedical Engineering*, 53(4):662–668, April 2006.

[51] Azadeh Yadollahi, Eleni Giannouli, and Zahra Moussavi. Sleep apnea monitoring and diagnosis based on pulse oximetery and tracheal sound signals. *Medical & Biological Engineering & Computing*, 48(11):1087–1097, Nov 2010.

[52] Massimo Zambon, Paolo Beccaria, Jun Matsuno, Marco Gemma, Elena Frati, Sergio Colombo, Luca Cabrini, Giovanni Landoni, and Alberto Zangrillo. Mechanical ventilation and diaphragmatic atrophy in critically ill patients: an ultrasound study. *Critical care medicine*, 44(7):1347–1352, 2016.

[53] S Zlochiver, M Arad, MM Radai, D Barak-Shinar, H Krief, T Engelman, R Ben-Yehuda, A Adunsky, and S Abboud. A portable bio-impedance system for monitoring lung resistivity. *Medical engineering & physics*, 29(1):93–100, 2007.

Chapter 2

Fundamentals of Ultrasound and Acoustic Wave Propagation

Ultrasound is a sound wave characterized by medium velocity, particle displacement, pressure, density, and temperature. Its frequency is out of the range for human ear which is 20 Hz to 20kHz. Unlike an electromagnetic wave, it requires a medium to travel, hence it can not propagate in a vacuum. It is based on vibration of particles in the same way of the applied force. The acoustic impedance of a medium is defined as:

$$Z = \rho c = \frac{p}{u} \tag{2.1}$$

where u is the velocity of particle oscillating in the medium, c is the speed of sound in the medium (m/s), ρ the density of the medium (kg/m^3) and p is the applied compressional force on a surface per unit area and is expressed as in (N/m^2) or Pascals.

If an AC voltage is applied to a piezoelectric ceramic (piezoelectric transducer) of a certain shape, there is a specific frequency f_r at which the ceramic vibrates strongly. This frequency is called the resonant frequency and depends on the shape of the transducer. When a piezoelectric transducer is subjected to stress T, it produces dielectric displacement

Table 2.1 Acoustic Properties of Biological Tissues [10].

material	Speed (m/s)	Attenuation Coefficient (dB/cm)	Acoustic Impedance ($kg/m^2.s$ or Mrayl)
Air	343		0.0004
Aluminum	6420	0.002	17
Silver	16	5.14	-
Ultrasound Gel	-	1.6	-
Water	1480	0.002	1.48
Blood	1550	0.18	1.61
Fat	1450	0.63	1.38
Muscle	1550	1.3-3.3	1.62
Bone	3360	5.0	6.0

D which is a linear function of T:

$$D = d \;\; T \qquad (d : piezoelectric\ strain\ constant) \tag{2.2}$$

In contrary, when electric field E is applied across electrodes of piezoelectric substance, it produces distortion S being a linear function of the electric field.

$$S = d \;\; E \qquad (d : piezoelectric\ strain\ constant) \tag{2.3}$$

2.1 Properties of a piezo transducer

To clarify some basics about the ultrasound technique and fundamentals, a summary of these information is listed in the following parts.

- **Assignment of Axis**

  Figure 2.1 shows the directions are designated by 1, 2, and 3, corresponding to axes

X, Y and Z of the classical right-hand orthogonal axis set, respectively, and rotational axes as 4, 5 and 6 as well. The direction of polarization (axis 3) is established during the polling process by a strong electrical field applied between the two electrodes. Since the piezoelectric material is anisotropic, the corresponding physical quantities are described by tensors. The piezoelectric coefficients are listed accordingly.

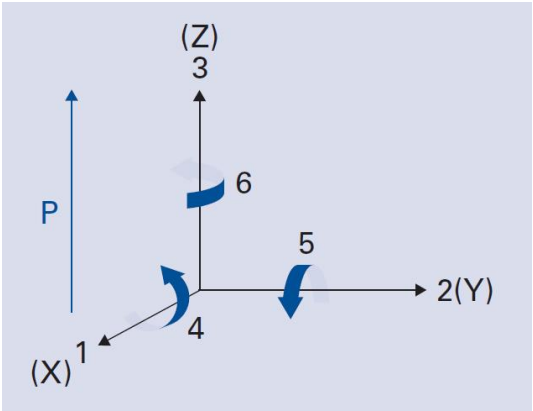

Figure 2.1 Assignment of Axis

- **Permittivity** ε: The relative permittivity, or relative dielectric coefficient, ε is the ratio of absolute permittivity of the ceramic material and the permittivity in vacuum ($\varepsilon_0 = 8.85 * 10^{-12}$ F/m).

  ε_{33}^{T} is permittivity in the direction 3 when an electric field is applied in parallel to the direction 3, under constant mechanical stress condition (T = 0).
  ε_{11}^{S} is the permittivity when electric field and dielectric displacement are in direction 1 at constant deformation (S = 0: "clamped" permittivity).

- **Piezoelectric Charge or Strain Coefficient-d_{ij}**

  It is the ratio of induced electric charge to mechanical stress or vice versa (T = constant). For instance, d_{33} is mechanical stress induced per unit of electric field applied in V/m or charge density in C/m^2 per unit pressure in N/m^2, both in direction Z or 3 which is the polarization direction.

- **Piezoelectric Voltage Coefficient -** g_{ij}

  It is the ratio of the electric field E to the effective mechanical stress T. As an example, g_{31} is the electric field induced in direction 3 per unit of mechanical stress in direction 1. In another word, stress is force per unit of area and not necessarily orthogonal.

- **Elastic Compliance** s_{ij}

  It is the ratio of the relative deformation S to the mechanical stress T. For example, s_{33}^{E} is the ratio of the mechanical strain in direction 3 to the mechanical stress in the direction 3, at zero constant electric field (E = 0 or short circuit).

- **Frequency Coefficient** N_i

  It has the relationship between the physical dimension of a body (A) and the corresponding resonance frequency (f_r):

  $(N = f_r.A)$

  The indices relates to the direction of oscillation. N_t is the coefficient for the thickness oscillation of a thin disk in the thickness mode operation and N_P is the coefficient of the planar oscillation of a round disk.

- **Mechanical Quality Factor** Q_m

  The mechanical quality factor Qm is the "sharpness of the resonance" of a piezoelectric transducer and is specified from the 3 dB band-width of the series resonance of the system. The reciprocal value of Q_m is the mechanical loss factor. The piezo transducer can be modeled by an equivalent circuit shown in Figure 2.2. So, the Q_m value could be obtained from either of the two methods from the equation 2.4. In this equation f_r is the resonant frequency, f_2 and f_1 are the two frequencies at which the amplitude

drops to –3 or –6 dB relative to the maximum

$$Q_m = \frac{1}{2\pi f_r R_1 C_1} \qquad or \qquad Q_m = \frac{f_r}{f_2 - f_1} \tag{2.4}$$

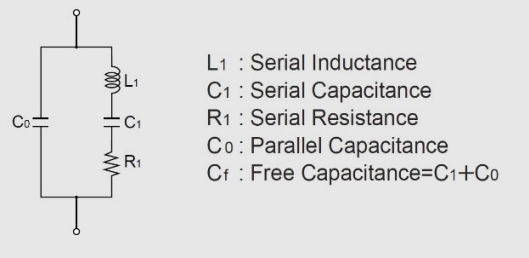

Figure 2.2 The piezo electric equivalent circuit

- **Coupling Factor k**

  This parameter shows the magnitude of the piezoelectric effect. It describes the ability of a piezoelectric material converting electrical energy into mechanical energy and vice versa. It is a determination of the square root of stored mechanical energy to the total applied electrical energy. For example:

  k_p the coupling factor for the planar radial oscillation of a round disk.

  k_t the coupling factor for the thickness oscillation of a plate.

- **Curie Temperature** T_c

  Curie temperature is the critical temperature at which crystals in the piezoelectric ceramic lose their spontaneous polarization and piezoelectric property.

- **Resolution**

  Axial Resolution: is the minimum distance that can be differentiated between two reflectors (objects or in this study, tissues) located parallel to the direction of ultrasound

beam. So, as the frequency increases, the resolution of object position tracking would be higher.

$$\theta_z = \frac{\lambda}{2} = \frac{c}{2f} \tag{2.5}$$

where c is the longitudinal speed in the medium and λ wave length in the medium. The piezo element thickness (t) is equal to:

$$t = \frac{\lambda_t}{2} = \frac{c_t}{2f} \tag{2.6}$$

c_t is the longitudinal speed in the transducer material and λ_t wave length in piezo.

2.1.1 Piezo Resonant Frequency and Vibration Modes

Vibration modes (resonant modes) of piezo ceramics depend on their shape, orientation of polarization, and the direction of the electric field. Each of these modes has unique resonant frequency and characteristics shown in Figure 2.3. In this research we utilized piezo transducers operating in the thickness mode.

2.2 Intensity of ultrasonic waves

The ultrasonic wave intensity is the average energy carried by a wave per unit area to the propagation direction over time. Since the power (P) is energy per unit time, it can be presented as the multiplication of force exerted by the pressure wave and medium displacement, divided by time. It could be said that the power is force multiplied by medium velocity density. Since the intensity, $i(t)$, is the wave power per unit area, it follows that:

$$i(t) = dP/dA = p(t)u(t) \tag{2.7}$$

where p and u are the pressure and medium velocity, respectively. In ideal case of

Vibration Mode	Shape/Vibration Mode	Resonant Frequency (fr)	Material Constant Symbol					
			k	d	g	Y^E	ε^T	N
Radial Mode	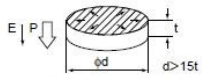 P : Direction of polarization E : Direction of electric field Thin disk with radial vibration mode. Polarization is oriented along the thickness of the disk.	$\frac{Np}{d}$	kp	d_{31}	g_{31}	Y_{11}^E	ε_{33}^T	Np
Length Mode	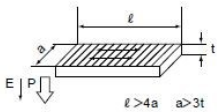 Thin rectangular plate, with the direction of vibration orthogonal to the polarization axis and with a single point of resonance.	$\frac{N_{31}}{\ell}$	k_{31}	d_{31}	g_{31}	Y_{11}^E	ε_{33}^T	N_{31}
Longitudinal Mode	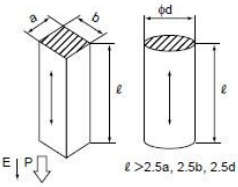 Square and cylindrical columns. Vibration is oriented along the direction of polarization. Only a single point of resonance.	$\frac{N_{33}}{\ell}$	k_{33}	d_{33}	g_{33}	Y_{33}^E	ε_{33}^T	N_{33}
Thickness Mode	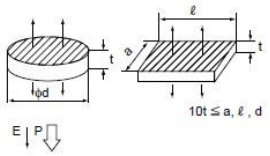 Disk and rectangular plates which are thin compared to their surface areas. They have multiple points of resonance in longitudinal vibration mode.	$\frac{Nt}{t}$	k_t	d_{33}	g_{33}	Y_{33}^E	ε_{33}^T	Nt
Shear Mode	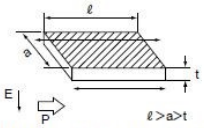 Disk or rectangular plates, with the electric field orthogonal to the direction of polarization, causing a shear vibration along the surface.	$\frac{N_{15}}{t}$	k_{15}	d_{15}	g_{15}	Y_{44}^E	ε_{11}^T	N_{15}

Figure 2.3 The piezo vibration modes [8]

sinusoidal propagation, the average intensity I, can be found by averaging the $i(t)$ for a cycle:

$$I = p_0 u_0 . \frac{1}{T} \int_0^T \sin^2 \omega t = \frac{p_0 u_0}{2} \tag{2.8}$$

where T is the period of wave, u_0 the peak pressure value and t_0 the medium velocity. By substituting the equation 2.1 to the above, we can conclude:

$$I = \frac{1}{2} \rho c u_0^2 \tag{2.9}$$

Most of the existing ultrasonic devices and the designed system for this research are based on pulsed ultrasound technique than the continues one. So, the amount of ultrasound intensity relies on some more parameters such as the pulse repetition factor (T_r) and pulse duration (τ) shown in Figure 2.4. Temporal averaged intensity, I_{TA}, is the average of generated ultrasonic wave intensities between two consecutive pulse bursts. Therefore, assuming the same amplitude and frequency of pulses applied to a transducer, the pulsed ultrasound has less energy applied to the human tissues than the continuous. There are two more parameters which refer to the physics of ultrasound waves, Spatial Peak intensity I_{SP} and Spatial Average intensity I_{SA} which is an average intensity over the ultrasound beam. The I_{SA} depends on the Beam Uniformity Ratio (BUR) which is the integral of area under the sensor, where the sound starts propagating, and reaches the 0.25 of the maximum value (or -6 dB) of I_{SP}.

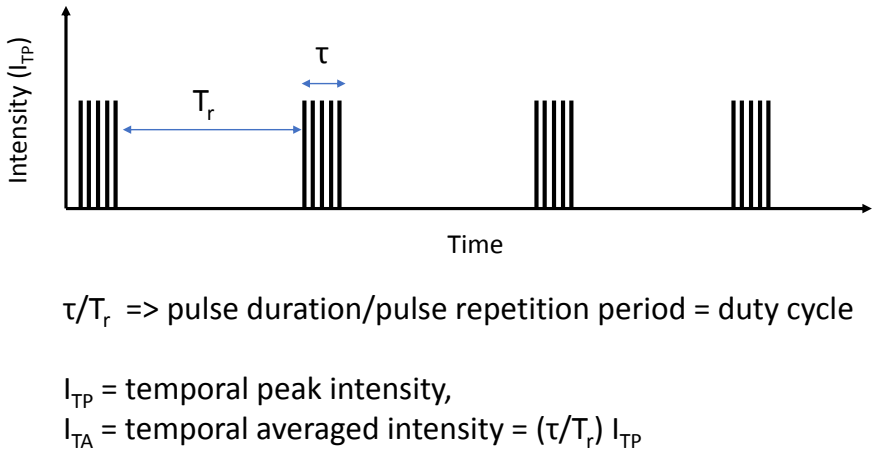

Figure 2.4 Train of pulses in time showing a temporal peak intensities I_{TP}, pulse repetition factor (T_r) and pulse duration (τ)

2.3 Biological effects of ultrasound

In biological tissues, a major portion of propagated ultrasound's energy is absorbed and converted to heat [5]. In low intensity ultrasound, the produced heat diffuses out rapidly. But in high intensities, adverse biological effects may happen if the produced temperature goes higher than 38.5 ℃[3] [11]. It may produce cavitation which can be harmful if bubble activity leads to collapsed transient cavitation events.

IEC Technical Committee 87 has provided an International Standard [7] draft named "Requirements for the declaration of the acoustic output of medical diagnostic ultrasonic equipment" which requires designers to consider and design acoustic outputs in a well-defined manner. Table 2.2 lists three maximum intensity values defined by the U.S. Food and Drug Administration (FDA)[2]. The Spatial Peak Temporal Average intensity I_{SPTA} and Spatial Peak Pulse Average intensity I_{SPPA} of an ultrasound device must be less than the acoustic intensities mentioned in this table in order to get the approval. The intensity of ultrasonic waves for our piezo transducer is calculated in Chapter 3.

Table 2.2 Recommendations for output exposure levels

Application	I_{SPTA} (mW/cm^2)	I_{SPPA} (W/cm^2)
Cardiac	720	190
Fetal Imaging & others*	430	190
Peripheral Vessel	94	190

* abdominal, Pediatric, Small Organ (breast, thyroid, testes, etc.).

2.4 Ultrasonic transducers and arrays

Piezoelectric crystals are rarely used as transducer materials in diagnostic ultrasonic imaging due to the weak piezoelectric effects. The most common is a polycrystalline ferroelectric ceramic material, lead zirconate titanate, Pb(Zr, Ti)O_3 or PZT, which have very strong piezoelectric properties. From different types of PZT transducers, PZT-5H is the most

common type used for ultrasound imaging. They work in thickness mode where the diameter (or width) is much larger than the thickness. Some characteristics of this type of piezo transducer are listed as below:

- Very high strain (charge) constants, permittivity, and coupling constants.
- Modest Curie temperature restricting its temperature range and thermal stability.
- Low mechanical quality factor.
- High charge output useful for sensing devices and generator elements.
- High strain output useful for large displacements at lower voltages.

The performance of medical diagnostic ultrasound instruments strongly relies on the properties of the transducer and it is important to have optimum sensitivity and resolution for different applications. The main issue in medical applications is the large mismatch between the piezoelectric ceramic and the load (water or tissue). Consequently, most of the energy is reflected back and forth within the rear and front faces of the ceramic, called ringing effect. Therefore, transmitted pulses into the load will be long and the axial resolution will be poor. The pulse duration affects the capability of imaging and detecting small objects and movements.

A common method to damp or lower these oscillations is to put an absorbing material to the rear face of the piezoelectric ceramic. Because most of the energy is absorbed by the backing, the transducer sensitivity is low which can be optimized by using a backing with a lower acoustical impedance. If the backing material has an impedance close to that of the ceramic, the pulse length transmitted and received will be short.

The sensitivity can be improved by a better matching layer between the sensor and the load. This can be done by using multi matching layers between the ceramic and the load

with various combinations of acoustic impedances and thicknesses. Because each layer has a different frequency band, the overall impulse response will be affected [6].

In a study [9], combinations of different matching and backing materials and thicknesses are examined. As a result, heavily backed ceramics have short pulses and broad bandwidth, while the sensitivity is low. Front matching layers on such transducers will increase the sensitivity and by carefully selecting the matching layers the pulse may be short even in this case. Also, there is not much improvement in two or more matching layers. A very broad and flat bandwidth can be achieved by a half-wave layer thickness but the shape of the echo pulse is then less satisfactory. Optimum sensitivity was obtained by front matching layers and air backing.

Various types of backing materials, such as tungsten-loaded epoxy and silver-loaded epoxy, have been used commonly with good success [11]. Different backing materials are listed in Table 2.3.

Table 2.3 Acoustic properties of matching and backing materials

layer	**Material**	**Acoutstic Impedance** (MRayl)	**Sound Velocity** (mm/ms)
Matching	Ceramic-loaded epoxy	2.8 to 11.3	1.5 to 3.9
	Glass	10.1 to 16	4.5 to 5.66
	Parylene	2.83	2.20
Backing	Tungsten-loaded epoxy	6 to 36	1.5 to 3.5
	Brass	40.6	4.7
	Carbon, pyrolytic	7.31	3.31
	Air	0.00043	0.334
Lens	RTV rubber	0.99 to 1.46	0.96 to 1.16
	Silicon rubber	1.03	1.05

The transducer's performance can also be improved by using front side acoustic matching layers. For a monochromatic plane wave, all the transmission occurs for a $\lambda_m/4$ thickness of material and acoustic impedance Z_m, where λ_m is the wavelength in the matching layer

material and Z_m can be measured from Equation 2.10 where Z_P is the acoustic impedance of piezoelectric element and Z_l the loading medium impedance. Desilets *et al* achieved a wide-band transducers by having a air-backed single matching layer of quarter-wave length [4]. The Equation 2.11 should be used for a single layer matching while for two matching layers, the impedance for two layers in Equation 2.12 should be used.

$$Z_m = (Z_P Z_l)^{1/2} \tag{2.10}$$

$$Z_m = (Z_P Z_l^2)^{1/3} \tag{2.11}$$

$$Z_{m1} = (Z_P^4 Z_l^3)^{1/3} \qquad Z_{m2} = (Z_P Z_l^6)^{1/7} \tag{2.12}$$

2.4.1 Types of Array elements

The essential element of each ultrasound transducer is a piezoelectric crystal, in order to generate and receive ultrasound waves. They differ in construction according to piezoelectric crystal arrangement, aperture (footprint) and operating frequency. Followings are most common types of transducers used in the critical ultrasound imaging shown in Figure 2.5 :

Figure 2.5 Some conventional ultrasound probes[1].

- **Linear Sequential Array**

  - Has as many as 512 piezo elements

  - Can have focused acoustic beam but not steered

  - High sensitivity

  - Field of view is limited.

- **Curvilinear (Convex) Array**

  - Similar to linear arrays, while having wider field of view.

- **Linear Phased Array**

  - Has less elements (128 elements),

  - All elements are used to transmit and receive each line of data,

  - Typical for restricted acoustic windows like cardiac imaging where the signal has to go through the ribs.

- **2D Phased Array**

  - For 3D imaging, similar to the linear Phased-Array transducers but more complex hardware and probe.

2.5 Ultrasound Sensor Design and Utilization in This Study

According to our system requirement in tracking the motion of soft tissue, we need a sensor with high sensitivity, low manufacturing cost and easy to drive with a simple circuit. So, we chose different piezo transducers based on our requirement in this research. These transducers were purchased from STEMINC company, Florida, USA.

When a transducer is excited by an electrical source, it rings at its natural resonant frequency. Transducers with air-backed, the mismatch in acoustic impedance between the air and the piezoelectric material causes the production of so-called ringing effect for pulse–echo applications. This is very undesirable because it lengthens the pulse duration. As will be

discussed later, the pulse duration affects the capability of tracking objects spaced close to the sensor.

In Chapter 3, we utilized a 1 MHz PZT4 transducer mounted on a plexiglass by a super glue. We found that the ringing effect intensity was higher than the reflected ultrasound waves from near tissues. So, in the Chapters 4 and 5 we used a kapton film as the front matching layer for a PZT-5J transducer operating at 2.2 MHz. With this transducer, not only the ringing effect is shorter, the sensitivity is higher which lessens the need to apply high voltage pulses across the transducer. The table 2.4 summarizes the properties of utilized transducers in this dissertation.

One main issue with piezo disk transducers operating at frequencies higher than 1 MHz is the transducer's electrode connectivity. One side of the sensor has to be interfaced with a matching layer with the overall thickness of $\lambda/4$ or less while having electrical connectivity to the circuit. Since the other side of sensor is covered by a backing material or left open as an air coupled backing, the connectivity in this side is not an issue. To address this requirement, we used a 125 μm thick Kapton (polyimide) film as a sensor substrate. Silver conductive traces are printed (flexible silver conductive ink) for the transducer's electrode connectivity using VOLTERA circuit printer. Kapton can be easily used as the matching layer as well as a substrate for the sensor circuit. Conductive silver epoxy is used to paste the transducer on the printed circuit. Having silver as the main component of epoxy, printed ink and transducer's electrode results in a good acoustic impedance matching between the transducer and the printed circuit layer. An advantage of impedance matching is the increased sensitivity of the transducer. To remove the air gap between the sensor and skin, placing ultrasound gel is needed. Skin, ultrasound gel and Kapton have 1.48, 1.6 and 3.16 Mrayl acoustic impedance values, respectively. A lower acoustic impedance can be reached by plastic based materials (2 to 3 Mrayl) instead of Kapton but their flexibility and conformality is less than the Kapton.

Table 2.4 Piezo Transducer Properties Used in This Dissertation

Property	Unit	Symbol	PZT-4	PZT-5J
Electromechanical coupling coefficient	—-	Kp	0.58	0.64
		Kt	0.45	0.45
Frequency constant	Hz.m	Np	2200	2060
		Nt	2070	2000
Piezoelectric constant	$*10^{-12}m/v$	d33	320	500
		d31	-140	-210
	$*10^{-3}Vm/N$	g33	25	24.2
		g31	-11.0	-10.4
Mechanical Quality Factor	—-	Qm	1800	85
Density	g/cm^3	ρ	7.9	7.8

2.5.1 Pulse Generation and Transducer Excitation

A pulsed ultrasound system contains an analog switch which in the transmit path (Tx) few differential pulses excite the transducer to generate ultrasound waves. Then the switch turns into the receive path (Rx) to amplify reflected ultrasound waves perceived by the transducer. Figure 2.6 depicts the signals from the Tx and Rx paths. Two parameters of burst counts and burst repetitions have impacts on the reading resolution. Burst counts are the number of pulses applied to the transducer. In this thesis I applied 5 differential pulses. Higher number of pulses will widen the width of reflected beams, reducing the axial resolution in detecting object movements. So. the burst duration is about µsec assuming the frequency of pulses is 1 MHz. As shown in Figure 2.6, the switch turns into Rx path at time 10 µsec. The piezo ringing effect is getting weakened by the time after this transition. Note that reflected signals due to the acoustic impedance miss-matches between the transducer and skin surface are mixed with the ringing signals within the period of 10 to 50 µsec. We have applied techniques such as short circuiting to diminish these effects, explained more in the following chapters. The same process will repeat after the burst repetition period, which is 50 times a second in the Chapter 3 and 30 in Chapter 4 and 5.

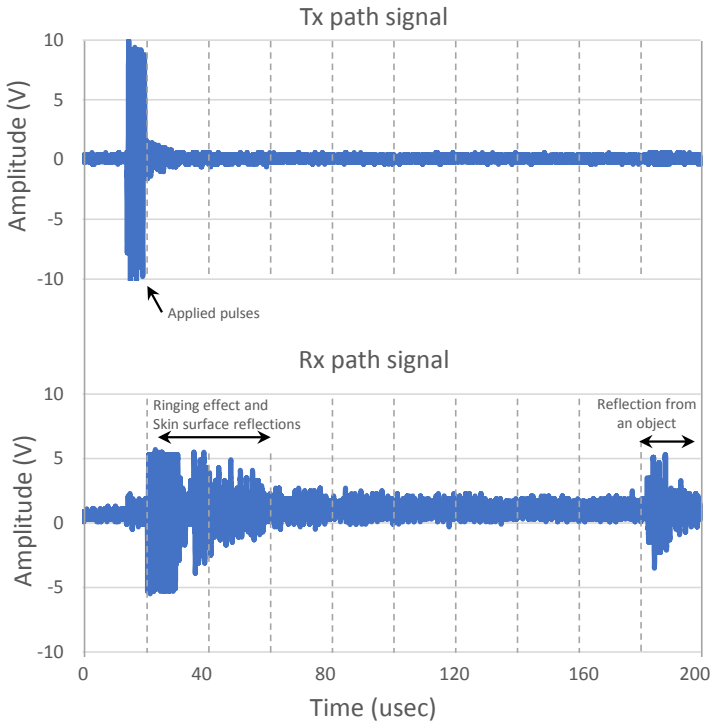

Figure 2.6 An example of transmitted (Tx) and received (Rx) signals from an object

Bibliography

[1] Ultrasound transducers. `http://www3.gehealthcare.com/en/products/categories/ultrasound/ultrasound_probes`.

[2] Information for manufacturers seeking marketing clearance of diagnostic ultrasound systems and transducers;. *U.S. Department of Health and Human Services Food and Drug Administration*, September 9, 2008.

[3] SB Barnett, GR Ter Haar, MC Ziskin, WL Nyborg, K Maeda, and J Bang. Current status of research on biophysical effects of ultrasound. *Ultrasound in medicine & biology*, 20(3):205–218, 1994.

[4] C. S. Desilets, J. D. Fraser, and G. S. Kino. The design of efficient broad-band piezoelectric transducers. *IEEE Transactions on Sonics and Ultrasonics*, 25(3):115–125, May 1978.

[5] F.J. Fry. *Ultrasound: Its Applications in Medicine and Biology*. Methods and Phenomena. Elsevier Science, 2013.

[6] G. Kossoff. The effects of backing and matching on the performance of piezoelectric ceramic transducers. *IEEE Transactions on Sonics and Ultrasonics*, 13(1):20–30, March 1966.

[7] lEC. Draft International Standard:. Requirements for the declaration of the acoustic output of medical diagnostic ultrasonic equipment. *International Electrotechnical Commission*, Document 87(CO) 11, Geneva, Switzerland,1990.

[8] muRata Co. Piezoelectric ceramic sensors. No.P19E-6.

[9] HW Persson and CH Hertz. Acoustic impedance matching of medical ultrasound transducers. *Ultrasonics*, 23(2):83–89, 1985.

[10] Roy C Preston. *Output measurements for medical ultrasound*. Springer Science & Business Media, 2012.

[11] K.K. Shung. *Diagnostic Ultrasound: Imaging and Blood Flow Measurements*. CRC Press, 2005.

Chapter 3

An Ultrasound Based Biomedical System for Continuous Cardiopulmonary Monitoring: A Single Sensor for Multiple Information

3.1 Abstract

Biomedical wearable sensors enable long-term monitoring applications and provide instantaneous diagnostic capabilities. Physiological monitoring can help in both the diagnosis and the ongoing treatment of a vast number of cardiovascular and pulmonary diseases such as hypertension, dysrhythmia, and asthma. In this paper, we present a system capable of monitoring several vital signals and physiological variables that determine the cardiopulmonary activity status. We explore direct measurements of multiple vital parameters with only one sensor and without special constraints. The system employs a PZT-4 piezo transducer stimulated by a suitable analog front-end. The system both generates pulsed ultrasound waves at 1 MHz and amplifies reflected echoes to track internal organ motions, mainly that of the heart apex. According to the respiratory motion of the heart, the proposed system

provides respiratory and heart cycles information. Promising results were obtained from six subjects with an average accuracy of 96.7% in heartbeats per minute (BPM) measurement, referenced to a commercial photoplethysmography sensor. It also exhibits 94.5% sensitivity and 94.0% specificity in respiration detection compared to an SPR-BTA spirometer signal as a reference.

3.2 Introduction

Health monitoring systems may contain many types of sensors, leading the world of Internet of Things (IoT) [6]. Non-invasive monitoring of living organs with high resolution is essential for observing physiological activity, mainly the breathing and heart rates as well as their patterns. In Chapter 1.2.1, we studied the importance of respiratory monitoring in a health care system. In addition to that, the obstructive sleep apnea (OSA) is another most common form of diseases in which breathing is interrupted by a blockage of airflow. Correct detection of OSA also requires heart rate variability analysis in addition to monitoring respiratory rate and pattern [3].

Numerous non-invasive devices for respiratory monitoring are proposed. In Chapter 1.2.1 we showed the lack of an ideal device for respiratory monitoring. As a health monitoring system, it is more advantageous if the device monitors more than one vital sign while operating under different body positions with fewer constraints on hardware resources and wiring connectivities. In this paper, we report an ultrasound-based organ motion tracking system to extract cardiopulmonary information such as respiration patterns, heart rate and its variation (HRV).

Capabilities of ultrasound systems in tracking the inner organ motions and blood flows, wall motion abnormality in heart [9] and some other information such as cardiac output measurements [5] were studied using medical ultrasound machines, such as an echocardiogram. They are expensive and can not be used as a wearable device. In this study, we focus on the

applicability of ultrasound sensor as a wearable device for health monitoring. The proposed system operates the same way as devices such as echocardiogram machine. However, this system has the potential to be utilized as a low-cost wearable device. We employed only one transducer in this study while the probe of medical ultrasound machines contains at least 50 transducers. Besides, this sensor is capable of monitoring the respiratory signal. The reported power consumption of this work is negligible compared to the existing ultrasound machines in the market.

An efficient and direct method to address the need for monitoring both heart and respiration cycles is observing the heart motions. The circumference of the normal adult rib cage expands by 3 to 5 cm during inhalation [15]. Moreover, respiratory motion of the heart on some patients in [13] and [4] shows that during inspiration, the heart moved inferiorly and underwent a craniodorsal rotation, and in few patients, they observed anterior movements as well. The amount of motions in [13] were $4.9 \pm 1.9mm$, on average for the caudally translation, and for some subjects $1.3 \pm 1.8mm$ on average for the anterior translation. On the other hand, the external intercostal muscles are most significant in respiration, having fibers that are angled obliquely downward and forward from rib to rib [7]. The contraction of these fibers raises each rib toward the rib above, with the overall effect of raising the rib cage, assisting in inhalation. Considering all motions due to the respiration, there is a possibility to extract heart and respiratory waveforms from ultrasound reflections from the heart and surrounding tissues.

In this paper, the point of interest to be tracked is the heart apex. So, we used only one sensory node consisting of a PZT-4 piezo transducer as a 1-D tracker of internal organs. We designed a mixed signal embedded system. The system operates in B-mode which plots ultrasound echoes as a function of intensity and time (depth) as an image. In this mode, the system generates ultrasound pulses discontinuously. By recording the intensity and time of flight (ToF) of reflected echoes from observing organs, the position of the organ can be

found. To determine the velocity and motion of the organ over time, the system records the amplitude and depth of specific points of reflections. The proposed system can have applications in situations where the person can not stay in front of sensors or remain immobile for a long time. On the other hand, some patients wear non-invasive ventilatory masks to help with breathing. This mask prevents the remote respiratory monitoring system from operating because the system measures the airflow of nasal or oral breathing. The proposed method can be of potential use for this situation.

A preliminary evaluation of the proposed system was done before [11]. In this chapter, the more extended data from the proposed ultrasound system at different conditions are collected. PPG sensor and spirometer as two primary and most common methods for heart and breath cycles monitoring are selected to evaluate and validate the performance of the system. It is to be noted that the data is collected for a healthy subject only to do the first-level system validation compared to the above mentioned state-of-art studies.

3.3 Physical Principles and Ultrasound Wave Generation

The sensor node is a piezo transducer mounted by epoxy on a plastic surface. The plastic surface acts as an acoustic matching layer. Only an acoustically conductive soft material, such as ultrasound gel, is needed to be rubbed on the skin surface to remove air gaps between the sensor and skin. There are many alternatives, such as water, baby oil or hand cream which have almost equal performance. So, the patient is not limited to use the ultrasound gel. The proposed system lessens the number of connected electrodes or sensors directly on the skin. Unlike ECG leads, the proposed system does not need adhesive (adhesive may cause irritations on sensitive skins, infants or injured bodies) to attach the sensor node on skin. One strap band is enough to hold the sensory head on its position and maintain constant light pressure on the sensor to the skin. Then the conductive medium enables a tight bond between the skin and the probe or transducer, letting wave transmissions directly to the

tissues underneath.

In soft tissues, about 80% of the ultrasound wave is absorbed by the tissue resulting in local heat production on cells. Attenuation coefficients and acoustic impedances of some specific tissue types and mediums [14] are listed in Table 3.1. A higher value of attenuation

Table 3.1 Acoustic Properties of Biological Tissues

Medium	Attenuation Coefficient (dB/cm)	Acoustic Impedance ($kg/m^2.s$ or rayl)$*10^6$
Water	0.002	1.48
Blood	0.18	1.61
Fat	0.63	1.38
Muscle	1.3-3.3	1.62
Bone	5.0	6.0

coefficient means more attenuated ultrasound wave passes the medium. For instance, bone with a very high attenuation coefficient hardly allows beam transmission through them. In addition, due to the high acoustic impedance mismatch between bone and tissues, there is a high-intensity beam reflection. For small upper body motions, the ultrasound waves emitted by the transducer can still pass through the rib cage bones gap while a big skin movement may results a noticeable sensor displacement, causing the ultrasound wave not to pass through the rib cage bones gap. This misplacement leads to an error in reading ultrasound reflection. Such big displacements rarely happen when the patient is not in intense motion.

In the pulsed ultrasound method, electrical pulses applied repetitively at a certain rate are called transmitted beams. In this design, the Pulse Repetition Frequency (PRF) equals 50 Hz and pulse duration $\tau \approx 5\ \mu s$ when 5 pulses are applied on piezo sensors. So, the Duty Factor $DF = \tau/PRF = 2.5 \times 10^{-4}$. Acoustic pressure and instantaneous acoustic intensity can be found from equation 3.1. Here, the $\rho.c$ is also called the acoustic impedance of the

medium.

$$I = \frac{p^2}{\rho.c} \ [W/cm^2] \qquad p = \frac{V}{M(f)} \ [P_a] \tag{3.1}$$

p = Instantaneous acoustic pressure

ρ = Density of the medium (Kg/m^3)

c = Speed of sound in the medium (m/s)

M = Sensitivity of sensor (V/P_a)

To address the safety of designed ultrasound system, intensity limits provided by the Food and Drug Administration (FDA) agency [1] should be considered. Two known intensities are measured to ensure that their level is below the limits assigned by the FDA. The system is capable to stimulate the transducer with maximum $\pm 20V$ differential pulses. When a maximum 40 V_{PP} ($\pm$20 V differential) voltage is applied on the transducer, the Spatial Peak Temporal Average intensity $I_{SPTA} = I_{SPPA} \times DF$ is equal to $15.4mW/cm^2$ where the Spatial Peak Pulse Average intensity is $I_{SPPA} = I/PD = 61.7(W/cm^2)$. PD is the pulse duration when the pulse pressure reaches 10% and 90% of its maximum value. The parameters are found smaller than the maximum intensities by FDA, being $I_{SPPA} = 190\ W/cm^2$ and $I_{SPTA} = 430\ mW/cm^2$. According to the Eq. 3.1, the ultrasound wave intensity is proportional to the applied voltage level with power of two.

Vibration (resonant) modes of piezo-ceramics depend on their shape, polarization orientation and the direction of the electric field. Each of these modes has unique resonant frequencies and characteristics. The axial resolution of ultrasound waves in a 1 MHz piezo disks, or the average accuracy of the sound waves, can be calculated as below (considering the average sound velocity in tissue $c = 1540m/s$):

Axial Resolution:

$$\theta_z = \frac{\lambda}{2} = \frac{c}{2f} = \frac{1540(m/s)}{2 * 10^6} \simeq 0.77\ mm \tag{3.2}$$

The piezo sound waves accuracy of 0.77mm suffices to measure the regular heart motions, as well as its movements due to the breathing cycles. Although piezo sensor's operation at higher frequencies improves the accuracy of the measurements, but the power consumption and system complexity increase accordingly, which is not beneficial for a round-a-clock or a wearable embedded monitoring system.

3.3.1 Pulse Generation and Observation

As discussed in the previous section, the average intensity of pulses depends on pulse repetition factor and the voltage level. Conventional medical ultrasound systems stimulate piezo sensors by high voltages (approximately 100V) to increase the wave intensity, resulting in the higher amplitude of echoes from deeper organs, while maintaining the limitations assigned by FDA. In this study, the goal is not detecting the movements of far tissues or even farther than heart left chamber. Practical experiments have shown that low energy acoustic pulses are enough to track the tissue, meaning a lower voltage pulse is sufficient to stimulate the transducer. In this study, we applied $\pm 8V$ differential pulses on transducer. Initial observations have shown that this voltage rating is sufficient for heart motion tracking. Monitoring for subjects with thicker skin and rib cage may need higher acoustic energies as the depth of penetration increases. Lowering the voltage not only decreases the intensity of pulses, which is proportional to the degree of two in Eq. 3.1, but also lessens the system power consumption. Although the change in transducer stimulation voltage from $\pm 20V$ to $\pm 8V$ results in less than 2 mA current consumption changes in this design, this amount would be considerable in a longer time power consumption. In addition, it is better to lessen the ultrasound wave intensities and inappreciable side effects on the body. However, ultrasound is known for an excellent safety record.

In ultrasound B and M Mode imaging, for every transmitted beam, there is a reflection carrying information on its frequency, phase, amplitude and the time of flight (ToF) of peaks. As the repetition factor increases, the refreshment of this information increases as well, whilst the I_{SPPA} rises proportionally which is not favorable. A trade-off between these two parameters resulted in the PRF = 50 Hz to achieve a suitable accuracy of 2% in reading every single record from reflected signals.

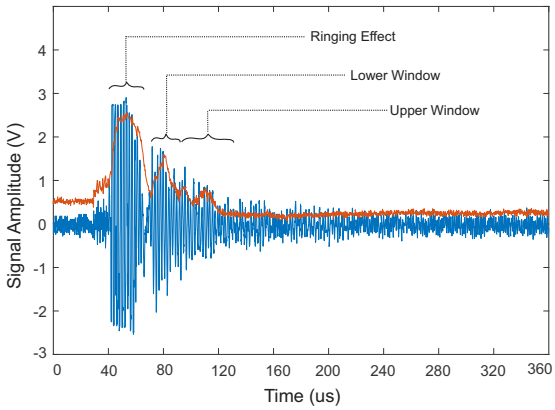

Figure 3.1 An example of amplified received (Rx) ultrasound waveform from transmitted beams (Tx) and its extracted envelop. 200 samples taken at 700 Ks/s, called a Record.

Fig. 3.1 shows an example of received waveforms when the sensor is placed on the chest. The orange wave is the envelope of echoes received. The required information lies under the peaks amplitude and their locations (ToF), explained more in Section 3.4. The biggest peaks marked on this figure are the result of sensors ringing effect. A low impedance electrical load for a short period is applied to diminish the ringing effect once the pulse generation ends.

Fig. 3.2 depicts a two minutes data recorded for a subject in rest without body movements to monitor the heart motions. This 6000 records is a series of the envelope signals, such as one shown in Fig. 3.1, recorded at every 20 ms. Results are similar to M-Mode ultrasound imaging where M stands for motion tracking over time. In this image, the two main systolic and diastolic heart cycles are evident more in the zoomed area in Fig. 3.2. The narrow yellow lines within samples 70 to 85 indicate the systolic cycles and samples 50 to 70 the

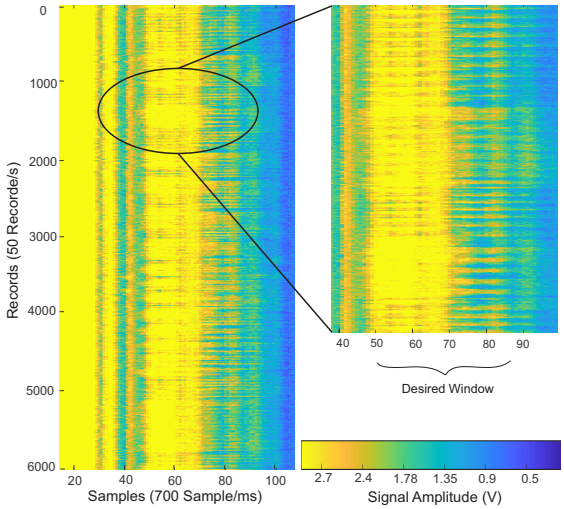

Figure 3.2 6000 records taken at every 20 ms. A data for a subject in rest with a zoomed area for better visualization.

diastolic.

3.4 System Architecture

Fig. 5.1 is the overall block diagram of the system designed and implemented to extract, monitor and record the ultrasound data and validate them with references. The ultrasound system consists of a semi high voltage stimulator and the receiver path to detect, magnify and digitize reflected echoes. The FPGA controls all blocks through digital pulses. It communicates serially to a computer for data collection and initialization. Electrical pulses are applied on a piezo transducer mounted by an epoxy on a thin hard plastic surface. The thickness of the plastic layer is chosen to be $\lambda/4$ to have the least reflections from this matching layer.

In order to increase the sense of reflections from deeper tissue levels, it is required to improve the signal to noise ratio (SNR). Increasing the amplifier gain of the receiver circuit does not improve the SNR significantly due to many noise resources such as sensor ringing effect, component and power supply noises. Moreover, it magnifies only low voltage electrical

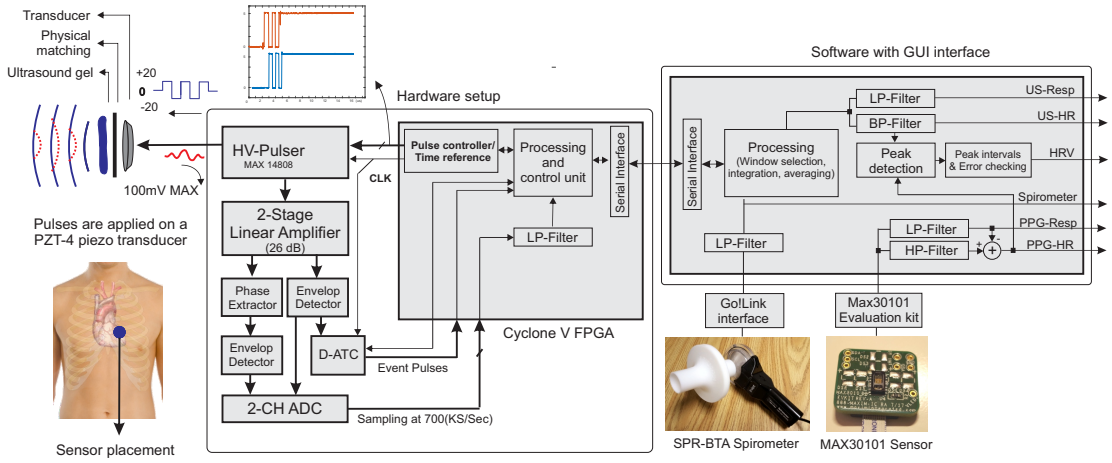

Figure 3.3 Ultrasound system designed to continuously measure and monitor heart and respiratory cycles. Spirometer and PPG sensors are used as references for ultrasound data validation.

signals from the transducer. There is a need to increase the amplitude of reflected acoustic waves. The simplest way is an increase in energy of transmitted acoustic waves, while maintaining FDA limits as discussed before, to obtain higher magnitude of reflections. Hence, a High Voltage (HV) Pulser is used to generate a differential pulses up to ± 20 volt to increase the intensity of ultrasound waves. An IC MAX-14808 performs as the front-end high voltage (HV) pulser, switch and damper in a single chip. A Cyclone V FPGA applies digital control pulses to the HV-pulser. This IC has embedded independent power supplies and level shifters that allow signal transmission without the external HV capacitors. It has integrated grass-clipping diodes to isolate the receive (Rx) path from high voltage spikes on the transmit (Tx) path. The IC operates in Three-Level mode for burst pulse generation, shown in Fig. 5.1, controlled by the two square pulses shown in this figure. It features an on-resistance 500Ω damping circuit to discharge the pulser's output internal node as soon as the transmit burst is over. Two controller signals from the FPGA control the operation into the Transmit Disable mode. In this mode, the T/R switch is ON and the sensor‘s output will be directed to the RX path while the damper is ON. The burst transmission period lasts 5 pulses, which is 5 us. In addition to the damping circuit, once the pulse generation is over, a zero voltage

will be applied on the piezo transducer, making a short circuit for less than 2 us, to decrease the impact of unwanted signals due to the sensors ringing effect.

A two-stage linear amplifier with a wide passive band-pass filter magnifies reflected ultrasound beams from undesired high and low frequency components of the signal. The magnified signal is passed to an envelope detector and a Dynamic Average Threshold Crossing (D-ATC) block[10], which helps to reduce the digital signal processing effort by finding indexes of the sampled signals where the amplitude passes a threshold value in each record [12]. It takes samples of the enveloped signal at the same frequency as the carrier signal (1 MHz), and the result of every sampled signal is a binary value. Each record stores an array of these logical values. Consecutive data of these records reveal the location of the signal amplitude's variations when a new record is compared with the latest one. This technique automates the calculation by finding the center-point of these variations to find the *desired window*. Fig. 3.2 shows an experimental dataset, where the center is sample number 70 and the amplitude of the signal in each record varies within the *desired window*, period of sample numbers 50 to 90. The *window*'s center index varies in different conditions such as body position or the thickness of chest tissues in different subjects. Based on observations, breathing impacts a negligible shift in the center point.

In shallow respirations, the peak location variations of the envelop signal are not evident due to the low axial resolution of the sensor and reflected waves. We observed that these variations are more evident in the phase of the reflections. Therefore, a phase shift comparator can relate the phase of the transmitted signals to the received echoes. This shift can be extracted by a simple analog switch. An analog multiplexer/demultiplexer with logic-level conversion, CD4053 from Texas Instruments, is used here. Logical voltage level of a square 1 MHz pulses handles the control of switch to divide its input signal (amplified received signals shown in Fig. 3.1) into two phases. Accordingly, the portion of the signal having different phase than the carrier is revealed. Due to the switch leakages, instability in the phase of

reflections, TX pulse jitters and system noise, the output is filtered by an envelop detector to filter the high frequency noises and spikes to extract the envelop of the signals are out of phase.

A 2-channel, 8-bit resolution, fast analog to digital converter (ADC) with the sampling frequency of 700Ks/s converts the two analog signals once the system switches to RX mode. For each record, 200 samples are taken from the signal, which lasts about 285 usec. This duration is the maximum time where echoes are observable in terms of the peak intensities and depth of the desired observation. It is worth noting that the energy of ultrasound waves attenuates as it moves through tissues. The amplitude decreases approximately by 1 dB per 1 MHz per 1 centimeter traveled. So, our ultrasound wave weakens by 1 dB for each centimeter of penetration.

By using the analog multiplexer as a phase extractor, the D-ATC block and envelope detector, we reduce the workload of the DSP unit. Although digital processing has other advantages, to apply the above mentioned processing and detections in digital, it requires a fast analog to digital converter with a sampling frequency of at least 2 MHz (by Nyquist sampling theorem) to reconstruct the original signal. In this case, to quantize the shift in phase in digital side with a good accuracy, the necessity for a faster than 2 Msamples/sec ADC increases. In addition, a sophisticated processing unit and ADC should be utilized to overcome the requirements for the information extraction. The data is logged and processed by MATLAB (Matrix Laboratory, USA) with a user-friendly GUI interface. The processing on ultrasound data could be done on FPGA. However, in order to make a better timing comparison between all three resources, it is done on a computer.

Fig. 3.2 shows an example of 6000 records taken at every 20 ms (120 seconds in total), while the subject starts with two breath-holds (with full inhalation and exhalation), then four slow breaths followed by eight fast breaths and ended with two other breath-hold. In this figure, the amplitude variations of each record over the time contains the information

on the heart and breathing rates. The X axis is Samples (taken at 700 KS/Sec) and Y axis is the sampling repetition or Records of 50 Records/sec. The integral of the signal or the mean value within the desired window (discussed in the last section) of each record gives a value (M_j).

$$M_j = \frac{1}{UB - LB} \sum_{i=LB}^{UB} S_{ji} \tag{3.3}$$

where j and i are the record and sample indexes respectively (on axises Y and X accordingly). The LB and UB are two lower and upper bounds of the *desired window* using data of the D-ATC block. A series of M_j values for all records produces a signal shown in Fig. 3.4A. Two low-pass and high-pass FIR filters, with cut-off frequency of approximately 0.5 Hz extract the low frequency element of the raw signal, which is the respiration trend (Fig. 3.4B), and the high frequency elements related to the heart cycles (Fig. 3.4D). High order FIR filters are used to filter because of linearity in phase which is a very important criterion for filter selection, especially for heart rate data.

3.5 Data Analysis and Experimental Results

3.5.1 Ultrasound Data Validation

Six healthy subjects with ages of 26 to 34 were asked to do the test. We applied two tests on each subject prolonged two minutes each, and the average of the two tests are reported in the table 4.1. Fig.3.4 depicts one out of two data sets of the first subject.

To validate the data obtained from ultrasound system, two references from which the breathing and heart rate can be calculated accurately are needed. Spirometers, pulse oximetry sensors (PPG) and electrocardiogram (ECG) are most known clinical and commercial references. Therefore, a SPR-BTA spirometer with GO!Link data logger is used to measure oral breathing in rest condition. A nose clip is used to prevent nasal breathing. This device

measures the amount of airflow not the volume. Accordingly, the signal level returns to zero in breath holds as shown in Fig. 3.4D.

As a real-time reference for the heart rate tracking, we used MAX30101 evaluation kit which provides a proven design to evaluate the integrated pulse-oximetry and heart rate monitoring integrated circuit of MAX30101 sensor. PPG sensor is selected as a comparative technique to the proposed ultrasound system. Some studies proposed the use of PPG sensors for respiration estimation as discussed in the Introduction.

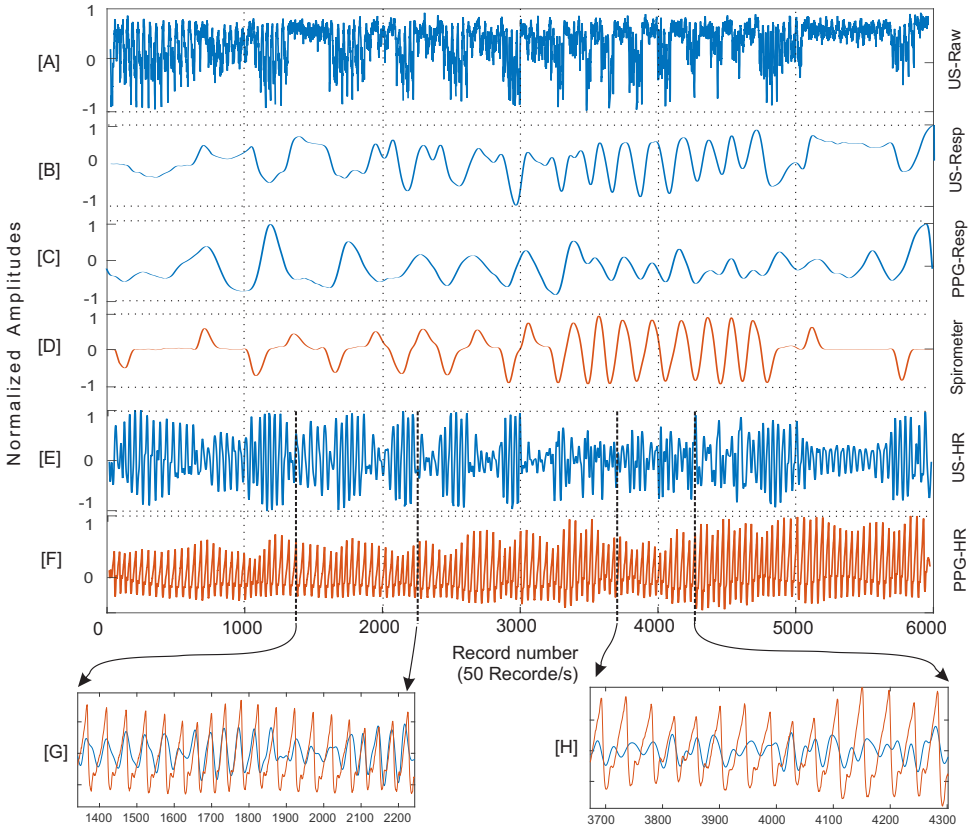

Figure 3.4 (A)Raw data resulted from a series of mean values for each record within the desired window in Fig. 3.2. (B)Low frequency component of the signal (A) shows breathing cycles. (C)low-passed signal of the PPG sensor as its respiratory waveform. (D)Spirometry signal as a reference to measure the airflow during respiration cycles. (E)High frequency component of the signal (A) represents heart rate (HR) signal. (F) Pulse oximetry heart rate signal as a reference for average heart beats and its variation (HRV) verification. (G) and (H) are zoomed area for a better representation of US-HR waveform versus PPG-HR and the impact of breathing on US-HR waveform.

3.5.2 Respiratory signal validation

In this study we used two low-pass and high-pass filters to extract the heart and respiratory cycles from the PPG sensor's data and compared its respiratory waveform with the spirometer to validate the reliability of this sensor as a respiratory monitoring.

Fig. 3.4B is the obtained ultrasound respiratory (US-Resp) waveform from the proposed system for a 2 minutes record. The first minute is a normal breathing started with two long breath-holds. It begins with a full inhalation and a full exhalation ends at 12 seconds. Note that only the first rising or falling edge of respiratory waveform for each cycle in Fig. 3.4D should be matched with Fig. 3.4B, because the spirometer is a flow-meter sensor not air volume. Moreover, the output of phase detector is added to the low frequency component of US-Resp for better sense of respiration. Except some minor delays at these edges such as around the record number 2000, the US-Resp shows a high correlation with spirometer. The second half of the waveform shows a very close agreement in deep and fast breathing with average breathing length of 3.5 second and ended with two long hold-breaths. In a study [2], they measured the diaphragmatic and cardiac motion during breath holds. They found an average velocity of 0.15 mm/sec of diaphragm at end expiration, which applies a pressure on the cardiopulmonary system. The impact of this motion is observed in the US-Resp waveform distinctly. For example, around record number 1300 in Fig. 3.4B where the subject had a full exhalation and suspension on his breath, the signal level lowers gradually, same as records around 5100.

Based on observations on 12 experiments of the 6 subjects, a weak correlation between the PPG and spirometer waveforms are found. According to the discussion on indirect methods for respiratory monitoring systems in the introduction, the PPG signal level has a late response to the breathing. In fast breathing, this response is evident when compared to a reference such as spirometer and the proposed ultrasound system, as plotted in Fig. 3.4C on records 3000 to 5000. The Fig. 3.4C is the low-pass filtered waveform of the PPG sensor's

data. It is evident in this figure that the signal contains some peaks and valleys where there is no breathing activity, such as the records 200 to 800 and 5000 to 6000.

In this study, subjects are asked to follow a similar breathing pattern as in Fig.3.4. Respiratory waveforms are statically analyzed using the following equations to find the sensitivity and specificity of the PPG and proposed sensor in reference to our gold standard.

$$Sensitivity = \frac{TP}{TP + FN} \tag{3.4}$$

In this equation, the true positive (TP) is the number of correctly detected full breathing operations and false negative (FN) is the number of breaths wrongly classified as negative. True negative (TN) means the time both the gold standard (spirometer) and the sensor do not detect any breathing.

$$Specificity = \frac{TN}{TN + FP} \tag{3.5}$$

For patients having sleep apnea, it is important to avoid false detection, which is the time the patient is suffocated but the sensor is showing a breathing operation. An example of this condition is evident in Fig. 3.4C from records 5000 to 6000. The PPG sensor shows an inhalation whilst the subject was holding his breath. Therefore, the False Positive (FP) is an important parameter in respiratory monitoring to be minimum, meaning a higher value of specificity.

3.5.3 Heart Rate validation and assessment

Fig. 3.4E shows the ultrasound heart rate waveform (US-HR) and can be compared with the reference signal in the time domain in Fig. 3.4F. The average heart rate measured by ultrasound sensor is 64.4 BPM and 68.7 BPM for PPG sensor, resulting 93.8% accuracy for

Table 3.2 A summary of experimental test results on five subjects.

Subject	Heart rate				Respiratory rate				
	US (BPM)	PPG (BPM)	Error (BPM)	Error in detecting true heart beats	Breaths (per min)	Sensitivity		Specificity	
						US	PPG	US	PPG
1	66.34	67.5	2.78%	9.10%	7.5	100%	88.20%	88.90%	84.20%
2	72.35	78	7.20%	14.20%	10	89.10%	80.30%	91.80%	83.70%
3	72.25	72.2	0.07%	9.02%	9	94.10%	84.20%	94.10%	94.40%
4	61.7	62.15	0.67%	12.70%	16	87.80%	57.50%	98.70%	82.50%
5	74.3	79.8	6.90%	18.10%	15	98.30%	38.50%	95.20%	55.20%
6	84.9	83.2	2.05%	9.03%	20	97.40%	65%	95.20%	74.50%
Average	71.9	73.8	3.30%	12.00%	12.9	94.50%	69.00%	94.00%	79.10%

the two minutes data in this figure. Two periods of these two waveforms are zoomed in Fig. 3.4H and G for better understanding of the signal shape, amplitude and phase which is discussed in details in next section.

To estimate the peak to peak time intervals of heart beats, peak extraction and zero crossings are two common techniques. In this application, the signal offset is subject to fluctuations due to reasons such as sensor displacement, body motions and scattered ultrasound waves from surrounded organs. So, peak to peak (PP) detectors performs more reliable and accurate time interval estimation. The PP time intervals of heart rate signals are extracted to validate the heart rate variability (HRV) of ultrasound system. Although the PPG sensor provides pulse rate variability (PRV), not HRV, there is a significant correlation between these two values when compared with ECG signal [8]. The heart rate signal of this sensor is shown in Fig. 3.4F.

Since the heart rate detection is based on the heart motions, any sort of external pressure to the pericardium sac can apply displacement to the heart, leading longer or shorter PP detection. Breathing is one of the known sources causing this error as shown in Fig. 3.4H where the heart rate signal has some unwanted or misaligned peaks compared to the reference which is the PPG signal. The error increases as the speed and intensity of breathing increase. Fig. 3.4G shows a very well matching compared to 3.4H. There is a minor error in detected

PP time around sample number 2070 which is a result of inhalation occurring at the same time as heart beat. Therefore, an error detector is added to the system to replace the detected PP time interval with the previous one if this time is higher than 30% of an average within past three PP intervals. On the other hand, skip a PP interval if its duration is less than 70% of the average. This error for each subject is listed in the Table 4.1.

Observations and results have shown higher error in heart beat detection and more conformal trend in respiration at faster and deeper breathing. However, a very high correlation between the ultrasound signals and references indicates that the proposed method is promising to be used in a human health tracking systems specially for real-time monitoring of breathing disorder and heart rate variation abnormality during sleep.

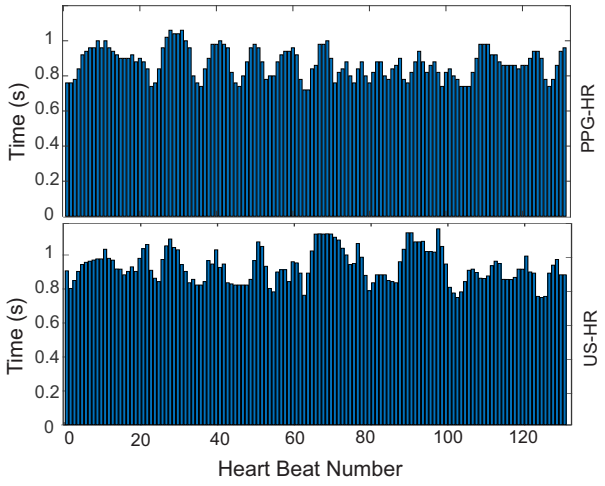

Figure 3.5 Peak to peak time intervals of Fig. 3.4E and F show heart rate variability (HRV) for ultrasound and PPG sensors visualizing 131 beats.

PP time intervals of ultrasound and PPG sensors are shown in Fig 3.5. The US-HR presents the same trend as PPG-HR except heart beats numbers 90 to 100 with a little error. This mismatch is a result of fast breathing explained before. For the whole two minutes, 131 beats are detected which matches with the average time of the whole PP intervals. In addition, the respiratory sinus arrhythmia biofeedback (RSA) is evident in Fig. 3.5 when compared to any respiratory waveforms in Fig. 3.4. The beats time intervals decreases

during inhalation, such as the inspiration at sample 1000 in Fig. 3.4B corresponds reduction in time around beats number 20 in Fig. 3.5.

Box plot of the obtained PP intervals for both PPG and US sensor for all five tests are summarized in Fig. 3.6. This figure shows the dispersion of intervals versus the mid point which is a median for each data set.

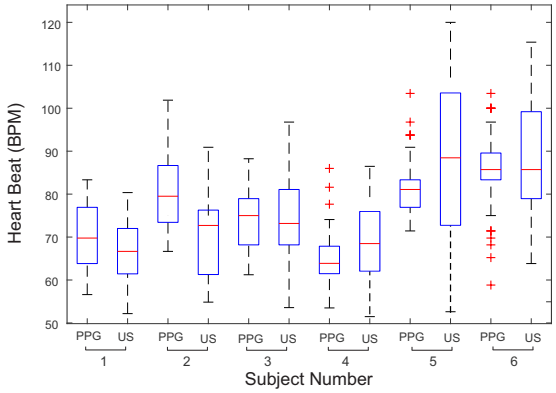

Figure 3.6 Statistical visualization of peak to peak (PP) time intervals of PPG and ultrasound (US) sensors for six subjects.

3.5.4 Hardware resources and noise analysis

The proposed system requires +3.3 voltage sources for the digital and analog integrated circuits and the differential ±5 to ±20 volts from an external DC linear power supply for the transducer stimulation. It consumes 34 mA for the digital and analog circuit. The transducer itself consumes less than 0.1 mA on different voltages. Only 393 logical blocks of a Cyclone II FPGA are used. The average SNR values for HR and RESP signals measured 2 and 3.2 dB, respectively, from the following equations:

$$P_n = \frac{1}{N} \sum_{j=1}^{N\_Records} M_j^2 \tag{3.6}$$

where M_j is the mean value in Eq.4.2 and the P_n is the power of signal when it does not contain any useful signal (the sensor is not placed on body). The same equation as 3.6 is

used to find the P_s, the power of signal+noise mixture, when the sensor is placed on the body and system is measuring heart or respiratory cycles. Finally, the SNR could be calculated by:

$$SNR = 10 \log_{10} \frac{P_s - P_n}{P_n} \tag{3.7}$$

Table 3.3 The designed hardware parameters summary

Parameter	Value	Unit
SNR(RESP)	3.25	dB
SNR(HR)	2.1	dB
Amplifier gain	20	dB
Total current	34 or less	mA
Sensor current	0.1 or less	mA
Voltage ratings	+3.3 and ±10	V
FPGA Logics	393	-

Skin motions can cause the movements of the sensor position. Large movements can induce the system failure to observe organ motions as the rib cage bones will block the ultrasound path from the transducer to the organ. However, the proposed system would not generate false positive detections even if the rib cage bones block the ultrasound path. An array of three to five sensors seating next to each other would help for better motion detection. Assuming a 0.5 to 1 centimeter space between each sensor guarantees that at least one transducer will observe motions, even if others are blocked by rib cages. As explained before about the desired window, our system looks into motions observed within this period of time. Any other noise, such as skin surface reflection, ringing effect and acoustic mismatch have the most amplitude on the signal within the period of 0 to 40 samples in Fig. 2, and least amplitude after the 40 samples which is our desired period. Therefore, the proposed system would be less affected by these other sources of noise.

Acknowledgment

This research was funded by McGill university [G130100 Start Up Fund Electrical and Computer Engineering] and Natural Sciences and Engineering Research Council of Canada [G245366 NSERC RGPIN-2018-05176].

3.6 Discussion and Conclusion

In this study, a novel approach for long-term monitoring of heart and respiratory as the two main vital signs was proposed. The aim was to design a multi-parameter monitoring system based on only one sensory node element and less wiring connectivity to the body. Derived waveforms from ultrasound signals carried two main information, higher frequency impulses resulted from the heart motions and lower frequencies of the signal due to the small respiratory motions of the heart and surrounded tissues. More investigation on the data revealed information correlated to the biofeedback of the cardiopulmonary systems, such as HRV, RSA and cardiac motion during suspended breathing due to the diaphragmatic pressures. Two clinical and commercial conventional methods for heart and respiratory monitoring systems are used to assess and validate the data obtained through the ultrasound system. The average accuracy of 96.7% is obtained for the heart beats per minute (BPM) measurements in reference to the PPG sensor for 6 healthy subjects. The respiratory waveform is also in good agreement with the waveform obtained from spirometer as a reference, having sensitivity and specificity of 94.5% and 94.0%, respectively.

The system lacks a good acoustic and electrical impedance matching. Improvements in this area can lead to a better SNR value and diminish the ringing effects. Our focus in further studies will be a comprehensive human test for validation of different subjects and body positions.

In addition, we observed that the derived respiratory waveform from this method is

sensitive to body motions or sensor displacements. The system-generated signal due to the impact of body or sensor motions could resemble as a respiratory signal if the frequency of motions is within the range of expected breathing rate. So, the system is more subject to false alarm production due to the motion artifacts. Another negligible drawback of the proposed technique in measuring the heart rate is the time the heartbeat occurs at the same time as the inhalation or exhalation. In this situation, one heartbeat could be masked since the amount of respiratory motion sensed from the heart is higher than a heartbeat. However, this problem could be resolved simply by applying the Doppler technique by finding the frequency shifts between the transmitted and received ultrasound waves. Apart from the problems mentioned above, there are many doors open to advance this sensor to obtain extra features such as cardiac output, all in one sensor. In the case of sensor displacement, there is a possibility of ultrasound wave blockage by rib bones. In this situation, the heart motions will not be sensed. We also found the respiratory signal susceptible to body motion artifact. So, instead of monitoring the respiratory motion of heart which is caused by diaphragm motions, we decided to monitor the motion of the diaphragm directly. Next chapter will discuss this new method for respiratory monitoring which provides a clear respiratory signal that is more independent of troublesome motion artifacts.

I also found that the 1 MHz PZT-4 piezo transducer has a longer period of ringing effect and is less sensitive to ultrasound wave reflections than a 2.2 MHz PZT-5 transducer used in the next two chapters. In addition, this higher frequency transducer will provide a finer and adequate axial resolution. Since the final goal is the development of a wearable device, power consumption is a key point must be taken into account. Although the higher frequency of transducer would provide better accuracy, the power consumption increases due to the faster switching of components such as the high voltage pulse.

Bibliography

[1] Food, Drug Administration, et al. Guidance for industry and fda staff information for manufacturers seeking marketing clearance of diagnostic ultrasound systems and transducers. *Silver Spring: US FDA*, 2008.

[2] Agnes E Holland, James W Goldfarb, and Robert R Edelman. Diaphragmatic and cardiac motion during suspended breathing: preliminary experience and implications for breath-hold mr imaging. *Radiology*, 209(2):483–489, 1998.

[3] María J Lado, Xosé A Vila, Leandro Rodríguez-Liñares, Arturo J Méndez, David N Olivieri, and Paulo Félix. Detecting sleep apnea by heart rate variability analysis: assessing the validity of databases and algorithms. *Journal of medical systems*, 35(4):473–481, 2011.

[4] Kate McLeish, Derek LG Hill, David Atkinson, Jane M Blackall, and Reza Razavi. A study of the motion and deformation of the heart due to respiration. *IEEE transactions on medical imaging*, 21(9):1142–1150, 2002.

[5] Yatin Mehta and Dheeraj Arora. Newer methods of cardiac output monitoring. *World journal of cardiology*, 6(9):1022, 2014.

[6] Shyamal Patel, Hyung Park, Paolo Bonato, Leighton Chan, and Mary Rodgers. A review of wearable sensors and systems with application in rehabilitation. *Journal of neuroengineering and rehabilitation*, 9(1):21, 2012.

[7] Peter S Rahko. Evaluation of the skin-to-heart distance in the standing adult by two-dimensional echocardiography. *Journal of the American Society of Echocardiography*, 21(6):761–764, 2008.

[8] Rainer-Dieter Bauer Martin Radespiel-Troger Michael Mueck-Weymann Robert Rauh, Robert Limley. Comparison of heart rate variability and pulse rate variability detected with photoplethysmography. *Proc.SPIE*, 5474:5474 – 5474 – 12, 2004.

[9] Zahra Alizadeh Sani, Ahmad Shalbaf, Hamid Behnam, and Reza Shalbaf. Automatic computation of left ventricular volume changes over a cardiac cycle from echocardiography images by nonlinear dimensionality reduction. *Journal of digital imaging*, 28(1):91–98, 2015.

[10] A. Shahshahani, D. R. Nafchi, and Z. Zilic. Ultrasound sensors and its application in human heart rate monitoring. In *2017 IEEE International Symposium on Circuits and Systems (ISCAS)*, pages 1–4, May 2017.

[11] Amirhossein Shahshahani, Sharmistha Bhadra, and Zeljko Zilic. A continuous respiratory monitoring system using ultrasound piezo transducer. In *Circuits and Systems (ISCAS), 2018 IEEE International Symposium on*, pages 1–4. IEEE, 2018.

[12] Amirhossein Shahshahani, Masoud Shahshahani, Paolo Motto Ros, Alberto Bonanno, Marco Crepaldi, Maurizio Martina, Danilo Demarchi, and Guido Masera. An all-digital spike-based ultra-low-power IR-UWB dynamic average threshold crossing scheme for muscle force wireless transmission. In *Proceedings of the 2015 Design, Automation & Test in Europe Conference & Exhibition*, pages 1479–1484. EDA Consortium, 2015.

[13] Guy Shechter, Cengizhan Ozturk, Jon R Resar, and Elliot R McVeigh. Respiratory motion of the heart from free breathing coronary angiograms. *IEEE transactions on medical imaging*, 23(8):1046–1056, 2004.

[14] K.K. Shung. *Diagnostic Ultrasound: Imaging and Blood Flow Measurements*. Wiley, 1998.

[15] Thitiporn Suwatanapongched, David S Gierada, Richard M Slone, Thomas K Pilgram, and Peter G Tuteur. Variation in diaphragm position and shape in adults with normal pulmonary function. *CHEST Journal*, 123(6):2019–2027, 2003.

Chapter 4

Ultrasound Sensors for Diaphragm Motion Tracking: An Application In Non-invasive Respiratory Monitoring

4.1 Abstract

This paper introduces a novel respiratory detection system based on diaphragm wall motion tracking using an embedded ultrasound sensory system. We assess the utility and accuracy of this method in evaluating the function of the diaphragm and its contribution to respiratory workload. The developed system is able to monitor the diaphragm wall activity when the sensor is placed in the zone of apposition (ZOA). This system allows for direct measurements with only one ultrasound PZT5 piezo transducer. The system generates pulsed ultrasound waves at 2.2 MHz and amplifies reflected echoes. An added benefit of this system is that due to its design the respiratory signal is less subject to motion artifact. Promising results were obtained from six subjects performing six tests per subject with an average respiration detection sensitivity and specificity of 84% and 93% respectively. Measurements were compared to a gold standard, SPR-BTA commercial spirometer. In this study, we also compared our measurements to other conventional methods such as inertial and photoplethysmography (PPG) sensors.

4.2 Introduction

Wearable devices providing non-invasive high resolution monitoring of living organs are essential in the hospital settings for observing physiological activity, mainly breathing and heart rate [25]. In the intensive care unit (ICU), almost all physiological parameters are measured and monitored, but the assessment of respiratory is lacking [22]. Normal function of the diaphragm is critical for effective ventilation during sleep in normal subjects [12]. Monitoring of respiratory activity is needed to detect respiratory disorders, such as the sleep apnea [11], cessation of breathing in infants [8] or dyspnea. Dyspnea relates to patients having difficulty breathing, whereas apnea refers to the cessation of airflow during sleep preventing air from entering the lungs. Besides the respiratory rate, depth and patterns are important [24]. Central sleep apnea (CSA) is another form of respiratory disease in which the brain temporarily fails to signal the muscles responsible for controlling respiration [10].

Numerous non-invasive devices for respiration monitoring have been proposed. Appropriate use of current monitoring systems and correct assessment of the provided data are essential in accurate diagnosis. Many of the previously mentioned conventional techniques for RR monitoring are impractical in real life conditions such as the patient being physically active or fully dressed. In a wearable health monitoring system, it is advantageous if the device monitors while operating under different body positions, with fewer constraints on hardware resources and wiring connectivities. In this paper, we report an ultrasound-based diaphragm motion tracking system to obtain a respiratory signal.

In an earlier study in Chapter 3, the ultrasound system based on motion tracking of the heart was employed to monitor heart and respiration rates [20] [21]. The PZT4 piezo transducer was placed on the chest in front of the heart. In this work, the sensor is placed in the zone of apposition (ZOA) to observe only the diaphragm motions. Therefore, the system is less sensitive to upper body motion and sensor displacement than the previous work. In addition, the obtained signals of this system from six subjects are validated against

a reference. The system uses one sensor, consisting of a PZT-5 piezo disk transducer as a 1-D tracker of the diaphragm. A mixed-signal embedded system designed to operate in B-mode which generates ultrasound pulses discontinuously and records ultrasound echoes as a function of intensity and time (depth). By recording the intensity and time of flight (ToF) of reflected echoes from observed organs, the position of the organ can be found. To determine the velocity and motion of the organ over time, the system averages the amplitude and depth of a specific period of reflections. This mode is called M-mode and is an analogous to recording a video of ultrasound images (B-Mode) focused on a specific area of images. This technique is widely used in ultrasound imaging for real-time measurements of heart rate and wall thickness [7]. In this paper, the data from the proposed ultrasound system is evaluated and validated against a spirometer as a gold standard and compared to the PPG and inertial sensors as two other methods. Results indicate the superiority of our ultrasound sensor in comparison to the inertial and PPG methods under different human body motion conditions. The data set is collected on subjects having no specific illness to do a system validation and performance evaluation.

4.3 Methods and Principles

4.3.1 Basics of ultrasound and sensor description

As mentioned before, the proposed system is based on ultrasound technique. Vibration (resonant) modes of piezo-ceramic transducers depend on their shape, polarization, orientation and the direction of the electric field. The transducer used in the sensor is a 2.2 MHz PZT5 piezo disk operating in thickness mode. One main issue in piezo disk transducers operating at frequencies higher than 1 MHz is the transducer's electrode connectivity. One side of the sensor has to be interfaced with an acoustic matching layer, with the overall thickness of $\lambda/4$ [23], while having an electrical conductivity to the circuit. λ is the acoustic wavelength

in the propagation medium. Since the other side of the sensor is covered by a backing layer or left open as an air-coupled backing, the connectivity of this side is not a problem. Hence, the piezo transducer is mounted by a silver epoxy on a Kapton (polyimide) film, 125 μm thickness. We printed a silver conductive pad (flexible silver conductive ink) on this film using VOLTERA circuit printer to connect the transducer's electrode to the rest of the sensor circuit. The printed substrate and finalized design is shown in Fig. 4.1. Having silver as the main component of this epoxy, printed ink and transducer's electrode result in a good acoustic impedance matching between the transducer and the printed circuit layer. Acoustic impedances and attenuation coefficients of some specific mediums and soft tissues were listed in Table 3.1.

The acoustic axial resolution of the sensor can be calculated as below by considering the average sound velocity of tissue as $c = 1540m/s$ and $f = 2.2MHz$ used in this study:

Axial Resolution:

$$\theta_z = \frac{\lambda}{2} = \frac{c}{2f} = \frac{1540(m/s)}{2 * 2.2 * 10^6} \simeq 0.35\ mm \tag{4.1}$$

K. M. Langen *et al.* [13] summarized the evaluation of the studies on diaphragm motion. The average peak-to-trough (PTT) diaphragm movement measured 13 mm in normal breathing and 39 mm during deep breathing. Hence, the axial resolution of 0.35mm should provide an adequate accuracy to measure the internal organ motion.

The selected piezo ceramic disc transducer has 15 mm diameter, which is wide enough to sense reflections within the two rib bones. *Ringing effect* is one of the issues to consider when designing an ultrasound system. In the previous work [20] [19], the transducer was operating at 1 MHz and the piezo ringing effect period masked reflected signals from near objects. Choosing higher frequency piezo transducers not only helps to shorten the ringing effect, it also improves the axial resolution. It is worth noting that the energy of ultrasound waves attenuates as they move through tissues. The amplitude decreases approximately by

1 dB per 1 MHz per 1 centimeter traveled [23]. So, the need to amplify more the reflected signals increases the power consumption of the circuit. Moreover, the system consumes more power in faster switching of components. Therefore, the 2.2 MHz piezo transducer from STEMINC is selected which optimizes our need for ringing effect, distance to observe objects (the diaphragm wall) and our need for power consumption.

4.3.2 Sensor Position

In this study, the goal is to investigate the motion of the diaphragm, thus the sensor was positioned on the zone of apposition (ZOA). The ZOA is the area of the diaphragm encompassing the cylindrical portion (the part of the muscle shaped like a dome/umbrella) which corresponds to the portion directly apposed to the inner aspect of the lower rib cage [5]. The piezo sensor is placed on the right side of the body, as it is easier to see the diaphragm through the liver window [17]. Following methods described in the literature [28],[14],[26],[27], the sensor was placed between ribs 8^{th} and 9^{th} at the mid-axillary line (Fig. 4.1). Having the sensor positioned in this zone will enable it to see both contraction and relaxation of the diaphragm. The diaphragm is an hyperechoic structure, which means that ultrasound can be reflected and measured [17]. Although the diaphragm is deeper than the thoracic rib cage, its motion can be seen by ultrasound from the intercostal space.

4.3.3 Study Protocol

As discussed, we are monitoring the internal organ motion, mainly the diaphragm wall. Our goal is the evaluation of the proposed system on subjects in different body motion and position conditions. Four practical tests were done in a resting state to ensure an accurate assessment versus the gold standard. Moreover, two additional tests were applied when the subject had upper body motion to examine the system under motion artifact. All tests were done in a sitting position. Tests are detailed as follows:

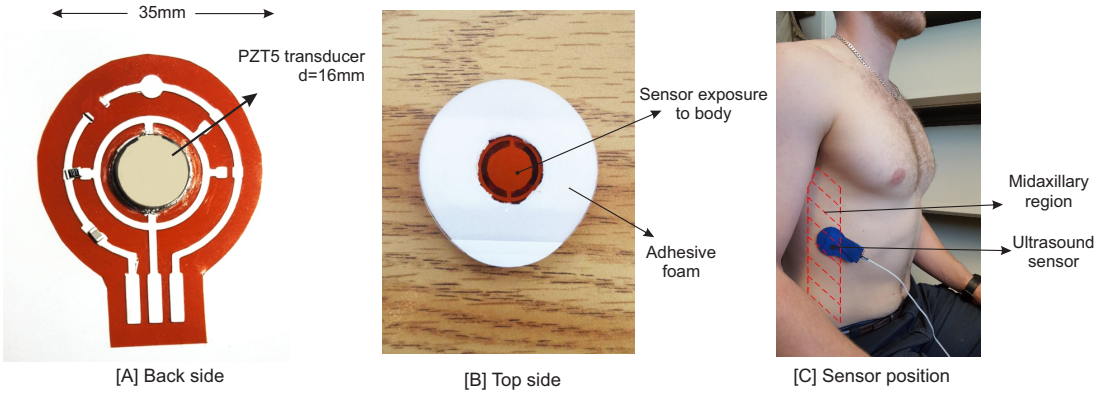

Figure 4.1 (A) The PZT5 piezo transducer mounted on a flexible printed PCB circuit. (B) The top side of sensor. A two-sided adhesive pad is used to hold the sensor on the body. The middle round area is filled by ultrasound gel. (C) Sensor position in the zone of apposition (ZOA). The sensor on back side is covered by a blue tape.

- Test-T1, Normal breathing: In this test the subject was asked to disregard the apparatus and breath normally.

- Test-T2, Normal breathing with two breath holds: In this test the subject starts with two or three normal breaths and then a long inhalation followed by a long exhalation. This test is done to evaluate the system on breath holds, or when the subject is in suffocation.

- Test-T3, Fast breathing: In this test, the subject breaths fast (between 25 and 40 breathing cycles per minute) to simulate breathing after an exercise.

- Test-T4, Normal and weak breathing: This test is to evaluate the capacity of the apparatus to detect small and slow breathing. The subject is asked to be at rest and breaths gently.

- Test-T5, Normal breathing with hand elevation: This test is intended to evaluate the skin movements when a subject abducts the arm up to shoulder and then completely up. As mentioned before, if the sensor is placed in front of a bone, then the measurements

are impossible due to the ultrasound wave blockage.

- Test-T6, Breathing with upper body motion and rotation: In this test the subject is asked to move his/her upper body randomly in all directions. This is to evaluate the ability of the apparatus when upper body motion is occurring.

4.3.4 Ethics Approval

All participants gave their informed consent which was approved by the appropriate ethics committee (Research Ethics Board II Office, McGill University, approval number 252-1117). There are no known risks associated with the experiments asked to be performed on the subjects. In some cases, it caused dry mouth which was eliminated by providing enough time interval between each breathing patterns and drinking water. Moreover, Ultrasound has been shown on many occasions to be safe when the acoustic waves are under thresholds [6]. In a study, a similar sensor was evaluated to prove the amount of ultrasound wave intensities being less than the threshold values [19].

4.3.5 Validation process

To validate the data obtained from the ultrasound system, a gold standard was required as a reference. Spirometer and plethysmography based devices are the most common clinical and commercial references. We used an SPR-BTA spirometer with GO!Link data logger software to measure oral breathing in sitting condition. A nose clip is used to prevent nasal breathing. This device measures the amount of airflow but not the volume. Accordingly, the signal level returns to zero in breath holds. Since the proposed measurement method is based on the volume of air the subject inhales or exhales, trapezoidal numerical integration is used to compute the approximate integral of the signal.

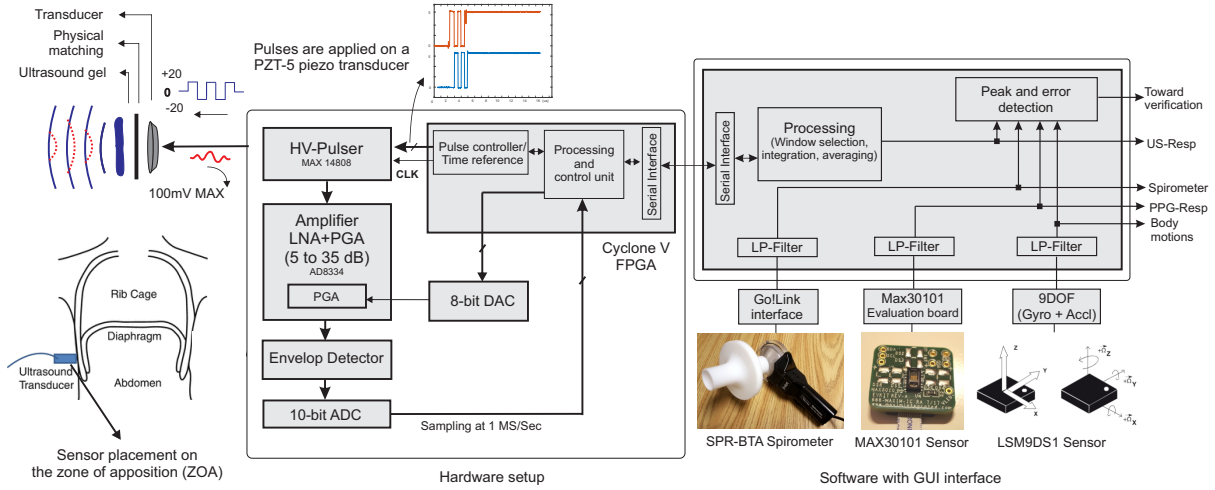

Figure 4.2 Ultrasound system designed to continuously measure and monitor respiratory cycles. Spirometer is used as a reference for ultrasound data validation, and compared with PPG and inertial sensors.

4.4 System Architecture

Fig. 5.1 shows the block diagram of the system designed and implemented to extract, record and monitor the ultrasound data, and validate it against the references. The digital and analog subsystems are employed; the analog sub-system has two main paths: a transmitter (TX) and a receiver (RX). A commercial IC MAX-14808 is deployed as the front-end high voltage (HV) pulser, switch and damper in a single chip. It hence acts as the transmitter and path separator. Also, this IC is a High Voltage (HV) Pulser used to generate a differential pulses up to ± 20 volt to increase the intensity of ultrasound waves. We employ the pulser in three main operation modes, controlled by two signals. First, the differential HV pulses are applied to the transducer and after 5 to 10 pulses, the voltage returns to zero and then the damper turns on for a short time to diminish the ringing effect and possibly stored high voltage charges. In the third step, once the internal switch is connected to the RX path, the receiver circuit amplifies the low voltage reflections from sensor.

A two-stage linear amplifier with a wide passive band-pass filter magnifies reflected ultrasound beams from undesired high and low frequency components of the signal. The

magnified signal is passed to an envelope detector which helps to reduce the digital signal processing work. According to the acoustic wave attenuation ratio of 1 dB per 1 MHz per 1 centimeter traveled in the tissue, our ultrasound wave weakens by 2.2 dB for each centimeter of tissue penetration. To increase the sense of reflections from deeper tissues, the gain of amplifier should increases linearly with the same ratio as the ultrasound waves attenuate. For this purpose, an analog front end (AFE) designed with an integrated low noise amplifier (LNA) followed by a variable gain amplifier (VGA). The gain is controlled by an analog voltage generated by a 10-bit digital to analog converter (DAC). Once the switch turns to RX path, the gain starts increasing from 10 to almost 30dB within 200 us. The gain is controlled by the FPGA immediately after the switch transition. So, there is no mismatch in time to generate asynchronous amplified signals. This time is chosen as it is the maximum period during which we expect to have the reflections. Finally, since the information of each echo is carried on the amplitude and flying time of reflections, the envelope of the signal is extracted. The envelope can be produced in an analog circuit with a simple rectifier and low pass filter or using Hilbert transform with the digitized values. The Hilbert transform method exhibits better performance, as it detects the true amplitude of the analytic signal. However, the analog subsystem will reduce the required ADC clock and processing units dramatically since the carrier frequency is removed.

To digitize the enveloped signal, we used a 10-bit resolution analog to digital converter (ADC) with the sampling frequency of 1Ms/s. It converts the analog signal once the system switches to RX mode for 200 samples (lasting 200 us).

A Cyclone V FPGA programmable logic device is programmed to control all blocks through digital pulses. The data is logged and processed by MATLAB (Matrix Laboratory, USA) with a user-friendly GUI interface. The processing on ultrasound data can be done completely on the FPGA. However, to make a better timing comparison between all three resources, the processing is done on the computer for the purpose of our experiments.

The hardware setup of the proposed system architecture is shown in Fig 4.3. The proposed system requires +3.3 voltage sources for the digital and analog integrated circuits and the differential ±5 to ±20 volts from an external DC linear power supply for the transducer stimulation. It consumes 34 mA for the digital and analog circuit. The transducer itself consumes less than 0.1 mA on different voltages. Only 393 logical blocks of a Cyclone II FPGA are used. Note that the hardware is built using an off-the-shelf 4-channel transceiver integrated circuit (IC). The same hardware will allow further analysis on multi-sensor or different transducer configurations, as discussed in Section 4.6.

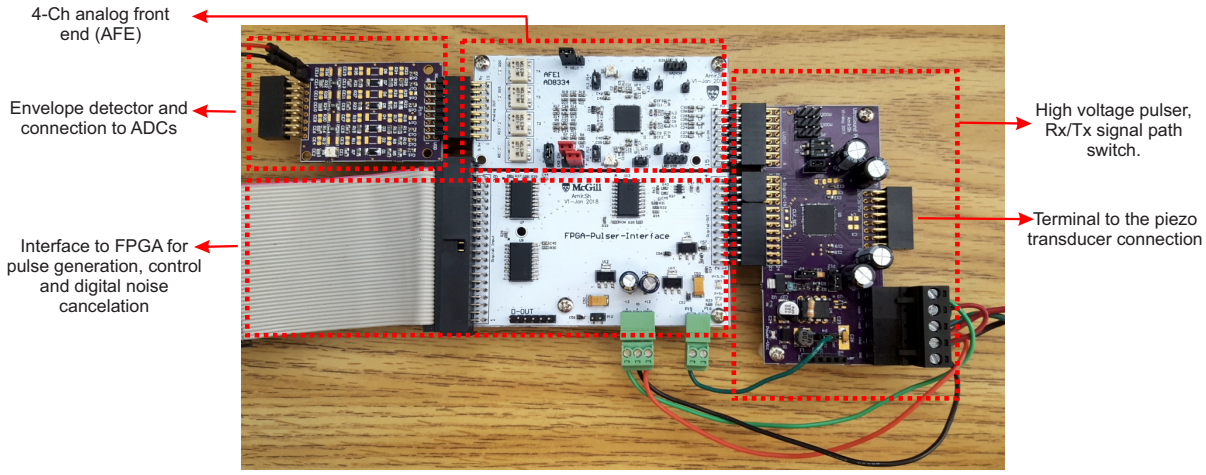

Figure 4.3 The designed 4-channel ultrasound system hardware setup consists of high voltage pulser, analog front end (AFE), envelop detector and ADC. It is interfaced to a Cyclone V FPGA board as a controller and data logger to the computer.

4.4.1 Pulse Generation and Observation

The average intensity of acoustic waves depends on pulse repetition factor and the voltage level. As the voltage applied on the transducer increases, the intensity of acoustic waves increases as well. And, as the repetition factor increases, the refreshment of this information increases as well. In this study, we are planning to measure the near tissue movements,

meaning low energy acoustic pulses are sufficient to stimulate the transducer. In this study, we examined our system by pulses on differential voltages from $\pm 5V$ to $\pm 20V$ applied on the transducer. Observations and measurements have shown that even ± 5 voltage rating is sufficient for the diaphragm motion tracking. Monitoring of subjects with thicker skin, fat and rib cage may require higher acoustic energies as the depth of penetration increases. Operation in lower voltages also consumes less energy and applies weaker ultrasound wave intensities, which might have the inappreciable side-effects on the body. However, ultrasound is known for its excellent safety record.

Fig. 4.4 shows an example of received waveforms when the sensor is placed on the ZOA. The blue and orange waveforms in Fig. 4.4.A are two examples of the envelope of echoed signals received in inhalation and exhalation, respectively. The required information lies under the peaks amplitude and their locations (ToF). The largest peaks marked on this figure at times less than about 20 us are a result of sensor's ringing effect and reflections from unmatched surfaces, from sensor to skin surfaces.

Fig. 4.4.B depicts a one minute of *Records* for a subject in rest without body movements to monitor the diaphragm wall motions. This 3000 records is a series of the envelope signals, such as one shown in Fig. 4.4.B, recorded at every 20 ms. Results are similar to M-Mode ultrasound imaging where M stands for motion tracking over time.

In this test, the subject started with three normal breathing. After that, two breath-holds (with full inhalation and exhalation), followed by normal breathing cycles continued to the end. In this figure, the amplitude variation of each record contains the respiration information. Since these peaks are results of internal organ motion, rather than external motion or skin surface, the obtained information is shown to be robust to the human motion. Additionally, the monitoring is based on a direct measurement of a physiological human activity, and not by an indirect method. To obtain the respiratory waveform, the integral of the signal or the mean value within the *desired window* of each record gives a value (M_j).

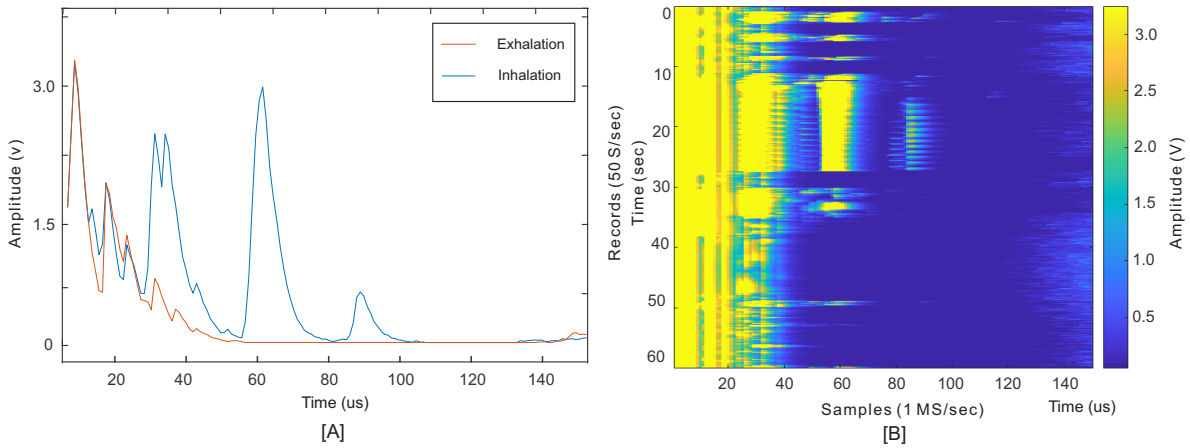

Figure 4.4 (A)An example of obtained signal sampled at 1 Ms/sec at the end of each inhalation and exhalation, each called a *Record*. (B) A one minute of *Records* taken at 50 Hz depicts the breathing cycles.

This is the period of time the ultrasound waves are reflected from the diaphragm. Reflections before this period are results of motion artifact, sensor ringing effect and small spikes from the internal switch when it turns into RX mode. For this study, the period is set from the time 22 to 100 us, so (M_j) can be found at:

$$M_j = \frac{1}{UB - LB} \sum_{i=LB}^{UB} S_{ji} \tag{4.2}$$

where j and i are the *record* and *sample* indexes, respectively (on axes Y and X). The LB and UB are the lower and upper bounds of the *desired window*, as explained above. A series of M_j values for all records produces a signal shown in Fig. 4.5 as US (ultrasound).

4.4.2 Data analysis and peak detection

A low-pass FIR filter is used to emit high frequency elements of the raw US signal, which is higher than 1 Hz. Same filters are used to apply on signals from the spirometer, the PPG and motion sensors. FIR filters of the same order (order 12) are used for filtering to ensure linearity in phase of filtered data which is an important criterion for filter selection, especially

for validation procedure. Since the respiration operation mainly changes the baseline of the PPG sensors data [3][4][15], the same technique utilized in this article. We applied a band-pass filter to extract the respiratory frequency from the raw PPG signal and eliminate the extremely low frequency or DC component of the signal. The respiratory signal is a non-stationary signal and all sensors data are processed in the time domain. A windowing percentile analysis [16] on all low-pass filtered sensor signals to detect positive peaks. Thus, a logical output for each signal was generated containing the logic '1' when the signal level passed the percentile threshold value and '0' when the signal was below the threshold. The logical waveforms showing the presence of each detected inhalation and exhalation in all signals are utilized in the statistical evaluations in Table 4.1. The percentile value is adaptive to the mean value of the signal in current and past windows.

4.5 Results

For all the listed tests, the inertial sensor was placed on the ultrasound sensor to monitor the body motion and motions due to the breathing. This sensor provides 3 axis accelerometer and gyroscope data at the same rate as ultrasound. We used MAX30101 multi-sensory board, which provides a proven design to evaluate the integrated pulse-oximetry and heart rate monitoring. PPG sensor is selected as a comparative technique to the proposed ultrasound system. Some studies proposed the use of PPG sensors for respiration estimation as discussed in the Introduction. But, to our best knowledge, there is no evident practical test of respiratory monitoring when the breathing is fast or the subject is moving. In this study, we evaluate the PPG under the same conditions as our proposed system.

Figures 4.5 and 5.5 show the signals of our ultrasound system (US), PPG, spirometer and motion sensors for a minute record, measured on subject number 4. It helps to compare waveforms visually and have a better assessment on the proposed system functionalities. Tests T1, T2, T3 and T4 in Fig. 4.5 are experiments without body motions and the T5-T6

tests in Fig. 5.5 are designed to evaluate the system with body motion. Our observations and analysis on the PPG data when the subject was moving showed uncertainty in the respiratory waveforms. Therefore, we skipped showing the PPG data for tests T5 and T6 in Fig.5.5. The accelerometer and gyroscope data in this figure show the seating position and motion of the body.

Among the gyroscope and accelerometer sensors data, the gyroscope was found to produce a better signal. Although the magnitude of data from these two sensors is extremely small, according to our data, the respiratory waveform from gyroscope is still more detectable than the accelerometer. Figures 4.5 and 1 to 5 clearly show the difference.

4.5.1 Ultrasound Data Validation - static body posture

The Test T1 in Figure 4.5 consists of 16 normal inhalations and exhalations per minute. As evident in this figure, the ultrasound system (US) has a clear breathing detection versus the reference (ESP). The PPG sensor's data follows the respiratory waveform with a lower accuracy and intensity while the gyroscope data has peaks which could be counted as wrong detections.

Test T2 consists of normal breathing with two breath holds. All subjects began with three normal breaths. Then, they were asked to hold their inhaled breaths for 10 to 20 seconds followed by a complete exhalation. The test continued with normal breathing to the end after the breath-holds. This test was done to simulate an apnea situation and feasibility of an apnea detection using the proposed respiratory monitoring. According to the signals of this test in Fig. 4.5, the PPG sensor was unable to follow the overall breathing patterns except three true detections in the beginning. Moreover, peak signals generated by this sensor could be realized as breathing activities. More signals in the appendix confirm this fact. The inertial sensor could provide a better signal than the PPG, however the sensor generated some peaks at the end which could be counted as breathing. In addition to the

breathing detection, the system is able to show the diaphragm efforts when applying pressure to open the airway. In a study by Holland *et al.* [9], they showed that breath holding does not eliminate motion of the diaphragm and the diaphragm moves upward during a breath hold with a constant velocity of 0.15 mm/sec. This phenomenon is evident in our data shown in Fig.4.5 US of Test T2. The mean amplitude of the signal lowers almost constantly by time.

Test T3 is the same as Test T1 except that the breathing is faster. This test is done not only to evaluate the performance of the proposed system but to compare against the PPG response to fast breathing. Our analysis showed a high correlation and breath detection of the ultrasound sensor versus the gold standard. However, four breaths were not detected by the ultrasound system, which is only 11% of the total breathing cycles in this test. Inertial Sensors performed better than PPG sensor in this test. Detailed results are listed in the Table 4.1 and Fig. 4.7.

Test T4 is similar to T1 except that to compare how the ultrasound sensor respond to weak and normal breathings versus the reference. The subject began with shallow breathing for almost 30 seconds and continued to normal breathing to the end. Our US signal could detect the weak breathing but the amplitude of the signal was low and failed at three points. Note that some subjects had a very weak breathing, which is the reason breaths detection was missing in Fig. 4.5-T4. During the same test, the PPG sensor did not provide any relevant signal regarding the weak breathing, and positive peak times in Gyro signal are not distinguishable with negative peaks. All sensors operated well in normal breathing for the second half of the test. It is worth noting that the US system rarely generate false readings.

4.5.2 Ultrasound Data Validation - dynamic body posture

In this section, the proposed system is assessed versus other methods when subjects had arbitrary upper body motions. Results are shown in Fig. 5.5. We performed Test T5 to

evaluate if the US sensor moves with hand elevation and its consequence on respiratory data. In this test, the subject started with two normal breaths with the arm relaxed on each side. Then, he abducted his right arm up to 90 degrees for two more breaths in that position, followed by the abduction of his arm up to almost 150 degrees and breathed two times again. Finally, he continued breathing while bringing the hand back to 90 degrees and the initial position. The right hand was chosen because the sensor was placed on the right side of the body. The skin around the ZOA shifted vertically following hand elevation. This shift caused the sensor to be displaced in front of a rib cage bone. Our analysis on subjects showed that the system operated ideally as long the elevation is up to the 90 degrees. The system failed to detect respiration a few times when the hand was elevated more than 90 degrees.

Finally in the Test T6, the proposed method was examined against upper body motion. An example of this test is shown in Fig. 5.5 while the subject bent to left and right for 25 seconds. Then, the subject was asked to do slower or more gentle motions for 10 seconds. The subject continued to the end by fast and big motions while was breathing normally. Reported results and observations showed a fairly correlated data versus the gold standard when the subject's body had motions. Although the sensor displacement on the first 25 seconds did not allow the system to track the diaphragm's movements (the similar issue in Test T5), the system showed better performance to the rest of tests, either in Fig. 5.5 or other reported data in the appendix. Due to the hand and body motions, the PPG data collection was skipped in these two tests as respiratory waveforms of these sensors are susceptible to motion artifacts [1].

Table 4.1 is a list of sensitivity, specificity and precision values of all methods with regard to the reference and plotted in Fig. 4.7 for an easier distinction. The sensitivity or true positive rate (TPR) is calculated by the equation below:

$$Sensitivity(TPR) = \frac{TP}{TP + FN} \tag{4.3}$$

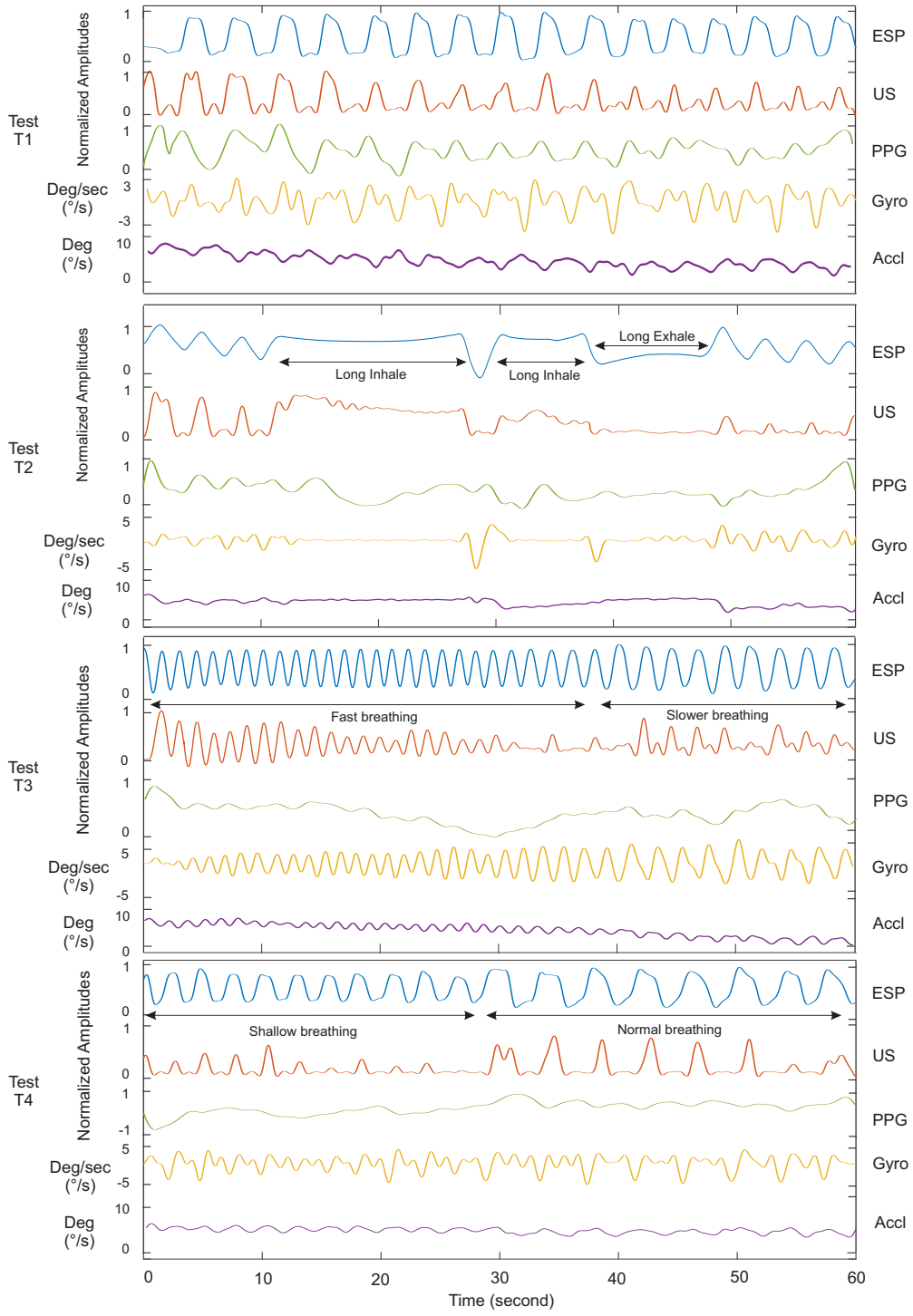

h]

Figure 4.5 Respiratory waveforms of subject 4 for the proposed ultrasound system (US) in comparison with spirometer (ESP), pulse oximeter (PPG) and motion sensor (Accl/Gyro). Only four out of six types of experiments are plotted in static body conditions.

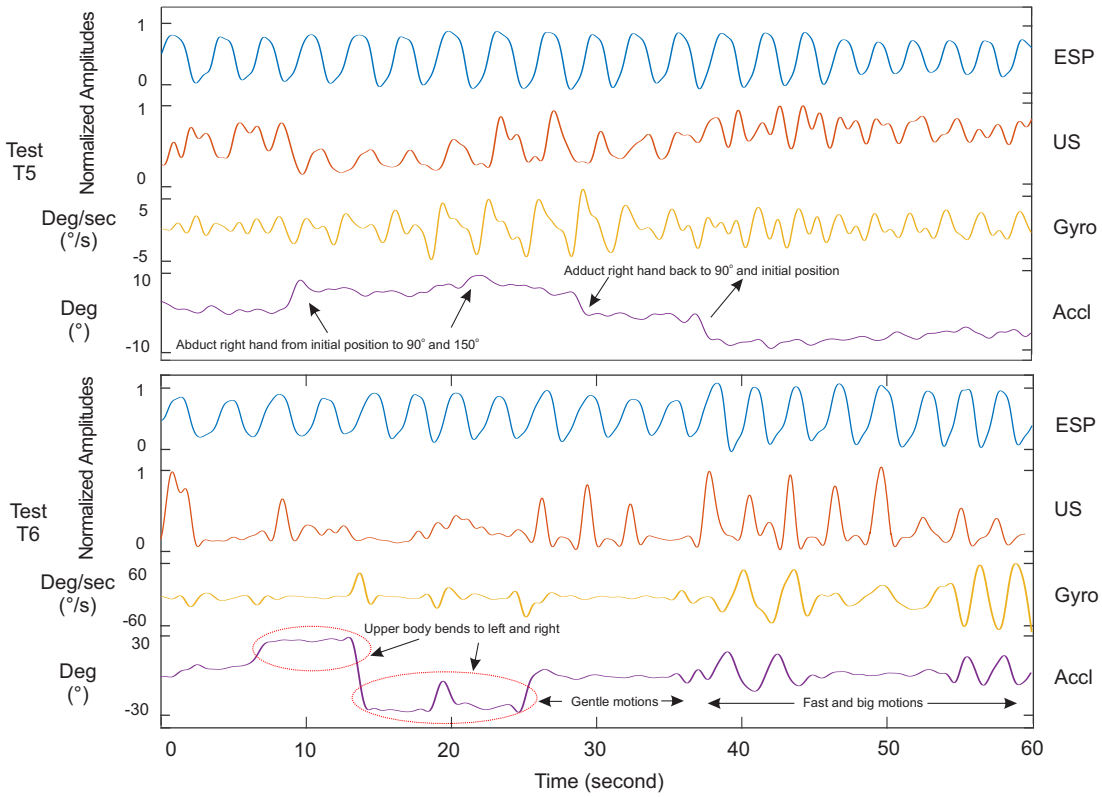

Figure 4.6 Respiratory waveforms of subject 4 for the proposed ultrasound system (US) in comparison with spirometer (ESP) and motion sensor (Accl/-Gyro) under human body motion condition. Since the PPG data is found to be sensitive to the motions, data collection is skipped for analysis in T5 and T6.

In this equation, the true positive (TP) is the number of correctly detected full breathing operations and false negative (FN) is the number of breaths wrongly classified as negative. In this table, the total number of breaths per minute of the spirometer is listed. True negative (TN) is considered positive when both the gold standard (spirometer) and the sensor do not detect any breathing. For example, if the spirometer and the sensor do not record any breathing when no breathing is occurring in between two breathing cycle or when the subject is holding their breath, it is considered a true negative. The specificity or the true negative rate is calculated to identify the proportion of non-breathings that are correctly identified. It can be calculated using below equation:

$$Specificity(SPC) = \frac{TN}{TN + FP} \tag{4.4}$$

In addition to sensitivity, precision or positive predictive value (PPV) is calculated by Eq. 4.5. In this equation, the false positive (FP) is the total number of breathing operations detected by an error. This error in ultrasound system could be a result of sensor displacement which rarely happened during our experiments. This value is noticeably high for the gyroscope. The statistics of the Test T6 are not calculated for the gyroscope, accelerometer and PPG sensors due to the extremely noisy and unusable data.

$$Precision(PPV) = \frac{TP}{TP + FP} \tag{4.5}$$

Table 4.1 Statistical measurements of all experimental tests on 6 subjects. Results are compared with the spirometer as a reference. The average number of breaths per minute of all tests are measured by spirometer. As shown in Fig. 4.5,T5 and T6, the inertial and PPG sensors are not applicable (N/A) for respiratory monitoring when the subject's body moves.

Test number	Breaths per minute	Sensitivity (%)				Specificity (%)				Precision (%)			
		US	Accl	Gyro	PPG	US	Accl	Gyro	PPG	US	Accl	Gyro	PPG
Test1	13	86	73	81	68	98	91	79	92	98	84	75	88
Test2	11	89	78	86	48	98	88	75	86	98	88	76	84
Test3	25	87	63	94	27	92	84	90	85	92	81	90	77
Test4	16	89	81	84	59	91	93	80	94	88	90	79	95
Test5	16	78	71	87	N/A	94	81	73	N/A	94	86	74	N/A
Test6	17	73	N/A	N/A	N/A	89	N/A	N/A	N/A	89	N/A	N/A	N/A
Average	N/A	84	73	86	51	93	86	79	86	94	87	79	89

According to the above mentioned results and visual observations, the author did not find a relationship between the body specification and system performance.

4.5.3 Non-respiratory movements

As mentioned before regarding the *desired window*, the system looks into reflected ultrasound waves from internal organs, mainly the diaphragm. Among all the subject tests of T6 in this

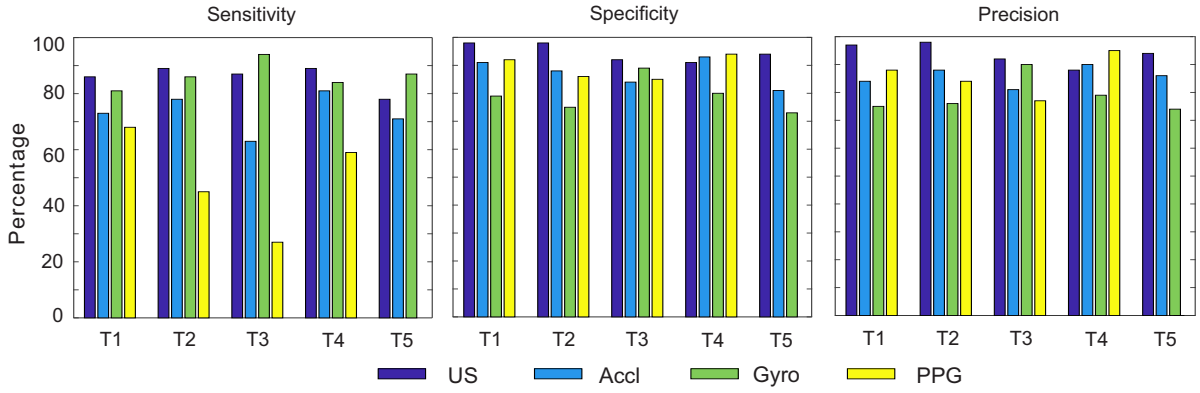

Figure 4.7 Graphical presentation of the values listed in the Table 4.1.

Table 4.2 Summary of subjects specifications. CC is the chest circumference.

ID	Age (year)	Height(cm)	Weight (Kg)	CC (cm)
1	36	173	73	84
2	29	176	65	81
3	26	175	75	84
4	25	183	95	88
5	27	165	50	74
6	34	175	70	74

article, none of the tests showed any correlation with body motion. In some tests where the subject held the breath for a longer time, there were some small peaks in the signal due to the heart operation. These spikes are visible in the most T2 tests of this article during the breath holds. Heart contractions transmit motions to the surrounded organs, such as the pericardium sac and the diaphragm [18].

4.6 Discussion

In reference to the provided data, the proposed ultrasound system provides a stable respiratory signal using only one sensor placed in the zone of apposition. Although the system is sensitive to large sensor displacements, respiratory signal could be monitored even in gentle body motions, at different breathing rates and intensities. In addition, it does not generate

false detection in comparison to the other employed methods. Based on observations over all experiments, a weaker correlation is found between the PPG, Accl and Gyro versus the spirometer as the gold standard in the T1 to T4 test methods. As per the discussion on indirect methods for respiratory monitoring systems in the introduction, the PPG sensor responds slower to the respiratory trend and non-responsive when the sensor or body is not physically stable. Respiratory-induced motions on the body are negligible compared to the human motions during daily activities. This is while the respiratory signal is detectable by the proposed ultrasound system even when the body is moving, as presented in all T6 tests in the Fig. 5.5 and appendix figures.

To improve the displacement sensitivity, an array of transducers will enable the system to track the diaphragm motion reliably in the future. In this way, at least one transducer will trace motion changes of the diaphragm even if others are blocked by the ribs. An array of 3 transducers placed side by side within the intercostal space could be a solution to overcome this issue. Note that transducers placed on a flexible material will not cause any discomfort nor inconvenience for the subjects.

Our tests show that when the subjects were performing long oral breathing test with the spirometer, they felt exhausted and dizzy when the test was reaching 50-60 seconds period. Further analysis is scheduled to apply prolonged tests based on a different reference. The system is using a bulky setup with one wired connection to the sensor. In the future, integrated wireless hardware will be developed to replace the wired connectivity and bulky evaluation setup. System evaluations during the noninvasive ventilated (NIV)[2] subjects will be addressed.

4.7 Conclusions

In this paper, we presented a direct respiratory monitoring system based on pulsed ultrasound technique. The sensor consists of a PZT5 piezo transducer mounted on a flexible

surface in direct-contact with the skin surface. The sensor should be placed in the zone of apposition (ZOA) on the right side of the body to observe the motion of diaphragm. The proposed diaphragm motion tracking sensor provides fairly good detection of respiratory cycles in different breathing patterns. The system was compared against a spirometer as the gold standard. In addition, we compared our measurements with inertial and photoplethysmography (PPG) sensors. Our ultrasound sensor was less affected by upper body motions in comparison to the inertial and PPG sensors.

In this work we found that the single piezo transducer is not sufficient to track the motion of diaphragm. The skin displacement is high at the situations which the user stretches his/her body or abducts his/her right hand higher than the shoulders. As a result of this displacement, the rib cages may block the ultrasound waves propagation into the body. Therefore, we designed a sensor with multiple similar piezo transducers to resolve the problem of a single transducer method. In this way, it is guaranteed that at least one transducer will observe diaphragm motions. The next chapter will describe the modified enhanced system for diaphragm motion tracking.

Bibliography

[1] Laurent Brochard, Greg S Martin, Lluis Blanch, Paolo Pelosi, F Javier Belda, Amal Jubran, Luciano Gattinoni, Jordi Mancebo, V Marco Ranieri, Jean-Christophe M Richard, et al. Clinical review: Respiratory monitoring in the icu-a consensus of 16. *Critical Care*, 16(2):219, 2012.

[2] G. Caironi, G. Gadda, R. Rossi, and Andrea Bellone. *Monitoring Patients During Non-invasive Ventilation: The Clinical Point of View*, pages 163–172. Springer International Publishing, Cham, 2016.

[3] Peter Charlton, Drew A Birrenkott, Timothy Bonnici, Marco AF Pimentel, Alistair EW Johnson, Jordi Alastruey, Lionel Tarassenko, Peter J Watkinson, Richard Beale, and David A Clifton. Breathing rate estimation from the electrocardiogram and photoplethysmogram: A review. *IEEE Reviews in Biomedical Engineering*, 2017.

[4] Peter H Charlton, Timothy Bonnici, Lionel Tarassenko, Jordi Alastruey, David A Clifton, Richard Beale, and Peter J Watkinson. Extraction of respiratory signals from the electrocardiogram and photoplethysmogram: technical and physiological determinants. *Physiological measurement*, 38(5):669, 2017.

[5] A Troyer De and Marc Estenne. Functional anatomy of the respiratory muscles. *Clinics in chest medicine*, 9(2):175–193, 1988.

[6] Food, Drug Administration, et al. Guidance for industry and fda staff information for manufacturers seeking marketing clearance of diagnostic ultrasound systems and transducers. *Silver Spring: US FDA*, 2008.

[7] Mario J. Garcia, Leonardo Rodriguez, Miguel Ares, Brian P. Griffin, Allan L. Klein, William J. Stewart, and James D. Thomas. Myocardial wall velocity assessment by

pulsed doppler tissue imaging: Characteristic findings in normal subjects. *American Heart Journal*, 132(3):648 – 656, 1996.

[8] Gregory P Heldt and Raymond J Ward III. Evaluation of ultrasound-based sensor to monitor respiratory and nonrespiratory movement and timing in infants. *IEEE Trans. Biomed. Engineering*, 63(3):619–629, 2016.

[9] Agnes E Holland, James W Goldfarb, and Robert R Edelman. Diaphragmatic and cardiac motion during suspended breathing: preliminary experience and implications for breath-hold mr imaging. *Radiology*, 209(2):483–489, 1998.

[10] S Javaheri and JA Dempsey. Central sleep apnea. *Comprehensive Physiology*, 2013.

[11] Akram Khan, Timothy I Morgenthaler, and Kannan Ramar. Sleep disordered breathing in isolated unilateral and bilateral diaphragmatic dysfunction. *Journal of clinical sleep medicine: JCSM: official publication of the American Academy of Sleep Medicine*, 10(5):509, 2014.

[12] Franco Laghi and Martin J Tobin. Disorders of the respiratory muscles. *American journal of respiratory and critical care medicine*, 168(1):10–48, 2003.

[13] KM Langen and DTL Jones. Organ motion and its management. *International Journal of Radiation Oncology• Biology• Physics*, 50(1):265–278, 2001.

[14] DK McKenzie, SC Gandevia, RB Gorman, and FC Southon. Dynamic changes in the zone of apposition and diaphragm length during maximal respiratory efforts. *Thorax*, 49(7):634–638, 1994.

[15] DJ Meredith, D Clifton, P Charlton, J Brooks, CW Pugh, and L Tarassenko. Photoplethysmographic derivation of respiratory rate: a review of relevant physiology. *Journal of medical engineering & technology*, 36(1):1–7, 2012.

[16] OMSignal. Validation of breathing rate algorithm during running.

[17] Aarti Sarwal, Francis O Walker, and Michael S Cartwright. Neuromuscular ultrasound for evaluation of the diaphragm. *Muscle & nerve*, 47(3):319–329, 2013.

[18] Andrew D Scott, Jennifer Keegan, and David N Firmin. Motion in cardiovascular mr imaging. *Radiology*, 250(2):331–351, 2009.

[19] A. Shahshahani, D. R. Nafchi, and Z. Zilic. Ultrasound sensors and its application in human heart rate monitoring. In *2017 IEEE International Symposium on Circuits and Systems (ISCAS)*, pages 1–4, May 2017.

[20] Amirhossein Shahshahani, Sharmistha Bhadra, and Zeljko Zilic. A continuous respiratory monitoring system using ultrasound piezo transducer. In *Circuits and Systems (ISCAS), 2018 IEEE International Symposium on*, pages 1–4. IEEE, 2018.

[21] Amirhossein Shahshahani, Zeljko Zilic, and Sharmistha Bhadra. An ultrasound based biomedical system for continuous cardiopulmonary monitoring: A single sensor for multiple information. *(Under review). IEEE Transaction on Biomedical Engineering (TBME)*, 2018.

[22] Ioanna Sigala and Theodoros Vassilakopoulos. Diaphragmatic ultrasound as a monitoring tool in the intensive care unit. *Annals of translational medicine*, 5(4), 2017.

[23] Nimrod M Tole, Harald Ostensen, World Health Organization, et al. Basic physics of ultrasonic imaging. 2005.

[24] Michele Umbrello, Paolo Formenti, Daniela Longhi, Andrea Galimberti, Ilaria Piva, Angelo Pezzi, Giovanni Mistraletti, John J Marini, and Gaetano Iapichino. Diaphragm ultrasound as indicator of respiratory effort in critically ill patients undergoing assisted mechanical ventilation: a pilot clinical study. *Critical Care*, 19(1):161, 2015.

[25] Emmanuel Vivier, Armand Mekontso Dessap, Saoussen Dimassi, Frederic Vargas, Aissam Lyazidi, Arnaud W Thille, and Laurent Brochard. Diaphragm ultrasonography to estimate the work of breathing during non-invasive ventilation. *Intensive care medicine*, 38(5):796–803, 2012.

[26] JULIETTE L Wait, PATRICIA A Nahormek, WILLIAM T Yost, and DUDLEY P Rochester. Diaphragmatic thickness-lung volume relationship in vivo. *Journal of Applied Physiology*, 67(4):1560–1568, 1989.

[27] M Zambon, L Cabrini, and A Zangrillo. Diaphragmatic ultrasound in critically ill patients. In *Annual Update in Intensive Care and Emergency Medicine 2013*, pages 427–438. Springer, 2013.

[28] Massimo Zambon, Paolo Beccaria, Jun Matsuno, Marco Gemma, Elena Frati, Sergio Colombo, Luca Cabrini, Giovanni Landoni, and Alberto Zangrillo. Mechanical ventilation and diaphragmatic atrophy in critically ill patients: an ultrasound study. *Critical care medicine*, 44(7):1347–1352, 2016.

Chapter 5

Diaphragmatic Motion Tracking Using Ultrasound Sensors for a Motion Independent Non-invasive Respiratory Monitoring

5.1 Abstract

The ability to assess reliably the respiratory rate reliably is vital in the application of remote health monitoring. A newly developed pulmonary monitoring system based on diaphragm wall motion tracking is evaluated under human physical activity. Diaphragm excursions are tracked by a designed ultrasound sensory system utilizing three ultrasound PZT5 piezo transducers. We evaluate the accuracy and reliability of this system in monitoring the diaphragmatic function and its contribution to the respiratory workload. We also examine inertial and photoplethysmography (PPG) sensors as two alternative methods. Measurements are compared to a spirometer as the gold standard. The tests are designed in this study to investigate the performance of employed sensors in both the stationary and non-stationary human body situations. We conclude that by the direct tracking of the diaphragm motion, the proposed ultrasound system is fundamentally robust to motion artifacts. Out-

standing results were obtained for the proposed system from six subjects in six different test models with average sensitivity, specificity and false alarm of 89.7%, 93.1% and 6.3%, respectively.

5.2 Introduction

In this study, we utilized only one sensor, consisting of three PZT5 piezo disk transducers as a 1-D tracker of internal organs. The internal organ is the diaphragm muscle observed from the zone of apposition. The transducers operate in the thickness mode with the resonant frequency of 2.2 MHz. A designed multichannel mixed-signal system generates and records ultrasound pulses and its echoes as a function of intensity and time (depth), called ultrasound B-mode operation. Intensity and time of flight (ToF) of reflected echoes from observing organs reveal the position of the organ in one dimension. To determine the velocity and motion of the diaphragm, the system averages the amplitude of reflections over the time in the specified depth. Previously, an ultrasound based system based on one transducer proposed by the authors [8]. The system showed a good correlation in respiratory detection versus the gold standard in different breathing patterns. However, the system witnessed a reading error due to the sensor displacement in situations where the subject moved or stretched his body a lot. In this paper, we propose an improved sensor versus the previous one and evaluated it under different body kinematics. The system shows less sensitivity to body motion than the previously proposed system. In Section 5.3, we explain where the sensor should be placed on the body and how the system is going to be evaluated with other methods. Section 5.4 describes the proposed multichannel ultrasound system with an array of transducers. Section 5.5 depicts sensor's outputs and procedures of validation and comparison against the gold standard for RR in addition to the PPG sensor as another method. Comprehensive data are collected to examine the sensor on six different healthy male subjects in different body kinematic situations such as quiescence, upper body daily

motions, big motions and body stretching. Finally, we discuss the implications of our work in Section 5.6.

5.3 Principles and System Evaluation Method

5.3.1 Sensor Position

In this study, our goal is investigating the motion of the diaphragm. So, the sensor was placed on the zone of apposition (ZOA). The ZOA is the area of the diaphragm encompassing the cylindrical portion (the part of the muscle shaped like a dome) which corresponds to the portion directly apposed to the inner aspect of the lower rib cage [3]. The sensor is placed on the right side of the body, as it is easier to see the diaphragm through the liver window [7]. Previous sensor with one transducer placed in the gap between the ribs was affected by big skin displacement due to possibility of ultrasound wave blockage by rib cages [8]. So, we have arranged three independent transducers in a triangular format in the improved sensor. According to the methods described in the literature [11],[5],[10], the sensor covers ribs 8^{th} and 9^{th} and the gap between them at the midaxillary line, shown in Fig. 5.1. In this configuration, it can be guaranteed that at least one transducer will always observe diaphragm motions through a rib cage gap. The diaphragm has an hyperechoic structure, which lets ultrasound waves reflected and measured with higher intensity than other surrounding tissues [7]. Normal diaphragm operation in this approach shows the diaphragm moving closer to the transducer with inhalation.

5.3.2 Data validation and processing methods

We used an SPR-BTA spirometer as our oral breathing reference for ultrasound data validation. This device is a flow meter, not the volume. Therefore, the signal level returns to zero in breath holds. Trapezoidal numerical integration is used to acquire the volumetric values

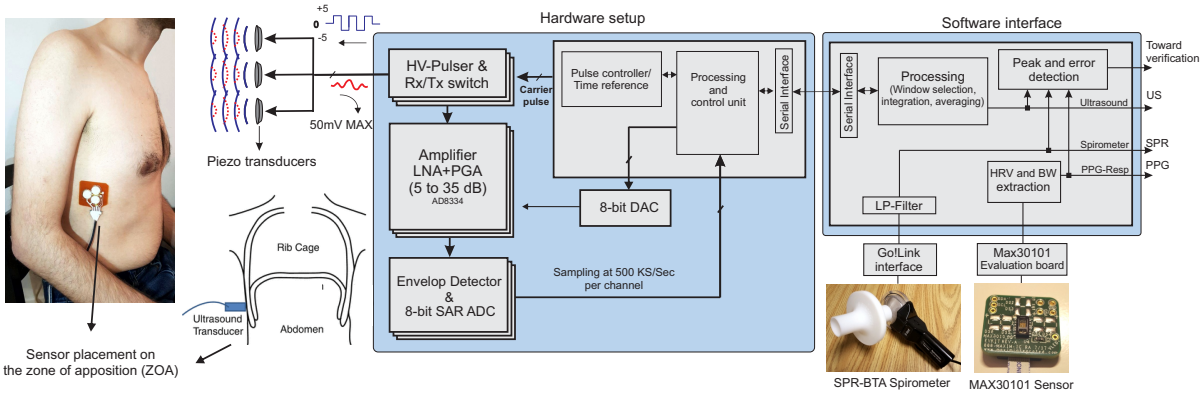

Figure 5.1 A) Piezo sensor placement on the body mounted by an adhesive pad. B) Ultrasound system designed to measure and monitor diaphragm motions as a respiratory monitoring system (US-RESP). The data is compared with spirometer, inertial and Photoplethysmography (PPG) sensors.

from airflow measurements. The proposed ultrasonic system is based on the volume of air the subject inhales or exhales, not the flow. The spirometer data is logged into a computer through GO!Link data logger. A nose clip is used to prevent nasal breathing.

Photoplethysmography (PPG) sensor is the most known sensor for heart cycle and oxygen level monitoring. As discussed in the introduction, some researchers utilized this sensor for breath monitoring. We employed a MAX30101 module consists of a PPG sensor and data logger to compare the PPG sensor performance against the reference and proposed ultrasound method. This module has an embedded accelerometer sensor which is used in this research to evaluate the impact of PPG sensor motions on its performance. The respiratory waveform can be extracted from the PPG via multiple modulations. Two of the most common methods are frequency modulation (FM) and baseline wander (BW) analysis [1]. Respiratory sinus arrhythmia (RSA) is a phenomenon by which the beat to beat heart rate interval is shortened during inhalation and lengthened during exhalation [9]. So, peak to peak time intervals of heart rate signal for each subject is obtained to form a heart rate variation (HRV) signal. It is expected that the trend of this signal corresponds to the respiratory signal. Changes in venous pressure due to changes in intra-thoracic pressure

during the breathing operation cause the baseline modulation of the PPG signal. We have used these two signals to monitor breathing with PPG. These two signals are plotted as PPG-HRV and PPG-Baseline in Figures 5.4-5.6.

Another accelerometer sensor is attached to the chest of subjects to monitor the chest motions during the breathing as well as body motions.

5.4 Ultrasound System Description

The piezo disk transducers employed in this work have electrodes on the two faces. One side of the sensor has to be interfaced to an acoustic impedance matching layer with the overall thickness of $\lambda/4$ (λ is wavelength), or less while having electrical connectivity to the circuit. The other side of the transducer can be covered by a backing material to reduce the transducer ringing effect. In this work, we used a 125 µm thick Kapton (polyimide) film as the sensor substrate. Silver conductive traces (flexible silver conductive ink) are printed on this film for the transducer's electrode connection to the circuit, using VOLTERA PCB circuit printer. Conductive silver epoxy is used to mount the transducer on the printed circuit. Since silver is the main component of epoxy, printed ink and transducer's electrode, this results in a good acoustic impedance matching between the transducer and the Kapton. Kapton as a flexible and resistant film is a proper substrate that can be easily used as the acoustic impedance matching layer between the piezo and skin. An advantage of impedance matching is the increased sensitivity of the sensor in sensing reflections. To remove the air gap between the sensor and skin, placing ultrasound gel or any similar soft gel is needed. The back of transducers are covered by a hot melt adhesive to prevent excessive vibrations (the ringing effect) and increase the axial resolution. Fig. 5.1-A shows the designed 3-channel sensor utilized in this research. All three transducers are excited at the same time to make sure that reflections are met at the same time as well.

The ultrasound system contains three parallel channels of pulser and analog front end

(AFE). The pulseres excite the transducers and the analog front ends magnify reflected ultrasound waves, as shown in Fig. 5.1B. Each pulser in this system is controlled by a digital circuit providing a 2.2 MHz carrier signal applied on the PZT5 piezo transducers, for 4 µsec duration. Once the pulse generation ends, the analog switch turns into Rx path to amplify and record reflections. In this design, burst repetition is done 20 times per second, meaning the same rate for every new reflection. Each reflection, called *Records* in this work, contains information about the observing organ position. Since the ultrasound wave attenuates linearly as it penetrates into the body, the reflected signals is amplified with the same rate to compensate the attenuation. So, a low noise amplifier (LNA) together with a programmable gain amplifier (PGA) magnify reflections in this manner. The amplitude and time of flight (TOF) of reflected signals are valuable information that needs to be captured and processed. So, the envelope of amplified signals is sampled at 500 kilo samples per second, for each channel. We employed an STM32F7 microcontroller to record and process the data. Finally, the captured data are transmitted to a computer for post-processing, validation with the reference and comparison with the other methods.

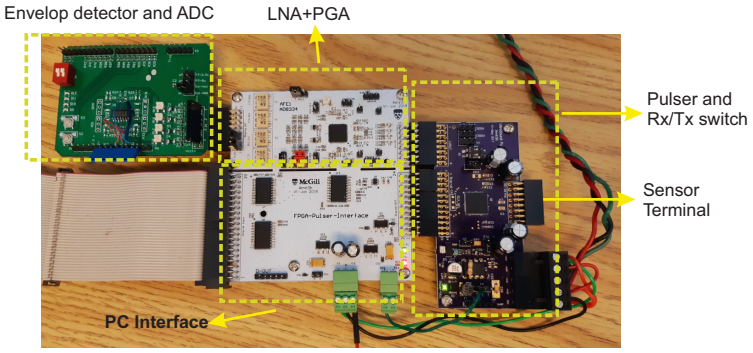

Figure 5.2 The designed 4-channel mixed signal hardware setup

The hardware setup of the proposed system architecture is shown in Fig. 5.2. The system applies differential pulses of maximum ±8 V on transducers for excitation. The hardware was built using off-the-shelf 4-channel pulser and transceiver integrated circuits (IC). In

this work, 3 out of 4 channels are used. This is just an evaluation design and it could be integrated into a small wearable design. The processing of ultrasound data could be done completely on the microcontroller. However, to make a better timing comparison between all three resources, processing was done on the computer for the purposes of our experiments.

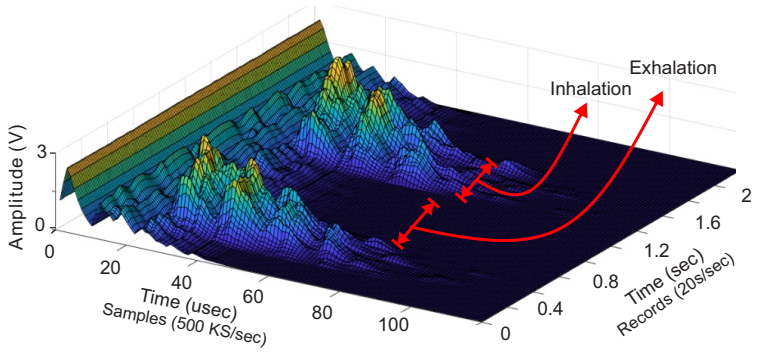

Figure 5.3 Two seconds data from ultrasound system when the subject inhales and exhales normally. Signals after the 20 µsec are the results of acoustic reflections from diaphragm wall motions.

Two seconds out of two minutes data (US signal in Fig. 5.4) from one transducer is plotted in the Fig. 5.3. In this figure, signals within 0 to 20 µsec are results of ringing effect and skin surface reflections. Signals later than 20 µsec are ultrasound waves reflected from internal organs. The period from 20 to almost 80 µsec on the Samples axis is called *desired window* (DW). An average of all samples within the DW of each record j results the value M_j. A series of M_j values represents the motion of the organ over the time, which is our respiratory waveform plotted in figures 5.4 to 5.7 as US. The following equation is used to find M_j for all channels (k):

$$M_j = \frac{1}{UB - LB} \sum_{k=1}^{3} \sum_{i=LB}^{UB} S_{k_i} \tag{5.1}$$

where i is the index of a sample S for channel k within the DW period. The LB and UB values are the Lower Bound and Upper Bound of the DW period, respectively. Since all transducers are tracking the diaphragm muscle excursion, ultrasound waves from this organ

will be reflected at almost the same time to all transducers. Also, any skin artifact will not impact on signals in the DW period which is a distinct advantage of our system. There is no crosstalk between transducers and overlapping of respiratory and non-respiratory signals observed in different channels. Moreover, reflections from nearby bones have no impact on the signal level within the DW period.

5.5 Experiments and Analysis

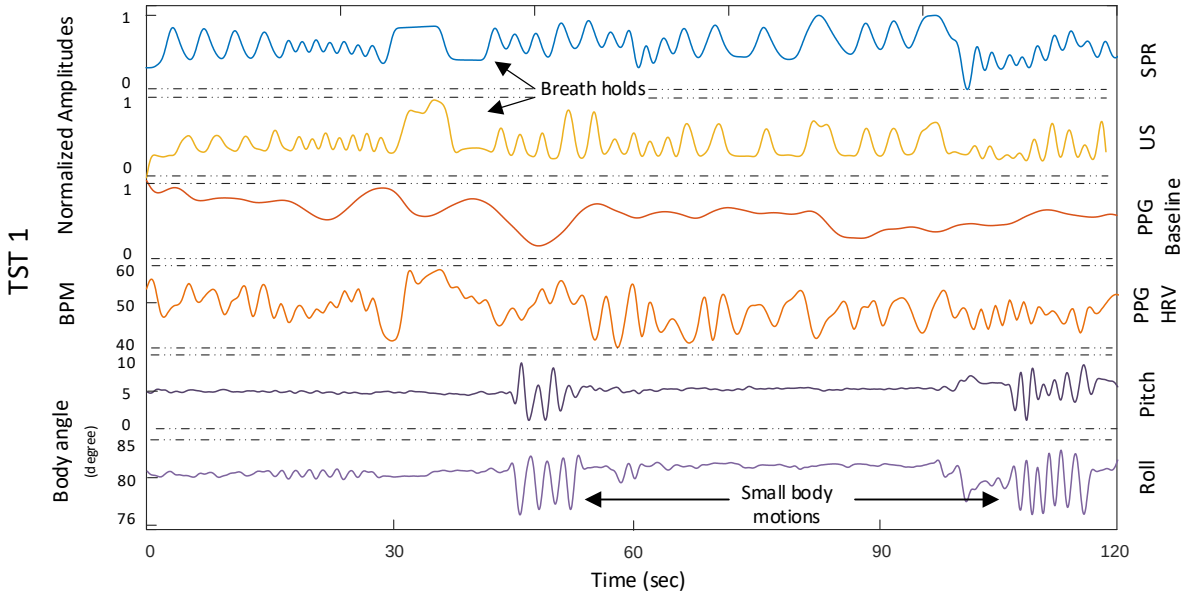

Figure 5.4 Respiratory waveforms of a subject as following sequence: spirometer (ESP) as the reference, proposed ultrasound system (US), Photoplethysmography (PPG) and its motion on the finger-tip, inertial sensor (Gyroscope and Accelerometer) to monitor body motions.

5.5.1 Study Protocol

As described, we are monitoring the internal organ motion, i.e., the diaphragm wall. Our goal is the evaluation of the proposed system on subjects in different body motion and position conditions, including sleep positions. Previously, we observed that the sensitivity of ultrasound sensor in breath detection decreased when there was a sensor displacement due

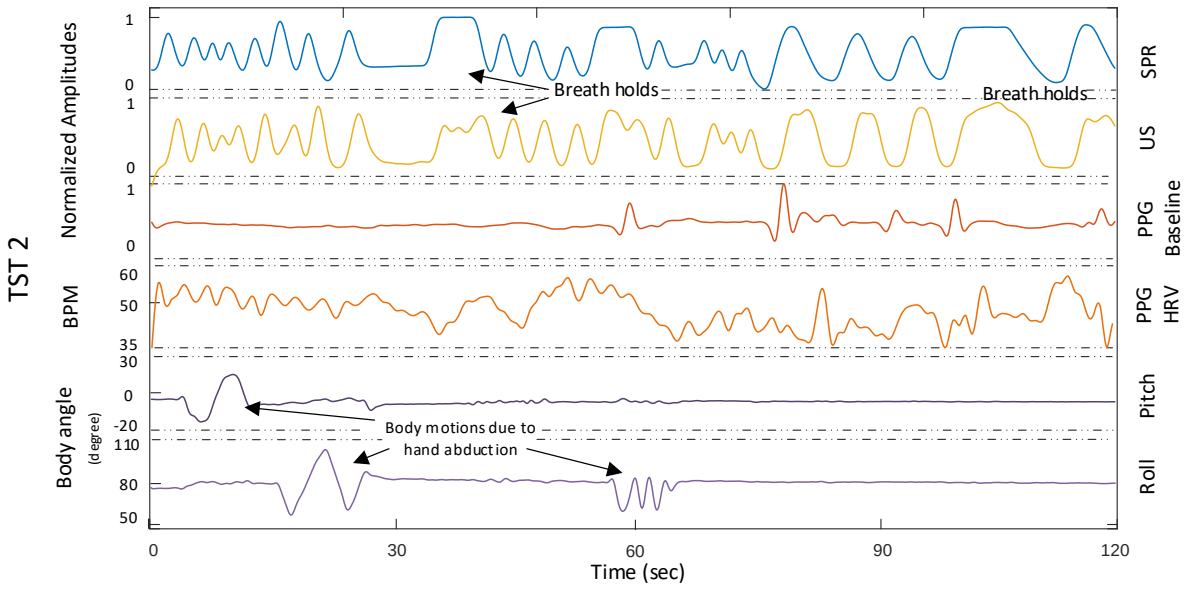

Figure 5.5 Respiratory waveforms of a subject as following sequence: spirometer (ESP) as the reference, proposed ultrasound system (US), Photoplethysmography (PPG) and its motion on the finger-tip, inertial sensor (Gyroscope and Accelerometer) to monitor body motions.

to the body motion or hand abduction [8]. So, in this study two tests are practiced that include these motions. This is intended to examine the sensitivity of PPG, ultrasound and inertial sensors to the motion artifact. Experiments are detailed as the following:

- Test-1 (T1): In this test the subject was asked to disregard the apparatus and breath normally, continue by a breath-hold and then normal and abnormal breathing. This test could be an instance of suffocation or having difficulties in breathing. The length of breath holding depended on the comfortableness of subjects and was typically between 5 to 25 sec.

- Test-2 (T2): Breathing normally while abducting hands up and down. This test is intended to evaluate the skin movements when the subject abduct (moves away from the body) their arms straight out at the shoulders and then completely up. Thereafter, the subject adducts (moves towards the body) his arms down to the normal condition. It is expected that at least one out of three transducers track the diaphragm motions

while there is such a big skin stretches and sensor displacement.

- Test-3 (T3): Breathing with random upper body motion and rotation. In this test the subject is asked to move his/her upper body randomly in all directions. This is to evaluate the ability of the apparatus when upper body motion is occurring. In contrast with the first two tests in which the PPG sensor was steady, the subject shakes his hand normally to examine the performance of the PPG sensor during hand motions.

- Tests T4 to T6 : One minute normal breathing in different sitting and sleeping positions. Researches have found that the diaphragmatic excursion (DE) varies in different body positions, such as sitting and supine [6],[2]. Takazakura *et al.* found that the DEs in the supine position were significantly greater than those in the sitting position. So, we evaluate the performance of our system in sitting position (T4), supine position (T5) and in left lateral sleep position (T6).

Table 5.1 Summary of subjects' physical specifications. CC is the chest circumference

Subject ID	BMI (kg/m^2)	Age ($year$)	CC (cm)
1	24.5	34	88
2	20.7	30	83
3	19.8	29	63
4	27.4	30	92
5	24.8	29	90
6	22.4	37	88

In this study, the experiments were conducted on six healthy subjects aged from 29 to 37, as listed in the Table I. They were instructed how to perform each breathing exercise before their recording sessions. We found oral breathing exhausting if it lasted longer than 2 minutes. So, we set the length of tests to a maximum of 2 minutes.

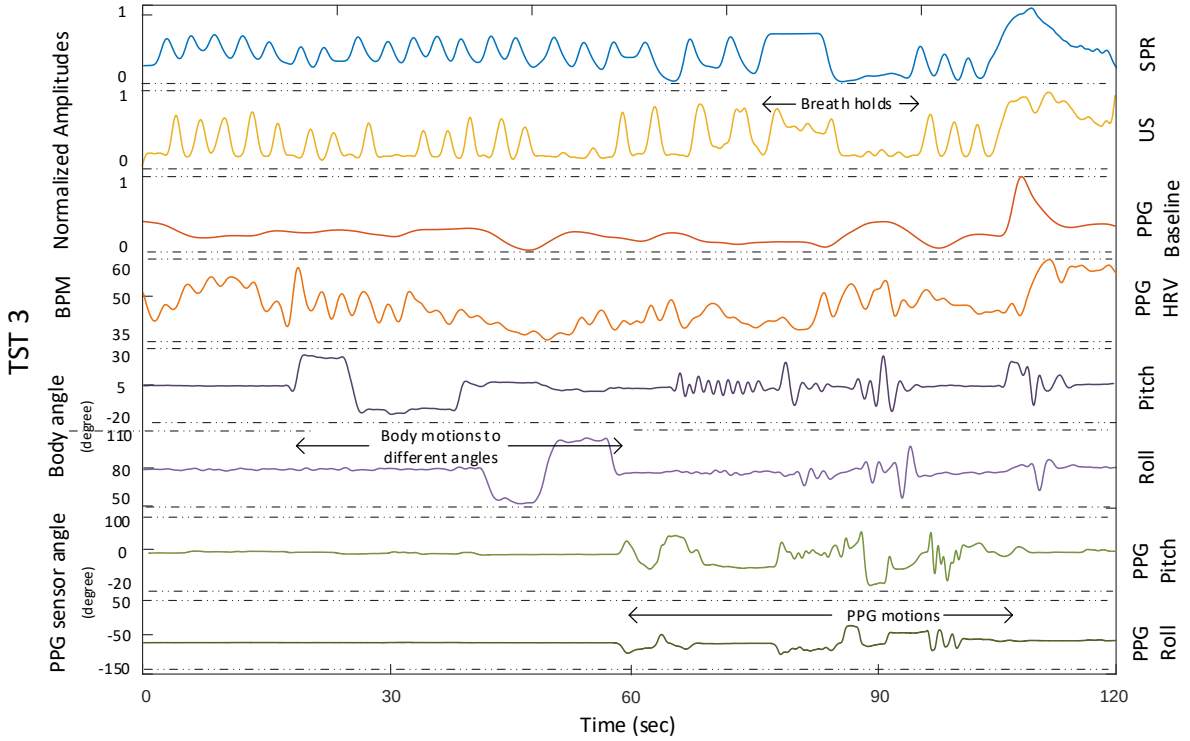

Figure 5.6 Respiratory waveforms of a subject as following sequence: spirometer (ESP) as the reference, proposed ultrasound system (US), Photoplethysmography (PPG) and its motion on the finger-tip, inertial sensor (Gyroscope and Accelerometer) to monitor body motions.

5.5.2 Graphical representation of respiratory signals

Signals of T1-T3 tests for a subject are plotted in figures 5.4 to 5.6 and T4-T6 tests are merged into Fig.5.7. SPR signal in these figures is the spirometer signal used as our respiratory signal reference for ultrasound (US) and PPG signals. The inertial sensor monitors both the respiratory signal and body motions. The subject body motions are plotted as pitch and roll angles and PPG motions are denoted as PPG pitch and roll.

In Fig. 5.4, the subject started with normal and fast breathing continued by a full inhalation and exhalation breath holds. The breath holding simulation is intended to evaluate how sensors detect breath pauses in disease such as apnea or Biot's breathing. The subject continued normal and abnormal breathing patterns to the end of this test. It is clear in

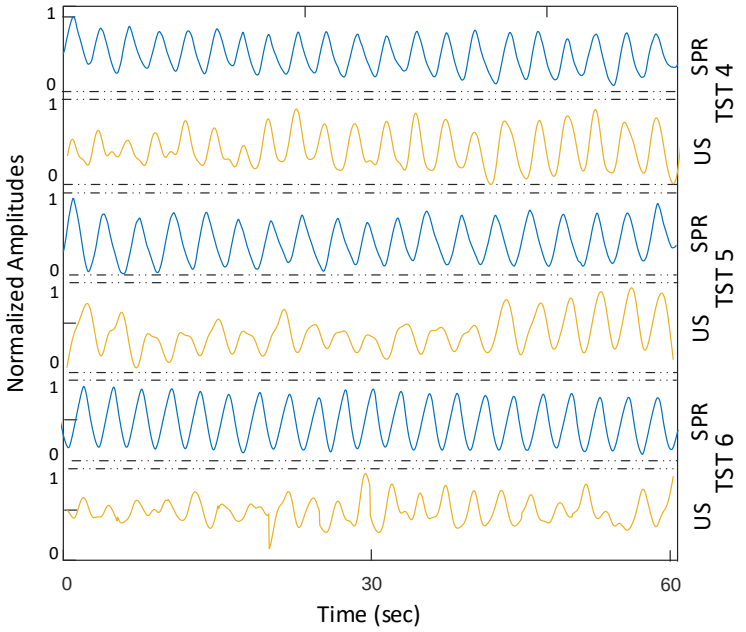

Figure 5.7 Respiratory waveforms of a subject in sitting (TST4) position, supine (TST5) and left lateral (TST6) sleep positions.

the Fig. 5.4 that the US signal is in a high correlation with the reference signal, while the PPG baseline signal has very weak correlation. Heart rate variation (HRV) analysis of PPG sensor is in a high accordance with the reference signal, except the breath holding period. Note that the high amplitude signals of pitch and roll in this figure (around times 55 and 115 seconds) are small motions of the body, not the respiratory motions of the chest.

Fig. 5.5 depicts the respiratory waveform of all sensors when the subject abducts and adducts his right hand. As explained before, skin displacements versus the rib cage could be the main bottleneck in using ultrasound for internal motion detection. This problem is simply resolved in this article by a three transducer sensor model. The ultrasound sensor never produced negligible false breathing detection. Due to the hand and minor body motions in this test, the PPG sensor failed in detecting correct breathing operation either from baseline amplitude or HRV variations. In this test, because of the body motions, the error rate of the inertial sensor in detecting RR increased, as reported in Table II for TST2.

An example of motion-based experiments is plotted in Fig. 5.6. In this test, the subject

Table 5.2 Summary of statistical measures of the performance on six subjects for tests TST1 to TST3. All values are in percentage.

Test number	Average breaths /length(min)	Ultrasound				Inertial Sensor				PPG-HRV				PPG-Base			
		Sens	Spec	Prec	FAL	Sens	Spec	Prec	FAL	Sens	Spec	Prec	FAL	Sens	Spec	Prec	FAL
TST 1	22	89.5	93.5	94.3	6.4	76.2	86.8	82.8	13.1	84.6	84.2	83.8	15.6	55	77.6	66.4	22.7
TST 2	21.8	92	94.7	94.8	5.2	50.6	80.2	67	19.9	86.4	91.2	90.8	8.8	33.2	79	58.4	20.9
TST 3	20.9	87.7	91.2	90.8	7.3	17.7	59.7	31	40.4	82	86.3	84.3	13.8	44.5	74.2	64	25.7
Average	21.6	89.7	93.1	93.3	6.3	48.2	75.6	60.3	24.5	84.3	87.2	86.3	12.7	44.2	76.9	62.9	23.1

bent to four directions by almost 30 degrees for a minute. So, the system experienced sensor displacements in four different directions. Except for the three failures in breath detection at times 32, 50 and 55 seconds, the sensor had a successful operation all the time. The subject continued breathing while motioning his fingers, hand and body in random directions. The ultrasound system could detect all the breathing and non-breathing periods whilst the PPG sensor showed uncertainty in this experiment from time 70 to 120 seconds. The PPG signal amplitude got changed due to its motions as evident in the PPG motion signals. Along with the whole test, the PPG sensor was fixed on the fingertip. It is obvious that the inertial sensor can not distinguish minor respiratory motions of the chest from the body motions. Obtained values from TST3 of inertial sensor in Table II imply this fact.

Fig. 5.7 illustrates all the US and SPR signals of tests 4 to 6. Since the main objective of these tests is to evaluate the performance of proposed system in different siting and sleep positions (as discussed in Section 5.5.A), the PPG and inertial sensors analysis are skipped in these experiments.

5.6 Results and Discussion

We have depicted the respiration detection ability of the proposed ultrasound sensor as well as PPG and inertial sensors as two conventional methods introduced by other researchers. This section evaluates all the methods statistically for all subjects and tests.

Table 5.2 reports the evaluation of the T1 to T3 tests results on all six subjects and

Table 5.3 reports the later T4 to T6 tests. We have used windowing percentile (of about 80%) analysis on all data to distinguish inhalation and exhalation cycles. This method is independent of the signal offset (baseline). However. even if there is no object (diaphragm) reflecting ultrasound waves, the amplitude of the signal is near to zero. So, any amplitude higher than a tunable threshold would be a certainly true inhalation. This is an advantage of this sensor for providing accurate data and simple processing effort. The percentile score is relative to the size of the window. A window size of 10 seconds and a dynamic percentile score of 60% to 80% were ideal combinations for this aspect. The total number of true and false detected events for the existing and non-existing breath operations are counted to calculate the sensitivity (true positive rate (TPR)), specificity (true negative rate (SPC)) and precision (positive predictive value (PPV)) values of the three methods with regard to our reference. False alarm ratio is added to this table to compare the probability of generating false positive patterns in different sensors. For applications such as sleep apnea, false breathing detection from a suffocated patient would lead to irreparable harms such as hypertension, heart disease including heart attacks and heart failure, diabetes and stroke.

According to the average values (average of 6 subjects in each test) in the Table 5.2, the proposed ultrasound sensor scored better than the PPG and inertial sensors for all sensitivity, specificity and precision values with about 90% and more. It also ranked first in generating the least false detections. In the previous work, the average of obtained sensitivity and specificity values were 73% and 89% respectively, for tests that involved body motions [8]. In this work, outcomes of Test3 were 89.7% and 93.1% for the sensitivity and specificity parameters.

Moreover, based on the Table III and Fig. 5.7, the ultrasound sensor had high sensitivity, specificity and precision for all tests 4 to 6.

The reader must note that the relationship and magnitude of RSA has been shown to be easily influenced and diminished by poor cardiopulmonary function and disease such as

coronary artery disease. In elderly people, the abnormal RSA is very prominent, while the importance of respiratory monitoring is higher for them. Poor physical fitness is another instance in which for both athletes and people who routinely exercise have higher prevalence of RSA than people who do not exercise [9] [4]. These reasons may exclude the PPG sensor as an applicable sensor for respiratory monitoring. Although the HRV analysis on the PPG sensor yields an acceptable accuracy (see Table 5.2), this sensor is still an indirect method for respiratory monitoring.

Table 5.3 Summary of statistical measures on six subjects for tests TST4 to TST6.

Test number	Ultrasound			
	Sens	Spec	Prec	FAL
Test 4	95.4	96.6	97.2	3.3
Test5	87.8	96.8	96.6	3.2
Test6	90.2	92.2	91.4	7.7
Average	91.1	95.2	95.1	4.7

5.7 Conclusion

In this paper, we evaluated a multichannel pulsed ultrasound system (US) for monitoring respiratory cycles in different human body motions as instances of daily activities. The system utilizes three PZT5 piezo transducers, mounted on a flexible surface, working in parallel to track the diaphragm motions observed from the zone of apposition (ZOA). The proposed sensor probes internal organ motion (the diaphragm muscle), rather than the external or surface motions of the body, making that extremely independent of patient's movements. The system output was examined by a spirometer as the gold standard. Inertial and photoplethysmography (PPG) sensors were employed to evaluate their operations as two alternative methods in comparison with the proposed system. The ultrasound system exhibits better performance than the PPG and inertial sensors under the body motions.

Bibliography

[1] Drew Birrenkott. Respiratory quality index design and validation for ecg and ppg derived respiratory data. *Report for transfer of status, Dept. Eng. Sci., Univ. Oxford, Oxford, UK*, 2015.

[2] Alain Boussuges, Yoann Gole, and Philippe Blanc. Diaphragmatic motion studied by m-mode ultrasonography: methods, reproducibility, and normal values. *Chest*, 135(2):391–400, 2009.

[3] A Troyer De and Marc Estenne. Functional anatomy of the respiratory muscles. *Clinics in chest medicine*, 9(2):175–193, 1988.

[4] WJ Hrushesky, D Fader, O Schmitt, and V Gilbertsen. The respiratory sinus arrhythmia: a measure of cardiac age. *Science*, 224(4652):1001–1004, 1984.

[5] DK McKenzie, SC Gandevia, RB Gorman, and FC Southon. Dynamic changes in the zone of apposition and diaphragm length during maximal respiratory efforts. *Thorax*, 49(7):634–638, 1994.

[6] Virender K Rehan, James M Nakashima, Aliza Gutman, Lewis P Rubin, and F Dennis McCool. Effects of the supine and prone position on diaphragm thickness in healthy term infants. *Archives of disease in childhood*, 83(3):234–238, 2000.

[7] Aarti Sarwal, Francis O Walker, and Michael S Cartwright. Neuromuscular ultrasound for evaluation of the diaphragm. *Muscle & nerve*, 47(3):319–329, 2013.

[8] Amirhossein Shahshahani, Carl Laverdiere, Sharmistha Bhadra, and Zeljko Zilic. Ultrasound sensors for diaphragm motion tracking: An application in non-invasive respiratory monitoring. *Sensors (Basel, Switzerland)*, 18(8), 2018.

[9] Fumihiko Yasuma and Jun-ichiro Hayano. Respiratory sinus arrhythmia: why does the heartbeat synchronize with respiratory rhythm? *Chest*, 125(2):683–690, 2004.

[10] M Zambon, L Cabrini, and A Zangrillo. Diaphragmatic ultrasound in critically ill patients. In *Annual Update in Intensive Care and Emergency Medicine 2013*, pages 427–438. Springer, 2013.

[11] Massimo Zambon, Paolo Beccaria, Jun Matsuno, Marco Gemma, Elena Frati, Sergio Colombo, Luca Cabrini, Giovanni Landoni, and Alberto Zangrillo. Mechanical ventilation and diaphragmatic atrophy in critically ill patients: an ultrasound study. *Critical care medicine*, 44(7):1347–1352, 2016.

Chapter 6

Conclusion and Potential Future work

I have introduced for the first time the application of ultrasound in M-Mode as a portable sensory device for human respiratory and heart monitoring. Ultrasound sensors as unobtrusive techniques are utilized to extract the chest and heart physical motions to monitor breathing cycles. A PZT piezo transducer operating at 1 MHz frequency was placed on the chest to trace the heart, relevant organs and the intercostal muscles motions. The extracted data revealed the heart rate, its variation relation with respiration and the respiratory cycles. With this method, the system was able to monitor the heart and respiratory signals using only a sensory node. The system could deliver the respiratory signal with 94.5% and 94.0% sensitivity and specificity, respectively. However, we found the respiratory waveform of this sensor sensitive to motion artifacts.

To improve the quality of the respiratory signal, I developed a flexible sensor made of Kapton film and a 2.2 MHz piezo transducer disk mounted on this film. With this sensor, the amount of near field reflections to the sensor got lower and the intensity of ringing effect reduced. I developed a mixed analog and digital signal hardware to excite the transducer and amplify the reflected signal. The sensor was placed in the zone of apposition (ZOA) in which the motion of the diaphragm can be observed easily. By tracking the motion of the diaphragm, a robust respiratory signal could be obtained. In this position, the sensor

will sense reflections only from the diaphragm wall. Therefore, there is no overlapping and undesired signals mixed with the respiratory signal. Since the system monitors the internal organ motions, the motion artifact has a minimal impact on the respiratory signal. The proposed method could provide the respiratory signal with 84% and 93% sensitivity and specificity, respectively. Sensor displacement due to skin motions was the only obstacle in deriving the respiratory signal. If a rib bone places in front of the transducer, it blocks ultrasound waves being propagated into the body. Therefore, the motion of the diaphragm cannot be sensed. To overcome this problem, I developed a 3-channel sensor with three piezo transducers mounted in star shape on the Kapton flexible film. In this way, even with the presence of skin motions and sensor displacement, there is at least one transducer able to trace the motion of the diaphragm. This method showed a remarkably better performance than the 1-channel design. Results were 89.7% and 93.1% for sensitivity and specificity under a more intense body motion. I found only 6.3% error as the false alarm when the system by mistake detects a respiration operation.

All the above-mentioned results were obtained from an extensively analyzed and evaluated data sets recorded from real subjects in reference to a spirometer as a gold standard.

6.1 Future Work

In this dissertation, I utilized a mixed of evaluation boards designed by myself to study the feasibility of using piezo transducers for an ultrasound-based respiratory monitoring. Therefore, the hardware setup was not optimized for power- and cost- effective concerns. On the other hand, I made a modular and flexible design to add freedom to the development procedure which makes the design bigger in size. Therefore, as a future work, this system could be integrated into a smaller and wearable design. So, the sensor, battery and wireless communication should be embedded into the design. This modular system supports up-to 8 piezo transducers operating in parallel. It is sufficient to have one or three channel

design for the purpose of respiratory monitoring. An inertial sensor could be integrated into the wearable sensor for a better understanding of patient activity and data fusion with the ultrasound sensor. It helps to understand better the presence of apnea, direction and intensity of body motions.

Another advantage of the proposed ultrasound sensor is the low voltage operation. The sensor is able to operate at ±5 volts for burst pulses while this value is more than ±10 for conventional ultrasonic systems in the area of medical imaging. So, based on our observations, not only the sensor does not heat up itself, the intensity of ultrasound waves are less than the thresholds defined by FDA (Chapters 1.2.1 and 3).

The basis of this dissertation is internal organ motion tracking. So far, we studied the utilization of a motion tracker in monitoring the operation of an organ such as the diaphragm muscle. However, there are many applications that this system could be utilized for diagnosis. We also proposed a new system for soft tissue artifact measurement and detection using an array of piezo sensors mounted on a flexible or rigid surface. Initial medical concepts are examined and some solutions are proposed based on the application under the test.

Knee laxity assessment is useful to discern knee injuries and the success of reconstruction procedures after the operation or therapy. The foundation of this diagnosis and treatments is manual clinical examination. Therefore, the assessment outcomes are subject to error in terms of observations and interpretations. Anterior and rotational knee laxity is usually evaluated manually with the Lachman, the anterior drawer or the pivot shift tests.

The Lachman's test is the most common technique to clinical evaluation as an important part of the gold standard in ACL injury detection [1], whilst this test is the most sensitive way [8]. The KT-1000 is the most common instrument in standardizing the anterior tibial translation [2] limited to only static antero-posterior (A-P) laxity evaluation, shown in Figure 6.1.

There are devices to measure anterior and rotational knee laxity to produce standard

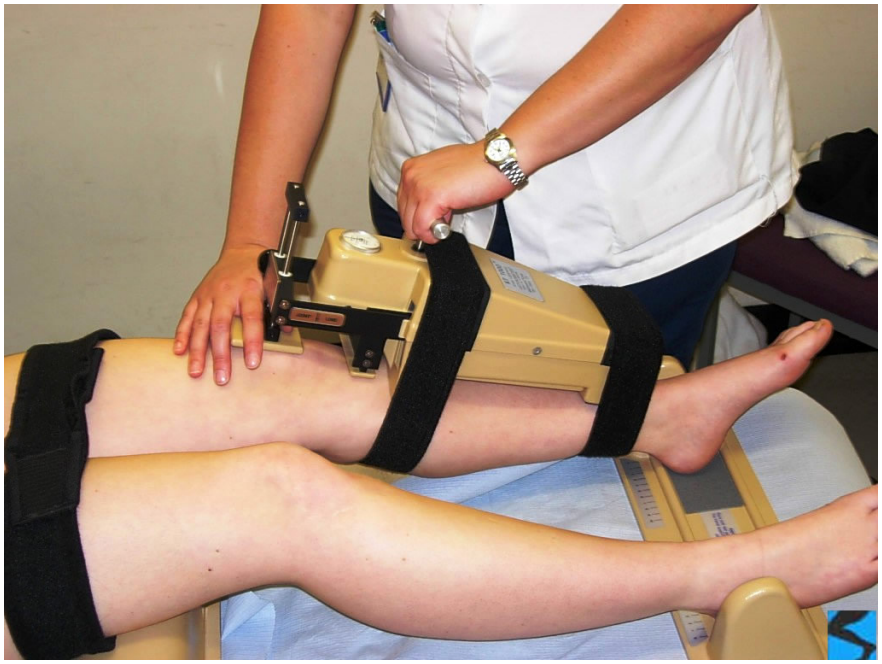

Figure 6.1 Anterior and posterior drawer tests using KT-1000 device[1] as a standard measurement tools

evaluation measurements. The Pivot shift test [6] is the most common clinical way as it tests the knee in more than one direction. Static tests, which evaluate the knee in one or several specific directions, are more interesting for laxity characteristics quantification. Some researchers used accelerometer sensors to find the laxity [7]. In a more accurate but expensive way, researchers used a workstation and a three-dimensional optical localizer to create images that represent knee kinematics [5].

Soft tissue artefact (STA) is a significant error source in skin marker-based measurement of human movement analysis, and are difficult to detect and eliminate non-invasively. This occurs to the extent that joint components in knee and laxity analysis that are suspect to small movements, will result in totally unreliable values. Most of the non-invasive devices rely on the exterior part of the leg than the tibia or femur. These methods suffer from the movement of soft tissue versus the bone. As a part of our developments, we introduced a method to measure the rotation and translation of soft tissue versus the bone non-invasively. This method utilizes an ultrasound sensor to find the relative motions of the sensor to

the bone and mapping the system outputs to the angular values. Figure 6.2 presents two examples of piezo transducer arrangements to detect the movement of bone versus the skin surface. Each model has its own pros and cons and requires a profound analysis to find out the best practical model.

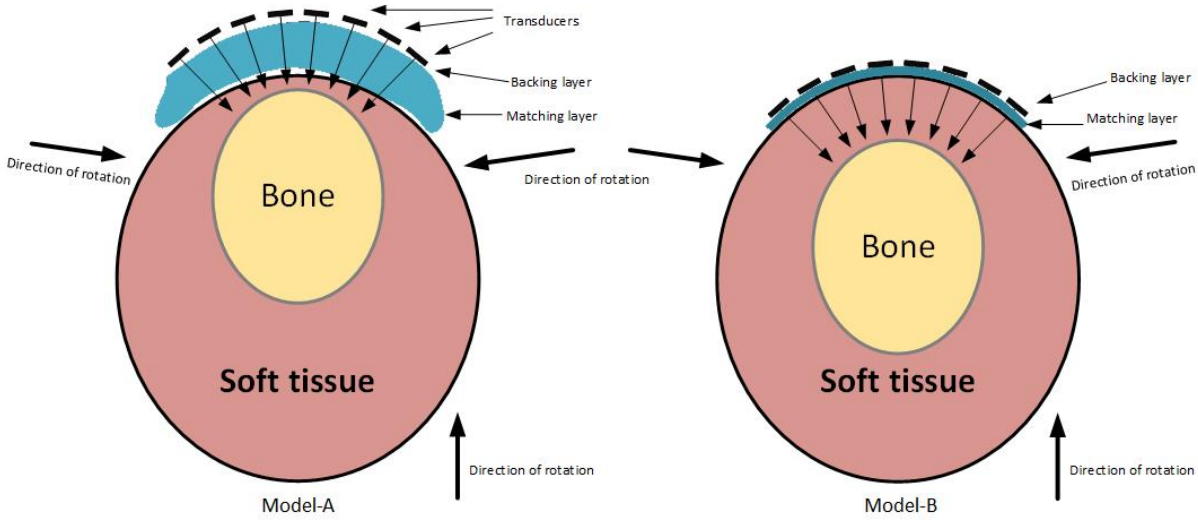

Figure 6.2 Three examples to design a model for soft tissue artifact measurement.

This new technique can be a solution to reduce the error in human kinematic movement analysis [4][3] and other clinical applications [9]. The utilized hardware in this thesis should be enhanced with an analog multiplexer to increase the number of ultrasound channels. A model of bone and soft tissue should be designed to simulate a real condition. This study requires extensive data processing by recording data from ultrasound and motions sensors fixed to the model. A learning algorithm could be applied to map the ultrasound data to the rotation and translation directions.

Bibliography

[1] Knee laxity testing device. `https://www.thekneedoc.co.uk/kt1000-knee-laxity-testing-device/`.

[2] Dale M Daniel, Mary Lou Stone, Raymond Sachs, and Lawrence Malcom. Instrumented measurement of anterior knee laxity in patients with acute anterior cruciate ligament disruption. *The American Journal of Sports Medicine*, 13(6):401–407, 1985.

[3] Helios de Rosario, Alvaro Page, Antonio Besa, Vicente Mata, and Efraim Conejero. Kinematic description of soft tissue artifacts: quantifying rigid versus deformation components and their relation with bone motion. *Medical & Biological Engineering & Computing*, 50(11):1173–1181, Nov 2012.

[4] Ugo Della Croce. Soft tissue artifacts in human movement analysis. In *Proceedings of the IXth International Symposium on the 3D Analysis of Human Movement*, 2006.

[5] Vincent Dessenne, Stéphane Lavallée, Remi Julliard, Rachel Orti, Sandra Martelli, and Philippe Cinquin. Computer-assisted knee anterior cruciate ligament reconstruction: first clinical tests. *Journal of Image Guided Surgery*, 1(1):59–64, 1995.

[6] HR Galway and DL MacIntosh. The lateral pivot shift: a symptom and sign of anterior cruciate ligament insufficiency. *Clinical orthopaedics and related research*, 147:45–50, 1980.

[7] Akira Maeyama, Yuichi Hoshino, Anibal Debandi, Yuki Kato, Kazuhiko Saeki, Shigehiro Asai, Bunsei Goto, Patrick Smolinski, and Freddie H Fu. Evaluation of rotational instability in the anterior cruciate ligament deficient knee using triaxial accelerometer: a biomechanical model in porcine knees. *Knee Surgery, Sports Traumatology, Arthroscopy*, 19(8):1233–1238, 2011.

[8] Martin Prins. The lachman test is the most sensitive and the pivot shift the most specific test for the diagnosis of acl rupture. *Australian Journal of Physiotherapy*, 52(1):66, 2006.

[9] Jiajia Wang, Zhongwen Lui, Zhihui Qian, and Luquan Ren. Soft tissue artifact evaluation of the cervical spine in motion patterns of flexion and lateral bending: a preliminary study. *PeerJ*, 4:e1893, March 2016.

Chapter 7

Appendix

Respiratory waveforms of other five subjects (subjects 1,2,3,5 and 6), in Chapter 4, are plotted on Figures 1 to 5. The proposed ultrasound system (US) is compared with the spirometer (ESP) as our reference, pulse oximeter (PPG) and motion sensors (Accl and Gyro). As mentioned before in Chapter 4 Section 4, since the PPG sensor is sensitive to the motions of the sensor and human body, the PPG data collection is skipped for Tests T5 and T6 of the following figures. Note that the Gyro and Accl signals are not necessarily synchronous with the breathing rates in the T5 and T6 tests. For the convenience of the readers, the amplitude of all signals was normalized to make the visual comparison easier. It is worth noting that the amplitude variations of the Gyro and Accl signals in the T5 and T6 tests were almost ten-times greater than the other four tests.

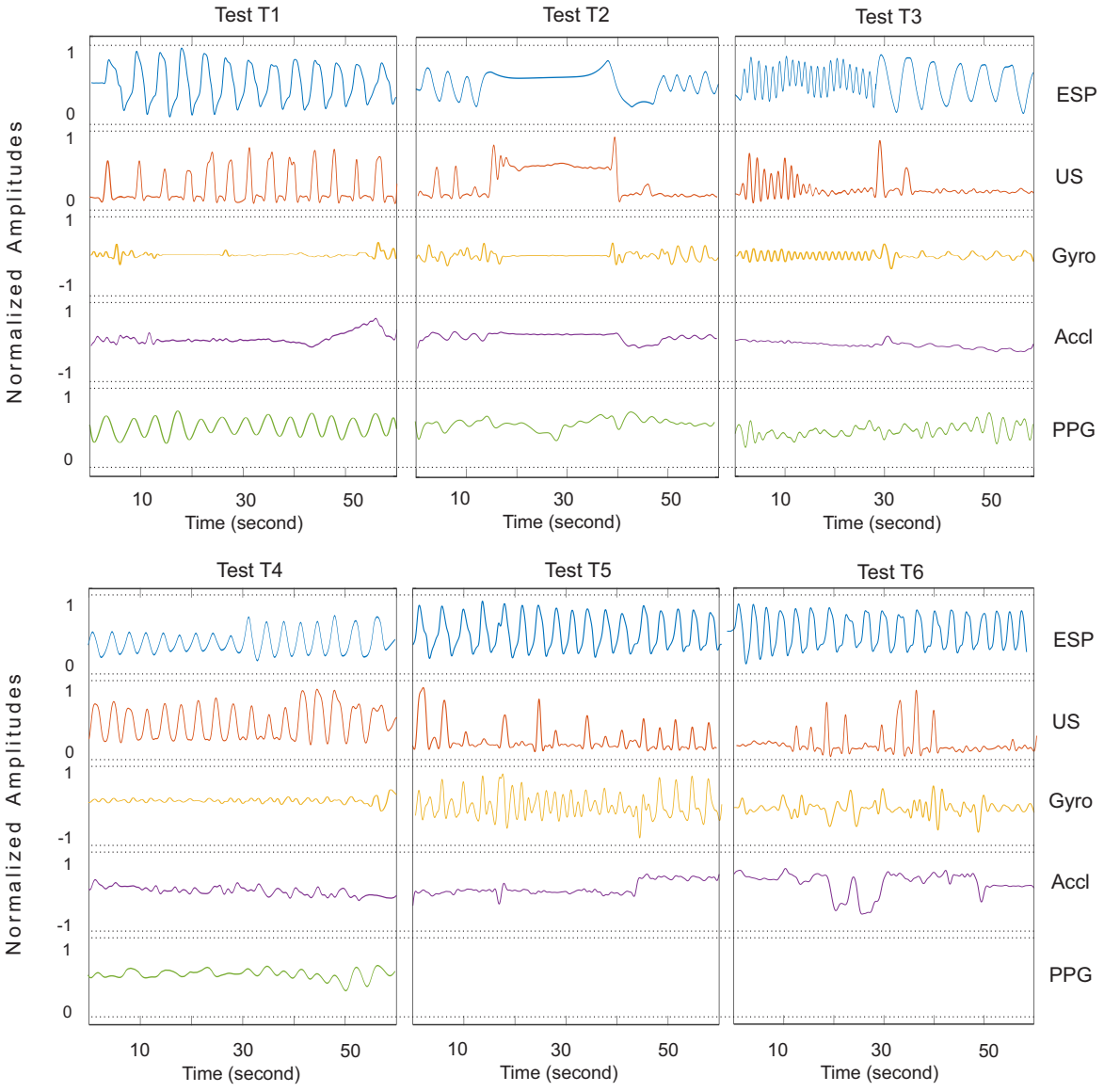

Figure 1 Respiratory waveforms of subject 1.

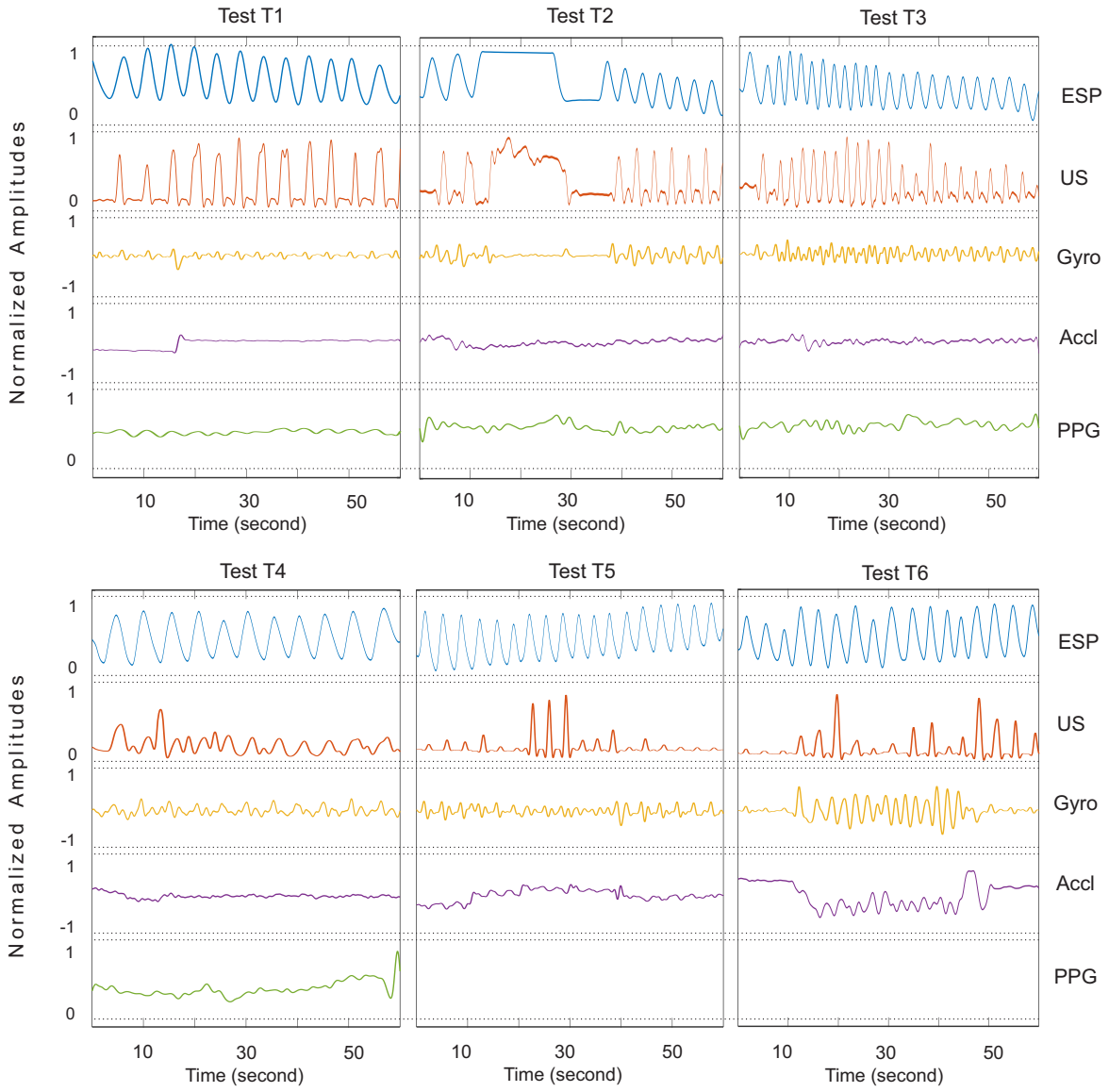

Figure 2 Respiratory waveforms of subject 2.

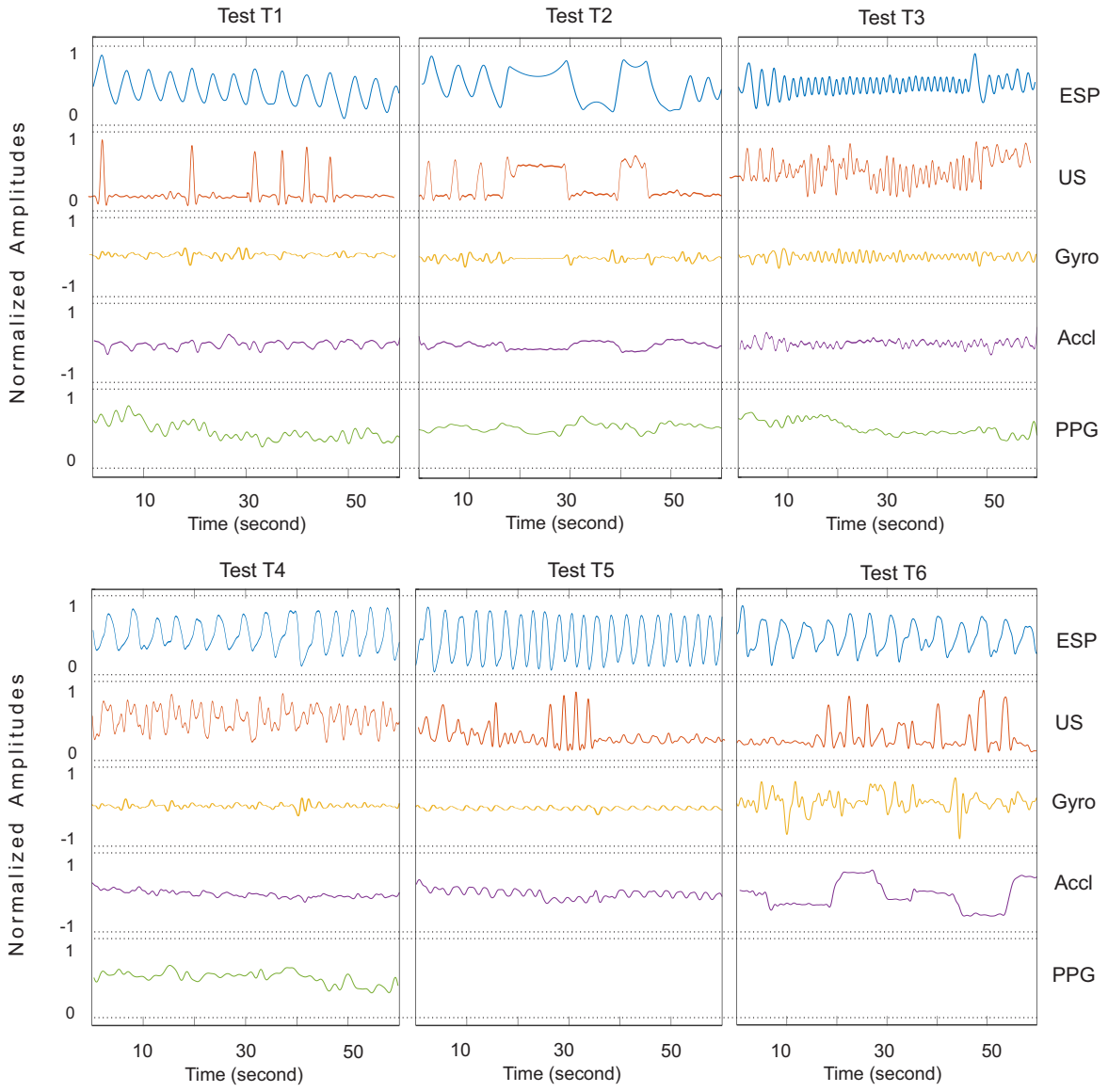

Figure 3 Respiratory waveforms of subject 3.

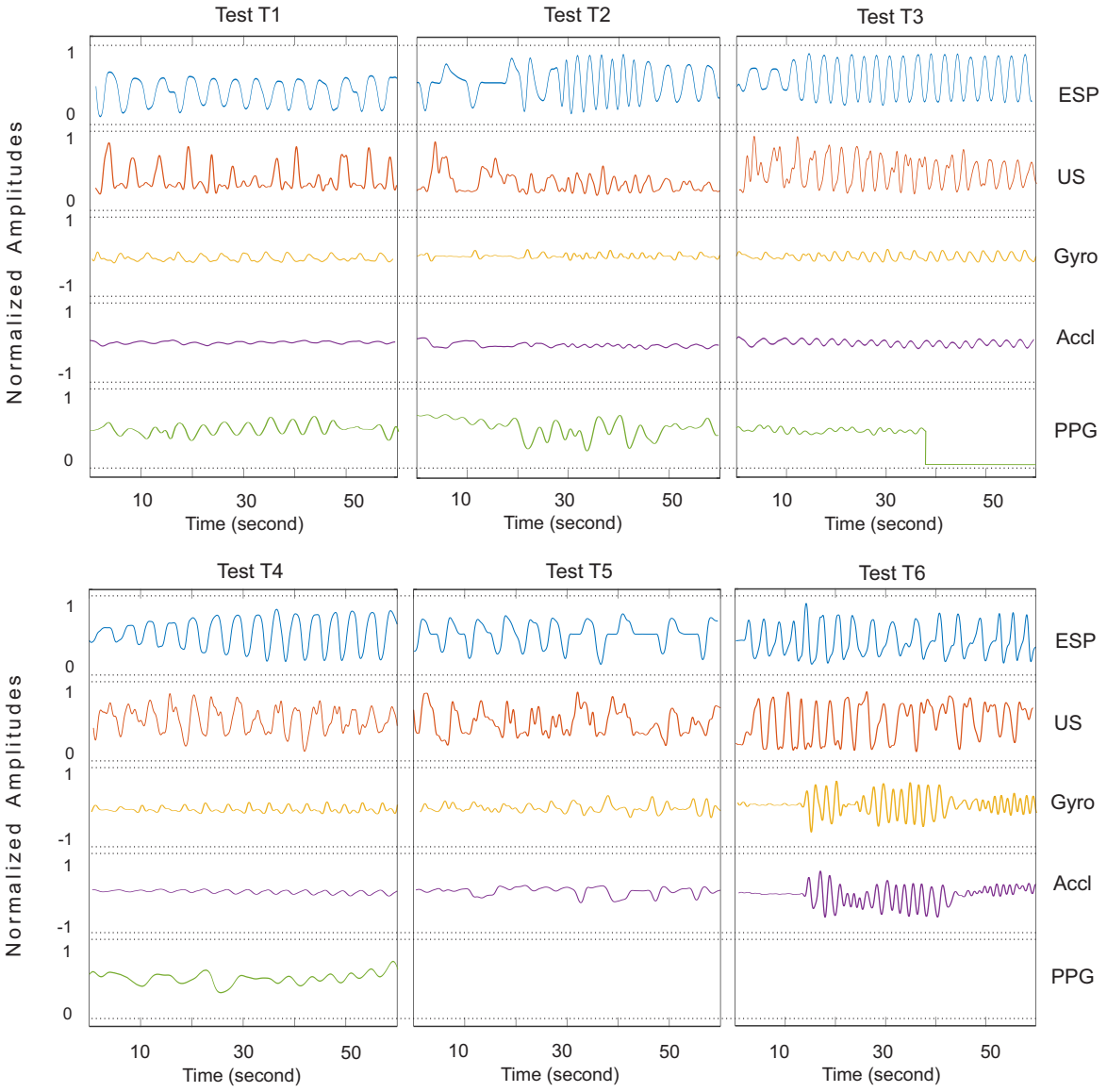

Figure 4 Respiratory waveforms of subject 5. The PPG sensor was detached from the subjects finger in the last 15 seconds.

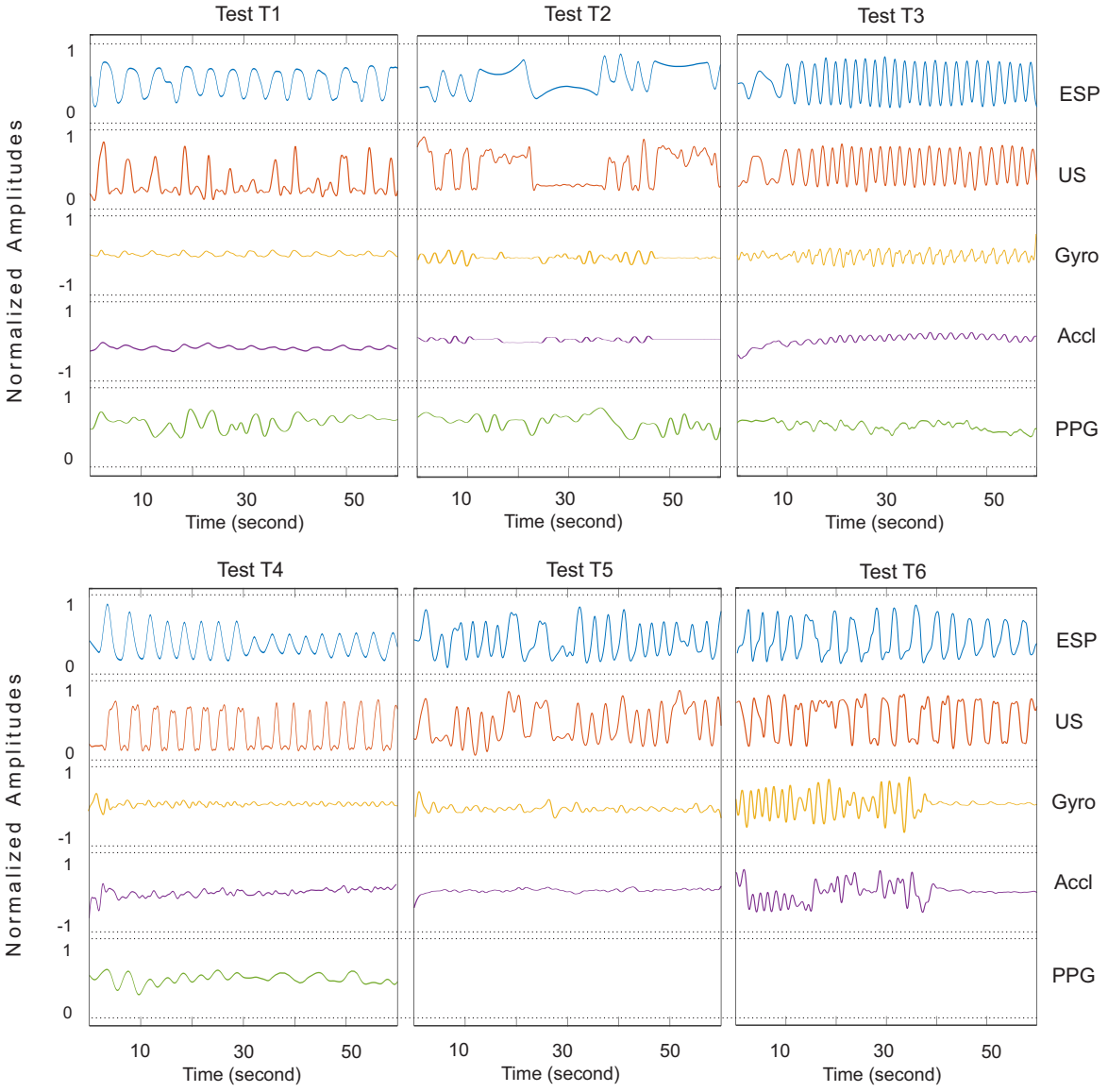

Figure 5 Respiratory waveforms of subject 6.